

1-1-1994

## Microstructure and deformation mechanism of thermoplastic elastomers/

Hun-Jan Tao  
*University of Massachusetts Amherst*

Follow this and additional works at: [https://scholarworks.umass.edu/dissertations\\_1](https://scholarworks.umass.edu/dissertations_1)

---

### Recommended Citation

Tao, Hun-Jan, "Microstructure and deformation mechanism of thermoplastic elastomers/" (1994).  
*Doctoral Dissertations 1896 - February 2014*. 833.  
<https://doi.org/10.7275/7bzd-0w08> [https://scholarworks.umass.edu/dissertations\\_1/833](https://scholarworks.umass.edu/dissertations_1/833)

This Open Access Dissertation is brought to you for free and open access by ScholarWorks@UMass Amherst. It has been accepted for inclusion in Doctoral Dissertations 1896 - February 2014 by an authorized administrator of ScholarWorks@UMass Amherst. For more information, please contact [scholarworks@library.umass.edu](mailto:scholarworks@library.umass.edu).



312066011022154



MICROSTRUCTURE AND DEFORMATION MECHANISM OF THERMOPLASTIC  
ELASTOMERS

A Dissertation Presented

by

HUN-JAN TAO

Submitted to the Graduate School of the  
University of Massachusetts Amherst in Partial Fulfillment  
of the Requirements for the Degree of

DOCTOR OF PHILOSOPHY

May 1994

Department of Polymer Science and Engineering

© Copyright by Hun-Jan Tao 1994

All Rights Reserved

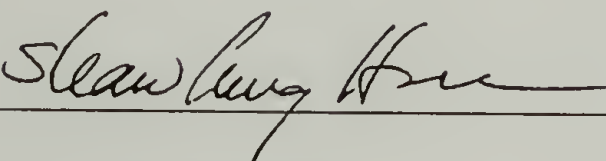
MICROSTRUCTURE AND DEFORMATION MECHANISM OF THERMOPLASTIC  
ELASTOMERS

A Dissertation Presented

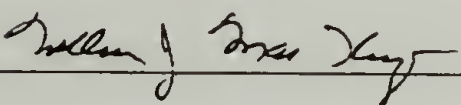
by

HUN-JAN TAO

Approved as to style and content by:



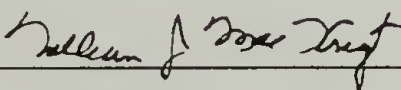
Shaw L. Hsu, Chair



William J. MacKnight, Co-Chair



H. Henning Winter, Member



William J. MacKnight, Department Head  
Polymer Science and Engineering

*To my Wife*

Wen-Ling

## ACKNOWLEDGEMENTS

It gives me great pleasure to acknowledge the guidance and support from my advisors, Professor Shaw Ling Hsu and Professor William J. MacKnight, through the course of this research. I would also like to thank Professor H. Henning Winter for his helpful suggestions.

My sincere thanks are due to Professor Howard D. Stidham, Professor Ying Kang Wang, Dr. Curtis W. Meuse, Dr. David M. Rice, Professor Z. S. Petrovic, Dr. Douglas A. Cates, Dr. Cun Feng Fan, Dr. Nick Reynolds, Professor Xuan Li, and Professor Xiaozhen Yang for their many helpful discussions and assistance.

I would like to express my thanks to all the members of my research groups and other friends for their help and the stimulating discussions. Of those I would like to mention particularly Shin-Long Chen, Mario Perez, Chao Cheng Chen, Sunghoe Yoon, Yuan Ren, Alice Ng, and Dr. Michelle Bellinger. I would also like to thank the Department who gave me this unexpected chance to come here and learn the most advanced polymer science and technology via those enlightening lectures and leading research environment.

Finally I am greatly indebted to my wife and my parents for their love, support, sacrifice, unfailing patience, understanding, and encouragement in the completion of this work.

ABSTRACT  
MICROSTRUCTURE AND DEFORMATION MECHANISM OF THERMOPLASTIC  
ELASTOMERS

MAY 1994

HUN-JAN TAO, B.S., NATIONAL TAIWAN UNIVERSITY

M.S., NATIONAL TAIWAN UNIVERSITY

Ph.D., UNIVERSITY OF MASSACHUSETTS AMHERST

Directed by : Professor Shaw Ling Hsu and Professor William J. MacKnight

Molecular simulation technique together with spectroscopic methods were utilized to study the phase separation behavior of thermoplastic elastomers. Several kinds of systems were investigated, which included diacetylene-containing polyurethane elastomers, polyurethane elastomers with monodisperse hard segments, and a bio-degradable polyester elastomer.

For the semi-rigid segmented polyurethane elastomers, we found that the chain rigidity of hard segment is the dominating factor responsible for their phase separation behavior. Chemical immiscibility, crystallization, and presence of hydrogen bonding are not necessary to drive phase separation even though they can promote it.

The phase diagrams for semi-rigid polyurethane elastomers associated with different lengths in hard/soft segments were explicitly calculated using molecular simulation technique based on rod-coil model. It was found that longer hard segment or *shorter* soft segments have higher degree of phase separation than their counterparts. This result was verified by vibrational spectroscopy. It was also shown that DSC is not appropriate to evaluate the phase composition of polyurethane elastomers.



The phase separation kinetics and the ultimate degree of phase separation for ultra-thin films of polyurethane elastomers are different from their bulk forms. Hard segments will also show preferential orientation onto the substrate surface. These are the direct consequence of hard segment chain rigidity effect. All the experimental results were successfully reproduced by Monte Carlo simulation based on rod-coil model.

Finally, the phase transformation process and mechanical deformation process of a bio-degradable thermoplastic elastomer, PHO, was investigated by FT-Raman spectroscopy and normal coordinate analysis. The long side-chains of PHO will form more extended conformations when PHO undergoes crystallization. It was also found that the strain-induced crystallization and crystalline break-up are not significant for deformed sample. We proposed that the high permanent tensile set associated with PHO comes from the amorphous part rather than from the crystalline part of the system.

# TABLE OF CONTENTS

	<u>Page</u>
ACKNOWLEDGEMENTS.....	v
ABSTRACT.....	vi
LIST OF TABLES.....	x
LIST OF FIGURES .....	xi
CHAPTER	
1. INTRODUCTION.....	1
1.1 Phase Separation Behavior of Thermoplastic Elastomers .....	1
1.2 Previously Proposed Mechanisms for the Phase Separation of Thermoplastic Elastomers .....	3
1.3 Characterization of Phase Separation Behavior.....	6
1.4 Prediction of Phase Separation Behavior.....	11
1.5 Objectives and Overview of this Work .....	12
References.....	14
2. APPLICATION OF A MOLECULAR SIMULATION TECHNIQUE FOR PREDICTION OF PHASE SEPARATED STRUCTURES OF SEMI-RIGID MODEL POLYURETHANES .....	16
2.1 Introduction .....	16
2.2 Method.....	18
2.3 Results and Discussions.....	33
2.4 Conclusions.....	43
References.....	45
3. A SPECTROSCOPIC STUDY AND THERMAL ANALYSIS OF PHASE SEPARATION BEHAVIOR IN DEACETYLENE-CONTAINING MODEL POLYURETHANES.....	48
3.1 Introduction .....	48
3.2 Experimental Section.....	50
3.3 Results and Discussion .....	54
3.4 Conclusions.....	72
References.....	73

4.	INVESTIGATION ON THE PHASE SEPARATION BEHAVIOR OF POLYURETHANE ELASTOMERS BY TWO-DIMENSIONAL WIDELINE SEPARATION NUCLEAR MAGNETIC RESONANCE SPECTROSCOPY .....	75
4.1	Introduction .....	75
4.2	Experimental Section.....	76
4.3	Results and Discussion .....	78
4.4	Conclusions.....	81
	References.....	82
5	A SPECTROSCOPIC ANALYSIS OF PHASE SEPARATION BEHAVIOR OF POLYURETHANE IN RESTRICTED GEOMETRY .....	83
5.1	Introduction.....	83
5.2	Experimental Section.....	85
5.3	Experimental Results.....	87
5.4	Model Used to Analyze Phase Separation Kinetics .....	89
5.5	Comparison of Simulation to Experiment.....	98
5.6	Analysis of Structural Anisotropy.....	99
5.7	Conclusions.....	102
	References.....	104
6	SPECTROSCOPIC STUDY OF THE CHAIN CONFORMATION CHANGES OF A BIO-DEGRADABLE POLYESTER ELASTOMER, POLY( $\beta$ - HYDROXYOCTANOATE), DURING THE PHASE TRANSFORMATION AND MECHANICAL DEFORMATION PROCESSES.....	105
6.1	Introduction .....	105
6.2	Experimental Section.....	107
6.3	Computational Methods .....	108
6.4	Results and Discussion .....	113
6.5	Conclusions.....	123
	References.....	126
7	GENERAL RESULTS AND RECOMMENDATIONS FOR FUTURE WORK .....	128
7.1	General Results.....	128
7.2	Recommended Future Work .....	130
	BIBLIOGRAPHY.....	132

## LIST OF TABLES

<u>Table</u>	<u>Page</u>
2.1	Structure, Volume, and the Average Size of the Subunits Calculated for the Hard and Soft Segments..... 22
3.1	Characteristics of As-Prepared Segmented Diacetylene- Containing Polyurethane Elastomers ..... 52
3.2	Molecular Weights and Molecular Weight Distributions of As-Prepared Segmented Diacetylene-Containing Polyurethane Elastomers ..... 52
3.3	Thermal Properties (DSC) of As-Prepared Segmented Diacetylene-Containing Polyurethane Elastomers..... 54
3.4	Infrared Results for As-Prepared Segmented Diacetylene- Containing Polyurethane Elastomers ..... 61
3.5	Assignments of the Major Bands in Raman Spectra (2500-1400 cm <sup>-1</sup> ) for As-Prepared and Cross-Polymerized Segmented Diacetylene-Containing Polyurethane Elastomers ..... 68



## LIST OF FIGURES

<u>Figure</u>	<u>Page</u>
1.1	Schematic representation of the phase separation process for segmented thermoplastic elastomers..... 1
1.2.	Schematic representation of the hysteresis associated with external deformation process for thermoplastic elastomers ..... 2
1.3.	Schematic representation of the crystallization mechanism for phase separation of polyurethane elastomers ..... 5
1.4.	Crosslinking effect on the $T_g$ for poly(propylene glycols)..... 8
1.5	Schematic representation of the degree of crosslinking effect on $T_g$ 's and $\Delta C_p$ 's ..... 8
1.6	Schematic representation of the splitting in the IR carbonyl stretching region by the hydrogen bonding effect..... 10
1.7	Schematic representation of the phase separation thermodynamics..... 12
2.1	A schematic drawing of single chain structure of an M24M hard segment..... 19
2.2	Calculated interaction energy terms between hard and soft segments for M24M/PPG model system..... 24
2.3	Simulated interaction energy $\Delta W_{hs}$ and the $\chi$ parameter for the M24M/PPG model system..... 26
2.4	Simulated chemical potentials for the M24M/PPG model system by using Flory's rod-coil model..... 29
2.5	Simulated phase diagram for M24M/PPG-2000 model system..... 29
2.6	Schematic drawing of the orientational order associated with hard segments ..... 32
2.7	Simulated chemical potentials for the M24M/PPG-2000 system at different temperatures..... 34
2.8	The effect of the hard segment length on the phase diagram..... 36
2.9	The effect of the soft segment length on the phase diagram..... 37
2.10	The effect of the hard segment length on the fraction of hard segments distributed in the hard segment rich domain, $F_{HH}$ ..... 40

2.11	The effect of the soft segment length on the fraction of hard segments distributed in the hard segment rich domain, $F_{HH}$ .....	41
2.12	Simulated hydrogen bonding strength at different temperatures for two isolated M24M hard segments described by the Maier-Saupe model .....	42
3.1	DSC traces for as-prepared diacetylene-containing polyurethanes .....	55
3.2	Schematic representation of the cross-polymerization of diacetylenes .....	56
3.3	Schematic representation of the non-crystalline hard-domain structure proposed by our previous study.....	57
3.4	Infrared spectra of as-prepared diacetylene-containing polyurethanes in Amide I region .....	60
3.5	Variation of fraction of hydrogen-bonded C=O for as-prepared diacetylene-containing polyurethanes as a function of temperatures .....	63
3.6	Infrared spectra of as-prepared diacetylene-containing polyurethanes in N-H region .....	64
3.7	FT-Raman spectra of as-prepared and cross-polymerized diacetylene-containing polyurethanes.....	66
3.8	FT-Raman spectra of cross-polymerized diacetylene-containing polyurethanes.....	69
4.1	Structures of the soft segment and hard segment for B4 polymer.....	77
4.2	Pulse sequence of WISE-NMR experiment used in this work with proton evolution, cross polarization (CP), and $^{13}\text{C}$ acquisition (AQ) with dipolar decoupling (DD) of protons .....	77
4.3	WISE-NMR spectrum of B4 polymer .....	80
5.1	Infrared external reflection spectra for the phase separation process of a 16 nm B2 polymer film on gold at 23°C.....	87
5.2	Avrami plots of isothermal phase separation kinetics for a 16 nm thick film on gold at 23°C.....	89
5.3	Comparison of Avrami exponents as a function of film thickness for B2 polymer at 23°C .....	90
5.4	Comparison of ultimate degree of phase separations as a function of film thickness for B2 polymer at 23°C.....	90

5.5	Schematic illustration of the domain growth at various time and the measurement of $X(t)$ by the probing points.....	92
5.6	Schematic illustration of film thickness effect on phase separation kinetics.....	93
5.7	Schematic illustration of the hard segment concentration profile from the hard domain surface to the isotropic phase .....	95
5.8	Changes in the concentration factor $F_c$ for different film thicknesses simulated by disk model .....	97
5.9	Simulated Avrami plots for several film thicknesses for disk model .....	97
5.10	Schematic illustration of the preferential orientation effect of hard segment in a ultra-thin film .....	100
5.11	Calculated orientation function of rods confined within two surfaces.....	102
6.1	Chemical structure of bacterially produced poly( $\beta$ -hydroxyoctanoate), PHO, random copolyester.....	106
6.2	Isotropic Raman spectra of n-hexane .....	110
6.3	Stereochemical representation of the model structure of PHO side-chain used in the normal coordinate analysis.....	111
6.4	Variation of the carbonyl stretching region for PHO crystallization process measured by FT-Raman spectroscopy.....	114
6.5	Variation of FT-Raman spectra in the region of $700-1200\text{ cm}^{-1}$ for PHO phase transformation process.....	115
6.6	Variation of optical circular dichroism for PHO phase transformation process .....	116
6.7	Measured isotropic Raman spectra for PHO at different level of phase transformation .....	118
6.8	Calculated isotropic Raman spectra for the PHO side-chain model structure as shown in Figure 6.3.....	119
6.9	Variation of carbonyl stretching region of stretched PHO's measured by FT-Raman spectroscopy.....	121
6.10	Variation of FT-Raman spectra in the region of $700-1200\text{ cm}^{-1}$ for deformed PHO samples.....	122
6.11	Model structure of PHO used for calculating the contour map of conformational energy.....	123

6.12	The contour map of conformational energy for the model structure shown in Figure 6.11.....	124
6.13	Schematic representation of proposed mechanism for the PHO permanent tensile set .....	125



## CHAPTER 1

### INTRODUCTION

#### 1.1 Phase Separation Behavior of Thermoplastic Elastomers

Generally speaking, most of the thermoplastic elastomers are block copolymers containing flexible blocks and rigid blocks. Typical examples are segmented polyurethane elastomers and styrene-butadiene-styrene (SBS) block copolymers.<sup>1</sup> It is well accepted that the phase-separated morphology is responsible for their elastic properties (Figure 1.1).

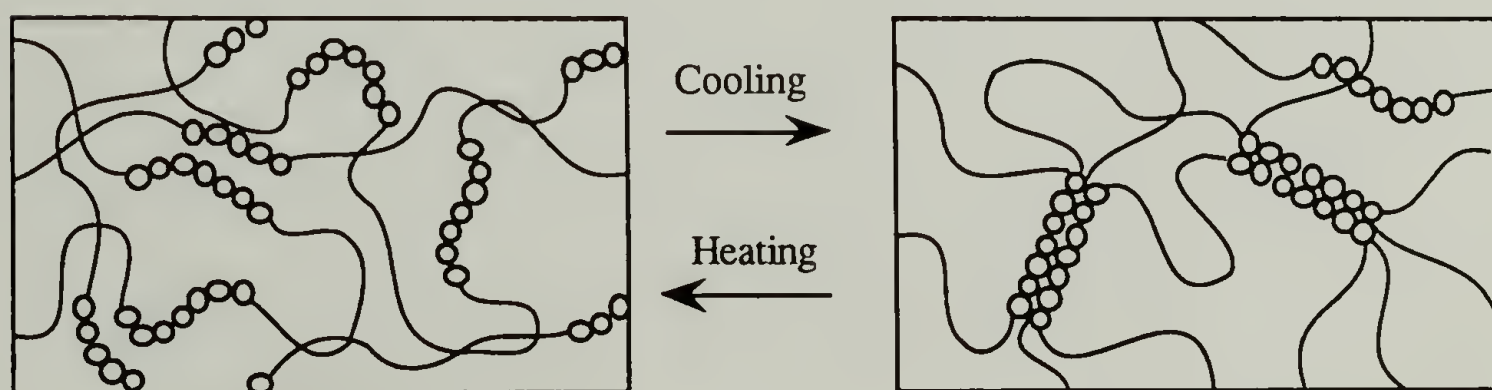


Figure 1.1 Schematic representation of the phase separation process for segmented thermoplastic elastomers. The solid lines stand for flexible segments and the circles stand for rigid segments.

By cooling the molten samples or by drying the solvent-casted films, phase-separated domains are formed which behave as the physical crosslinks between the flexible segments thus result in their elastomeric characters (Figure 1.1). The

advantage for thermoplastic elastomers is that the network formation/destruction process is reversible which is different from the permanent network structure associated with chemical crosslinks. This feature makes the processing more easier. However, because the cohesive energy of these physical crosslinking domains is not as strong as covalent bond, it is very likely to change the domain structures under external deformation and results in the deviation from ideal rubber behavior (for example, to produce a permanent tensile set as shown in Figure 1.2). Therefore it is essential to understand the factors controlling the morphology of phase-separated domains so as to improve their performance.

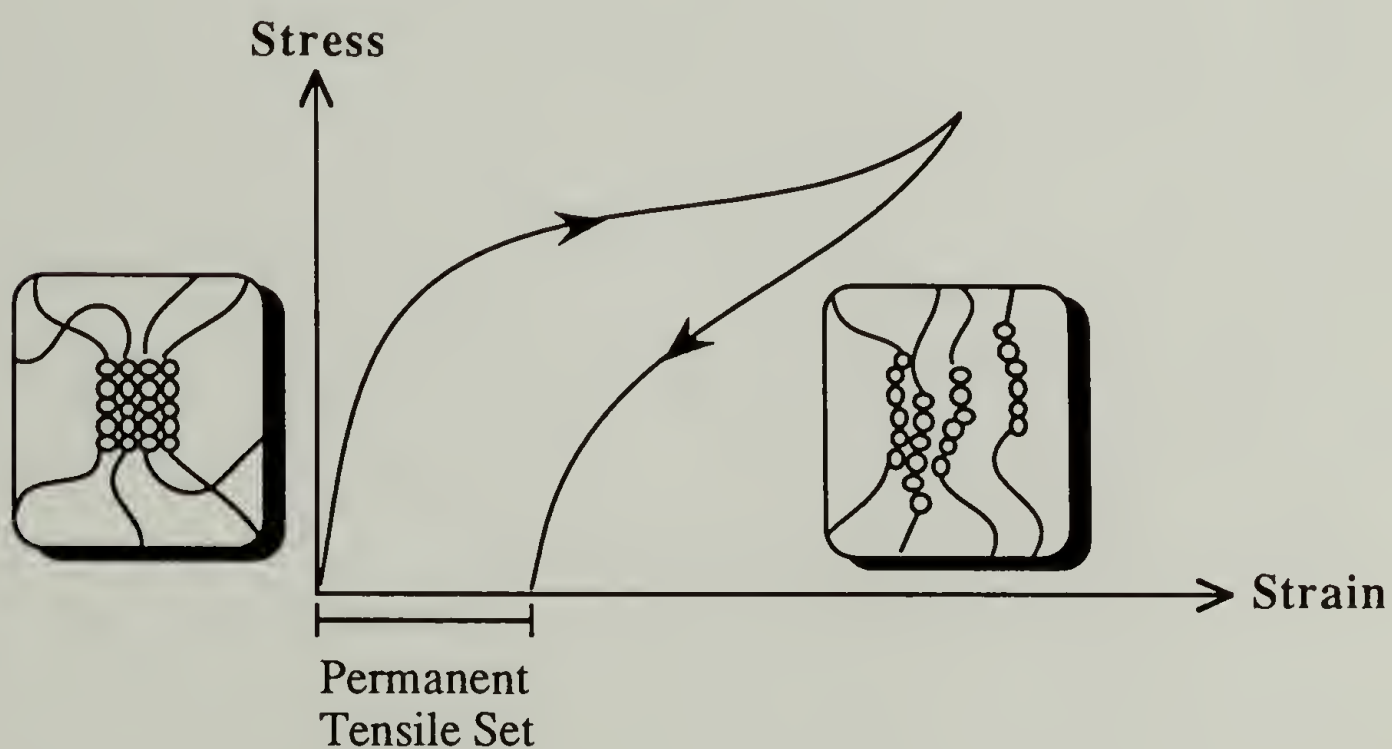


Figure 1.2 Schematic representation of the hysteresis associated with external deformation process for thermoplastic elastomers. Insets are the molecular model for the stress-induced structural change in the phase-separated domains.

Besides, the degree of phase separation is another important factor which can affect their final properties. It is also necessary to be more knowledgeable about controlling the degree of phase separation from the molecular microstructure point of

view. Accordingly, classification of phase separation mechanisms is necessary for these purposes.

## 1.2 Previously Proposed Mechanisms for the Phase Separation of Thermoplastic Elastomers

Several mechanisms have been proposed for illustrating the phase separation process.<sup>1-7</sup> They are briefly summarized as follows.

### (1) Chemical Immiscibility

Chemical immiscibility between distinct blocks is an important driving force for phase separation. Flory-Huggins theory,<sup>8-10</sup> which is shown in eq.(1.1),

$$\frac{\Delta G_m}{RT} = \frac{\Phi_A}{N_A} \ln \Phi_A + \frac{\Phi_B}{N_B} \ln \Phi_B + \chi \Phi_A \Phi_B \quad (1.1)$$

is widely utilized for this mechanism. In eq.(1.1),  $\Delta G_m$ ,  $\Phi$ ,  $N$ , and  $\chi$  stand for the Gibbs free energy change of mixing, the volume fraction, the degree of polymerization, and the interaction parameter between components A and B, respectively. The first two terms at the right side of eq.(1.1) are the combinatorial entropic contribution which are usually very small for polymeric systems. The dominating factor is the last term which corresponds to the enthalpic contribution and the non-combinatorial entropic contribution. A positive  $\chi$  with a value greater than the critical  $\chi$  parameter can cause the system to phase separate. For most of the cases, details regarding  $\chi$  parameter is not available and is usually estimated by<sup>2,5,7</sup>

$$\chi = \frac{V_r}{RT} (\delta_A - \delta_B)^2 \quad (1.2)$$

even though this equation applicable for non-polar systems only<sup>11,12</sup>. In eq.(1.2),  $V_r$  is the relative volume between components A and B, and  $\delta$  is the solubility parameter. The obvious drawback to use eq.(1.2) as an approximation is that it can only produce positive  $\chi$  parameter which is logically wrong. Furthermore, several experimental evidences indicated that the phase separation still can occur even in a negative  $\chi$  system.<sup>13,14</sup> Thus chemical immiscibility is not a necessary condition for phase separation.

## (2) Hydrogen Bonding Effect

Hydrogen bonding has been suggested to be an important driving force for some thermoplastic elastomers, especially for segmented polyurethane elastomers. It was proposed that phase separation of polyurethane elastomers can be driven by the strong hydrogen bonding between hard segments.<sup>4,6</sup> An association model was presented with this idea.<sup>2,15</sup> Association model adds one more term to the Flory-Huggins equation,  $\Delta G_{HB}/RT$ , which is associated with hydrogen bonding effect .

$$\frac{\Delta G_m}{RT} = \frac{\Phi_A}{N_A} \ln \Phi_A + \frac{\Phi_B}{N_B} \ln \Phi_B + \chi \Phi_A \Phi_B + \frac{\Delta G_{HB}}{RT} \quad (1.3)$$

However, the role of hydrogen bonding seems to be overemphasized for polyurethanes because experimental results have showed that phase separation still can be achieved for polyurethane elastomers which are free of hydrogen bonding.<sup>16,17</sup> Furthermore, from spectroscopic evidence<sup>18</sup> and from *ab initio* calculation<sup>19</sup> it was shown that the hydrogen bonding strength between hard-soft segments can be stronger than that between hard-hard segments for polyurethanes, or a negative  $\chi$ .



### (3) Crystallization

Crystallization of hard segments for polyurethane elastomers is sometimes taken to be the dominating driving force for their phase separation. For example, a critical hard segment length model has been proposed.<sup>20</sup> In this model, it is assumed that the hard segment lengths must be longer than a critical value to form crystalline structures, or to phase separate (Figure 1.3). The degree of phase separation is correlated to the degree of crystallinity. However, in most of the cases the 'crystalline' structures in the hard segment rich domains are found to be ill-defined by WAXS measurement.<sup>6</sup> Furthermore, several well phase-separated polyurethane elastomers were found to possess non-crystalline domains.<sup>21</sup> Crystallization as a necessary condition for phase separation is questionable.

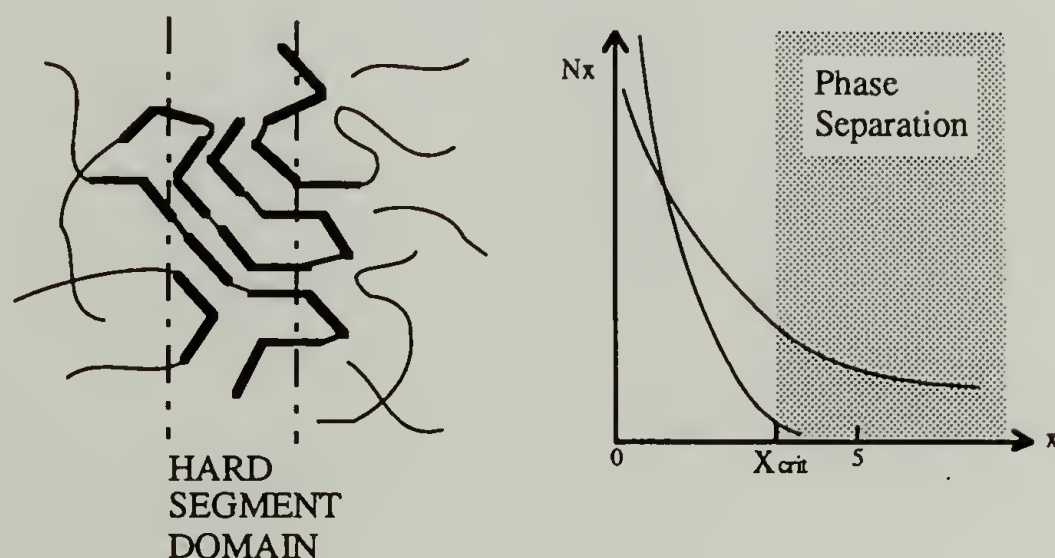


Figure 1.3 Schematic representation of the crystallization mechanism for phase separation of polyurethane elastomers : only hard segments which are longer than the critical length can phase separate into the crystalline domains. (from ref. 20)

#### (4) Diffusion

A kinetic model for the phase separation of polyurethane elastomers has been proposed.<sup>22</sup> In this model, the phase separation is assumed to be controlled by kinetic instead of by thermodynamic reason. Cahn-Hilliard-Cook-Binder theory<sup>23,24</sup> was utilized to illustrate this idea. For a two-component system undergoing phase separation, the phase separation rate  $R(q)$  can be expressed by

$$\begin{aligned} R(q) &= -Mq^2 \left[ \frac{\partial^2 f}{\partial \phi_0^2} + 2Kq^2 \right] \\ &= -D_{app}q^2 - 2MKq^4 \end{aligned} \quad (1.4)$$

where  $D_{app}$  is an apparent diffusion coefficient,  $M$  is the mobility,  $\partial^2 f / \partial \phi_0^2$  is the second derivative of free energy of mixing with respect to composition  $\phi_0$ , and  $K$  is the interfacial free energy density. Along with this idea, it was proposed that flexible hard segments will phase separate more completely or quickly than rigid ones.<sup>25</sup>

### 1.3 Characterization of Phase Separation Behavior

Several techniques have been utilized to analyze the phase separation behavior of thermoplastic elastomers. The ones usually employed for polyurethane elastomers are briefly summarized as follows.<sup>1,4,5,7</sup>

#### (1) Thermal Analysis (DSC)

Differential scanning calorimeter (DSC) is a popular technique for studying phase separation behavior of polyurethane elastomers. It is presumably that thermal properties are solely determined by the concentration effect ('copolymer effect'). Thus

the fraction of soft segments dispersed in soft segment rich phase,  $F_{ss}$ , was traditionally evaluated by

$$F_{ss} = \frac{(\Delta C_{p,PU}/W_{s,T})}{\Delta C_{p,soft}^o} \quad (1.5)$$

where  $\Delta C_{p,PU}$ ,  $W_{s,T}$ , and  $\Delta C_{p,soft}^o$  are the polyurethane soft segment heat capacity jump at its glass transition temperature, the weight fraction of soft segment in the system, and the heat capacity jump for pure soft segment, respectively. The composition in the soft segment rich phase was usually estimated by the following Fox equation:

$$\frac{1}{T_{g,PU}} = \frac{W_{H,i}}{T_{g,H}} + \frac{W_{S,i}}{T_{g,S}} \quad (1.6)$$

where  $T_{g,PU}$ ,  $T_{g,H}$ ,  $T_{g,S}$  are glass transition temperatures of polyurethane, of pure hard segments, and of pure soft segments, respectively;  $W_{H,i}$ , and  $W_{S,i}$  are the weight fractions of hard segment and soft segment in the isotropic phase. Most experimental data suggest that the  $T_g$  and  $\Delta C_p$  values depend not only on phase composition, confinement of soft segment chain ends to phase-separated domains will also affect these values ('cross-linking effect'). The crosslinking effect is much more important than the copolymer effect. For example,  $T_g$ 's of crosslinked poly(propylene glycols) (PPG) are higher than their linear forms by 56°C and 27°C for molecular weights of 1000 and 3000, respectively (Figure 1.4).<sup>26</sup> Furthermore,  $T_g$ 's and  $\Delta C_p$ 's of soft segments were also found to be dependent on the degree of crosslinking (Figure 1.5).<sup>27</sup> Therefore, it is not adequate to use DSC to evaluate the phase compositions of polyurethane elastomers.

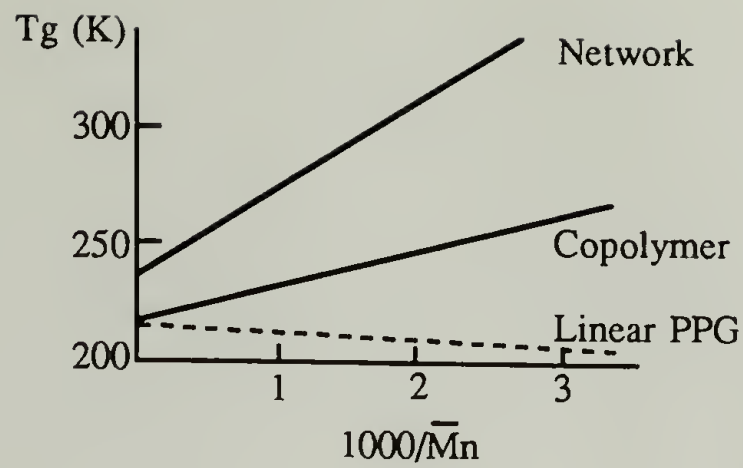


Figure 1.4 Crosslinking effect on the  $T_g$  for poly(propylene glycols). (from ref. 26)

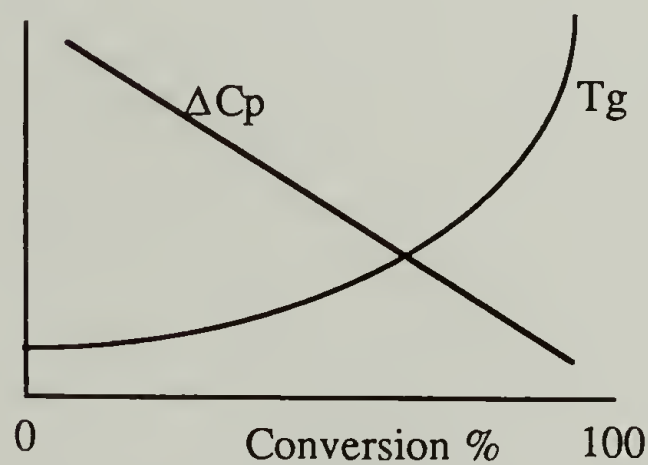


Figure 1.5 Schematic representation of the degree of crosslinking effect on  $T_g$ 's and  $\Delta C_p$ 's.

## (2) Small-Angle X-ray Scattering (SAXS)

SAXS can be used to reveal the phase-separated structure due to fluctuations in electron density. For a two-phase system with diffuse interphase and thermal fluctuations, scattering intensity  $I(q)$  can be expressed by<sup>25,28</sup>

$$I_{\text{obs}}(q) = K_p q^{-4} \exp(-q^2 \sigma^2) + I_b \quad (1.7)$$

where  $I_{\text{obs}}(q)$ ,  $q$ ,  $K_p$ ,  $\sigma$ , and  $I_b$  are respectively measured intensity, magnitude of the scattering vector, a constant related to the area of interface per unit volume, diffuse-



interface thickness parameter, and scattered intensity due to the thermal fluctuations.  $\sigma$  is related to the interphase thickness  $E$  by  $\sigma \approx (12)^{-1/2}E$ .  $I_b$  is assumed to be a constant in the Bonart method.<sup>25,28</sup> The degree of phase separation can be related to the integrated scattered intensity  $Q$  by

$$Q = \int_0^{\infty} [I_{\text{obs}}(q) - I_b] q^2 dq \quad (1.8)$$

while the interdomain spacing  $d$  could be estimated by using the Bragg equation

$$d = 2\pi/q_{\text{max}} \quad (1.9)$$

Detail information of the phase-separated structure can be obtained by deconvolution of SAXS pattern. But the results depend on the morphological model employed.

### (3) Solid State NMR

Solid state nuclear magnetic resonance spectroscopy (NMR) has been used for studying polyurethane elastomers, particularly their dynamics. For example, the fraction of slow and fast components, which are associated with the hydrogens in hard segment rich domains and in soft segment rich domains. This can be accomplished by using  $^1\text{H}$  magnetization relaxation spectrum by<sup>29</sup>

$$M(t) = M_f e^{-t/T_{2f}} + M_s e^{-t/T_{2s}} \quad (1.10)$$

where  $M(t)$  is the magnetization as a function of time,  $M_f$  and  $M_s$  are the initial magnetizations of the fast and slow components, and  $T_{2f}$  and  $T_{2s}$  are the spin-spin relaxation times of the fast and slow component. Similar method was used in  $^{13}\text{C}$  spin-lattice relaxation experiment.<sup>30,31</sup>

#### (4) Infrared Spectroscopy

Infrared spectroscopy (IR) is a useful tool for the phase separation study. For example, carbonyl stretching region typically exhibits two components for polyurethane elastomers. The higher and lower frequency components are associated with free carbonyl groups and hydrogen-bonded carbonyl groups, respectively.<sup>2</sup> If the soft segments are polyethers, the higher and lower frequency bands correspond to the hard segments in the dispersed phase and in the hard segment rich phase, respectively. The degree of phase separation can be estimated by the relative intensity of these two bands (Figure 1.6).

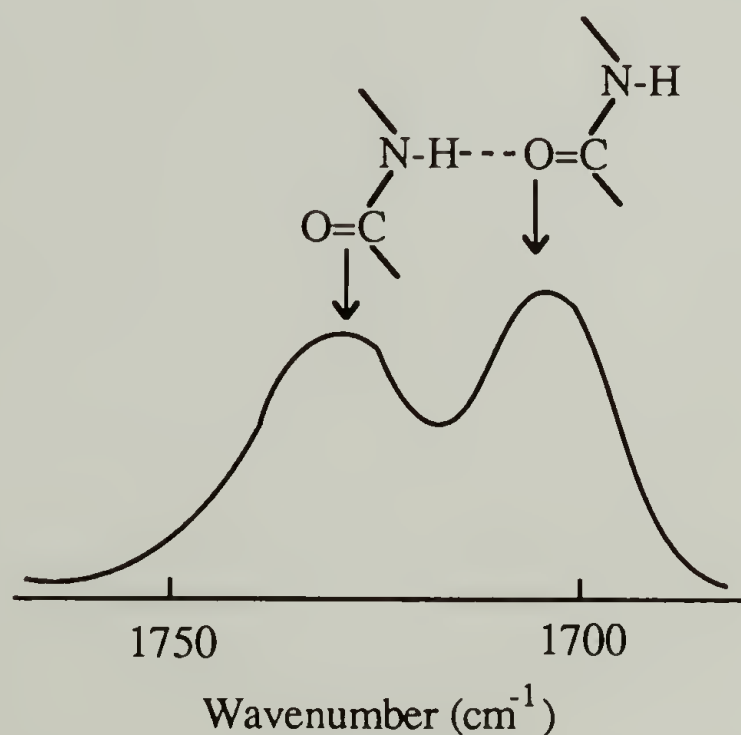


Figure 1.6 Schematic representation of the splitting in the IR carbonyl stretching region by the hydrogen bonding effect.

#### 1.4 Prediction of Phase Separation Behavior

The goal for the phase separation study is to accurately predict the phase diagrams for various systems. Even though at present no single theory is able to achieve this aim, a general approach is available from thermodynamic considerations. The principle to calculate the phase diagram is to calculate the Gibbs free energy change of mixing,  $\Delta G_m$ ,<sup>2,7,10,11</sup> defined by

$$\Delta G_m = \Delta H_m - T\Delta S_m \quad (1.11)$$

where  $\Delta H_m$  and  $\Delta S_m$  are changes in the enthalpy and entropy during mixing. The chemical potential for each species,  $\mu_i$ , can be derived by

$$\mu_i - \mu_i^o = \left( \frac{\partial \Delta G_m}{\partial n_i} \right)_{T,P,n_j} \quad (1.12)$$

where the superscript <sup>o</sup> stands for the standard state;  $T$ ,  $P$  and  $n_i$  are the temperature, pressure, and the number of moles of the  $i$ th species, respectively. The coexistence curve, or binodal curve, is determined by

$$\mu_i^\alpha = \mu_i^\beta \quad (1.13)$$

where  $\alpha$  and  $\beta$  denote two distinct phases. The spinodal curve is determined by

$$\left( \frac{\partial \mu_i}{\partial \phi_i} \right)_{T,P} = 0 \quad (1.14)$$

where  $\phi_i$  is the volume fraction of species  $i$ . Finally, the critical point can be determined by

$$\left( \frac{\partial \mu_i}{\partial \phi_i} \right)_{T,P} = \left( \frac{\partial^2 \mu_i}{\partial \phi_i^2} \right)_{T,P} = 0 \quad (1.15)$$

How these parameters vary as a function of composition are illustrated in Figure 1.7. The calculation of  $\Delta G_m$  depends on the system characters and a universal theory is not existent. However, several theories applicable to different conditions have been proposed. Reviews in this area are available.<sup>7,11</sup>

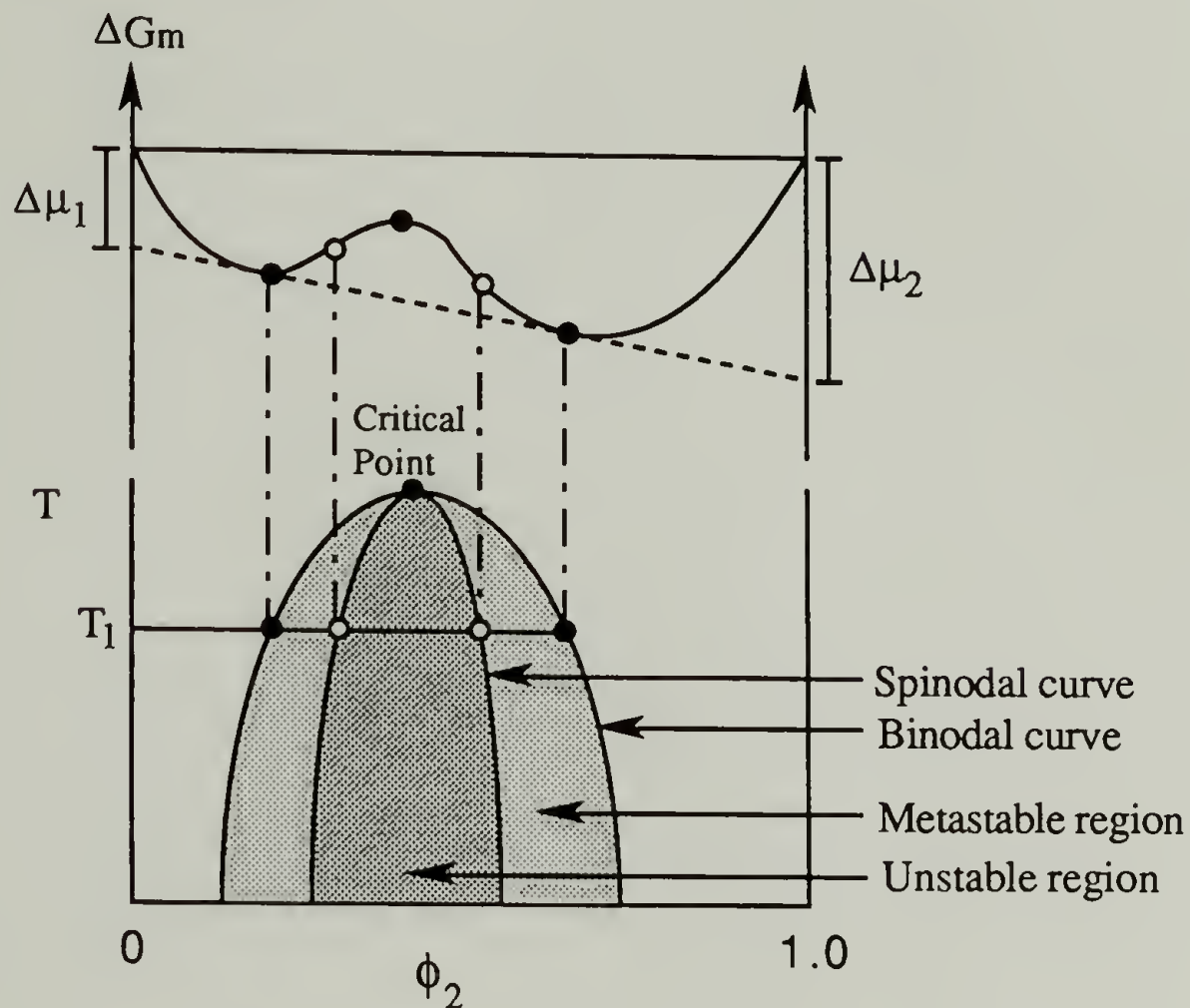


Figure 1.7 Schematic representation of the phase separation thermodynamics. Upper part : Gibbs free energy of mixing as a function of concentration in a binary system. Lower part : phase diagram.

### 1.5 Objectives and Overview of this Work

From the above discussion it is clear that thermoplastic elastomers form phase-separated structures, although the driving forces and structure-property relationships are still not clear. As a consequence, sometimes the interpretations of characterization results are in dispute due to the lack of proper mechanisms. Therefore we would like to



Finally, crystallization of the hard segments is not necessarily the driving force and a requisite condition for phase separation. Numerous studies show that the structure in the hard-segment domains is not crystalline.<sup>1,14-16</sup>

Clearly, further analysis is necessary to support and guide experimental studies for improved understanding of the phase separated structures of polyurethanes. A number of theories for prediction of polymer miscibility behavior have been presented.<sup>17-19</sup> Although, in some instances, the shape effect has been considered and specific interactions incorporated, a common assumption is that all chains are flexible. This assumption is inapplicable for consideration of miscibility behavior of hard-soft polyurethane segments. Greater emphasis has recently been focused on the effects of chain rigidity on miscibility behavior.<sup>20-23</sup> Hølyst and Schick, for example, proposed a rod-coil theory to calculate phase equilibrium behavior of rod-rod, rod-coil mixtures, and rod-coil block copolymers.<sup>22</sup>

An alternate approach has been pursued in our laboratory. In a previous study, a combination of the Flory-Huggins theory and a molecular simulation technique was applied to miscibility studies of three types of binary mixtures including solvent with solvent, polymer with solvent, and polymer with polymer.<sup>24</sup> Molecular simulation is utilized to calculate the interaction parameter in the Flory-Huggins theory, including heat of mixing associated with pairwise interactions and the number of possible interaction partners, i.e. coordination number. The pair energies are obtained by averaging a large number of configurations generated by *Monte Carlo* method as well as considering the constraint associated with excluded volume. The temperature dependence of the interaction parameter  $\chi$  is obtained with the formalism developed in the earlier study. In several examples, the calculated upper critical solution temperatures were compared with experimental values. This combination of Flory-Huggins theory and molecular simulation technique provides an opportunity to study

the thermodynamic behavior of a binary mixture without possessing previous knowledge or experimental data for the systems considered.

To extend the applicability of the molecular simulation approach to polyurethane systems, the inherent chain rigidity needs be considered, a concept encountered in studies of the isotropic-anisotropic transition of liquid crystalline polymers.<sup>25</sup> Flory, in deriving an isotropic to anisotropic transition in liquid crystalline polymers, considered the repulsive force associated with the chain rigidity effect. In such an instance, an anisotropic phase can coexist with an isotropic phase even if the interaction between polymer and solvent is favorable. Phase separation results from the entropic rather than enthalpic term. A positive  $\chi$  parameter can enhance phase separation; Even a negative  $\chi$  system may have phase separation, however. Chemical incompatibility is not requisite for phase separation if the difference in chain rigidity is significant.

A molecular simulation study with the following features has been conducted: 1. Prediction must be applicable for a mixture of rod and flexible segments; 2. The existence of molecular parameters are identifiable with the polymers being studied; 3. Phase separation can occur even with a negative  $\chi$  parameter. Furthermore, the relative importance of various secondary interactions is also of interest. An extension of our molecular simulation technique incorporating chain rigidity to explain polymer miscibility behavior is presented here.

## 2.2 Method

**A. Chemical Structural Units Considered.** The hard segments utilized in our simulation study are as follows: "M24M" designates one 2,4-Hexadiyn-1,6-diol in the middle as the chain extender with an MDI [4,4'-Methylenebis(phenyl isocyanate)]

unit at each end. MDI units are capped with a methyl group. The structure is presented in Figure 2.1.

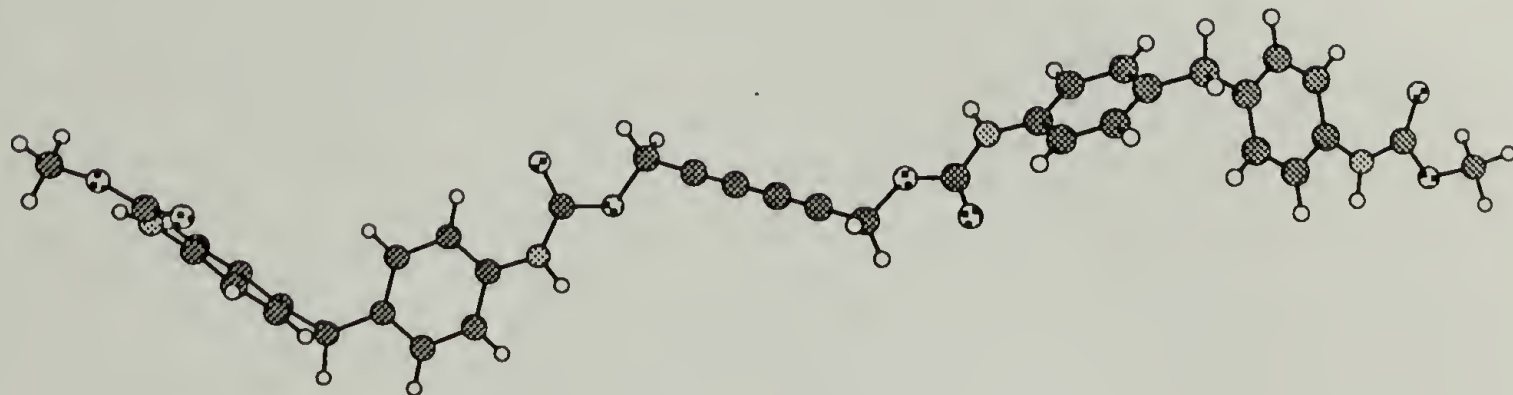


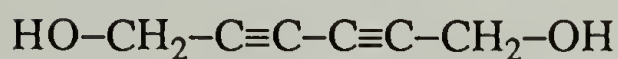
Figure 2.1 A schematic drawing of single chain structure of an M24M hard segment.

Similarly, "M24M24M" refers to a hard segment with two 2,4-Hexadiyn-1,6-diol units and three MDI units. The soft segments are PPG [poly(propylene glycol)] with molecular weights of 1000, 2000, and 3000. The hard segments are monodisperse in molecular weight. Schematic drawings of the monomer units are as follows :

MDI



2,4-Hexadiyn-1,6-diol



PPG





PPG is chosen as the soft segment in our experimental program to avoid complexities arising from soft segment crystallization. Hard segments were chosen for numerous reasons: 1. Hard segments with short MDI units do not form crystalline hard segment domains and thus perturbing effects arising from crystallinity are eliminated; 2. The diacetylene segment is more rigid than the butanediol (BD) chain extender typically used, thus simplifying our calculation; 3. By studying photo- and thermal- reactivities of the diacetylene segment, some of our assumptions and calculations can be verified.<sup>15</sup>

**B. Calculation of Free Energy of Mixing- Extension of Our Previous Model.** The actual calculation of the free energy of mixing,  $\Delta G$ , depends on the specific theory or model employed, with the Flory-Huggins lattice method perhaps being the simplest. In the previous study, the basis for providing a methodology incorporating molecular simulation techniques for studies of mixing behavior of binary systems was developed.<sup>24</sup> The model is incomplete as non-combinatorial entropic terms were not considered. In addition, interactions between polymers were approximated only by interactions between polymer segments occupying a similar *lattice* size. A question arises as to how accurate pairwise interactions,  $\Delta w_{ij}$ , can be obtained to represent interactions in the actual condensed state. Use of molecular mechanics to minimize energy using several selected configurations was determined not to be representative of the interaction energy for binary mixtures exhibiting normal Boltzmann distributions. Since relative movement of the two interacting segments is quite small at low temperatures, molecular dynamics samples only localized configurational space, unless very fast computers are utilized, therefore, cannot provide accurate interaction terms easily. From the pragmatic view, to improve the reliability of calculation of  $\Delta w_{ij}$  as a function of temperature, including constraints arising from excluded volume, an approach incorporating the *Monte Carlo*



technique was established to take into account and properly weigh a large number of relative orientations of the two molecules. In order to eliminate bias introduced by the chosen configurations, a crucial step for reliable calculation of interaction energies,  $\Delta W$ 's, is to establish an efficient algorithm for sampling relative orientations of a pair of interacting molecules. By calculating the specific interaction energies of the configurations which satisfied Metropolis statistics, we were able to calculate the interaction energy at various temperatures.<sup>24</sup>

In this study, to satisfy a requirement for use of the lattice model in calculating the interaction energy between hard and soft segments, each hard segment is divided into several subunits occupying a volume similar to the PPG soft segment. The M24M hard segment is then decomposed into 4 subunit-1, 2 subunit-2, and 4 subunit-3. M24M24M consists of 6 subunit-1, 4 subunit-2, and 6 subunit-3. The structures of the subunits are tabulated in Table 2.1 where their volumes are defined as the volumes within the van der Waals surfaces and calculated by the uniform finite element method.<sup>26</sup> The cubic root of the volume is taken as the average size for each subunit. Traditionally, the interaction energy,  $\Delta W_{hs}$ , for the two types of entities with similar size and spherical symmetric geometry can be defined as follows

$$\Delta W_{hs} = W_{hs} - \frac{1}{2}(W_{hh} + W_{ss}) \quad (2.1)$$

where  $W_{ij}$  is the intermolecular interaction between  $i$  and  $j$ . "h" denotes the hard segment and "s" denotes the soft segment. The interaction parameter,  $\chi$ , is defined as

$$\chi = \frac{Z \Delta W_{hs}}{RT} \quad (2.2)$$

where  $Z$  is the coordination number.

Table 2.1 Structure, Volume, and the Average Size of the Subunits Calculated for the Hard and Soft Segments.

	STRUCTURE	VOLUME( $\text{\AA}^3$ )	AVERAGE SIZE( $\text{\AA}$ )
<u>HARD SEGMENT</u>			
subunit -1	O-(C=O)NH	143.27	5.2
subunit -2	CH <sub>2</sub> C $\equiv$ C	131.08	5.1
subunit -3	C <sub>6</sub> H <sub>4</sub>	196.5	5.8
<u>SOFT SEGMENT</u>			
subunit	CH <sub>2</sub> C(CH <sub>3</sub> )HO	284.77	6.6

The uncertainty in this number will influence the critical temperatures calculated, and, in some cases, significantly. This number can be determined by methods described earlier.<sup>24</sup> The most simplistic way is to calculate the cohesive energy density of one or more pairs of interacting segments using periodic boundary conditions. Our earlier studies have shown that various techniques yield a value of 6-7 for the systems described. In addition with  $Z = 6$ , the calculated critical temperatures fit experimental data most accurately for the molecular or polymeric systems studied.<sup>24</sup> Therefore, in this study, we have used the number 6 for every segment pair as an assumption. Pairwise secondary interactions including van der Waals and hydrogen bonding are explicitly considered. By assuming that the interaction energy is proportional to the number of subunits in the hard segment, the hard-soft segment interaction,  $W_{hs}$ , for the M24M/PPG system is calculated as

$$W_{hs} = \frac{1}{10} (4E_{s1} + 2E_{s2} + 4E_{s3}) \quad (2.3)$$

where  $E_{si}$  represents the intermolecular interaction between the soft segment and subunit  $i$  in the hard segment. Similarly for the hard-hard segment interaction,  $W_{hh}$ , we have

$$W_{hh} = \frac{1}{100} (16E_{11} + 16E_{12} + 32E_{13} + 4E_{22} + 16E_{23} + 16E_{33}) \quad (2.4)$$

In a similar fashion, the interaction energies of the M24M24M/PPG system are

$$W_{hs} = \frac{1}{16} (6E_{s1} + 4E_{s2} + 6E_{s3}) \quad (2.5)$$

$$W_{hh} = \frac{1}{256} (36E_{11} + 48E_{12} + 72E_{13} + 16E_{22} + 48E_{23} + 36E_{33}) \quad (2.6)$$

In these cases, we have assumed that the probability of contact points is identical along the chain. The  $E_{ij}$ 's represent interactions between  $i$  and  $j$  subunits of the hard segment. This assumption is adequate for flexible hard segments in either hard segment rich or soft segment rich domains. For the case of rigid hard segments, this approximation assuming that contact points between two rods are random remains adequate for the isotropic phase as there is no preferential orientation between the two chain segments. In other words, the defined enthalpic interactions are consistent with the Flory-Huggins model. It is obvious that this is not the case for rigid hard segments in the hard segment rich domains because, in this case, the hard segments display preferential orientation between themselves. It is therefore necessary to introduce another parameter,  $V$ , as described below, to describe the enthalpic contribution to the free energy.

The classical force-field characteristic of interatomic interactions, whether intramolecular or intermolecular, is the single most important and essential parameter governing the accuracy of simulation techniques. The energy of a system, which can



be a single molecule, a pair of molecules, or even a condensed state assembled with a large number of molecules, is defined by different energy terms. Covalent interactions may be described by terms such as bond, valence angle, torsion, and hybridization. Terminology describing nonbonded interactions includes van der Waals, electrostatic, and hydrogen-bonding interactions. The specific force field used in our study has been previously defined.<sup>27</sup> The *POLYGRAF* software is from Molecular Simulations, Inc. The necessity for incorporating partial charges depends on the specific force fields used. Some contributions from charges have been incorporated in the force field.<sup>27</sup> It has been shown that explicit incorporation of charges appears unnecessary.

The interaction energies for various pairwise interactions of the M24M/PPG system calculated as a function of temperature are shown in Figure 2.2.

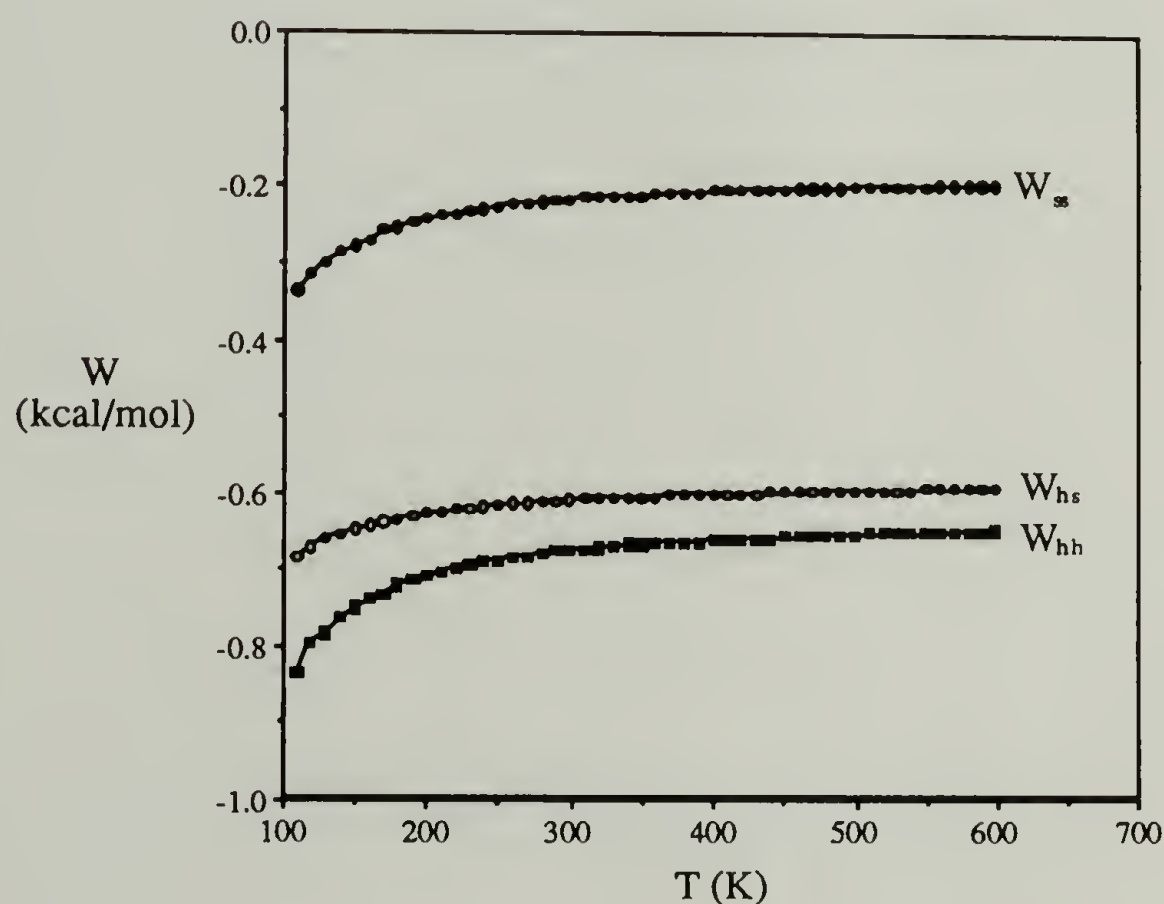


Figure 2.2 Calculated interaction energy terms between hard and soft segments for M24M/PPG model system.



The M24M24M/PPG system shows a similar result. In both cases, the hard-hard segmental interaction,  $W_{hh}$ , is the most favorable and the soft-soft interaction,  $W_{ss}$ , the least favorable. The calculated interaction energy,  $\Delta W_{hs}$ , and the  $\chi$  parameters, both negative, are shown in Figure 2.3. The negative  $\chi$  values obtained suggest that phase separation should not occur in the temperature range of interest according to the Flory-Huggins theory, in direct contradiction to known polyurethane morphology. This inherent contradiction arises either from the simulation technique, including force field, or inapplicability of the Flory-Huggins theory to polyurethane elastomers. Accurate structural predictions for a broad spectrum of molecules and macromolecules have demonstrated the reliability of the force field.<sup>24,27</sup> The simulation technique, including the *Monte Carlo* method proposed, has also proven effective.<sup>24</sup> Experimental data have shown that a negative  $\chi$  is possible for the polyurethanes, and our calculated  $\chi$  values are in reasonable agreement with those measured.<sup>6,7</sup> For example,  $\chi$  parameters can be as low as -3 for systems with relatively weak specific interactions and as low as -12 for those with strong specific interactions.<sup>28</sup>

**C. Modifications of Earlier Algorithms.** The principal deficiency with use of the Flory-Huggins theory is that it is applicable only for flexible chains. Modification of the theory incorporating chain rigidity is thus necessary for polyurethanes. The model hard segment of M24M in the single chain conformation is shown in Figure 2.1. In the MDI unit, the rotational barrier of various dihedral angles can be in the range of 1.8 to 7 kcal/mol. There is little possibility for chain conformation to deviate from the straight segment shown schematically in Figure 1.1 thus making it impossible to satisfy the basic assumption of the Flory-Huggins theory, i.e. flexible chains.

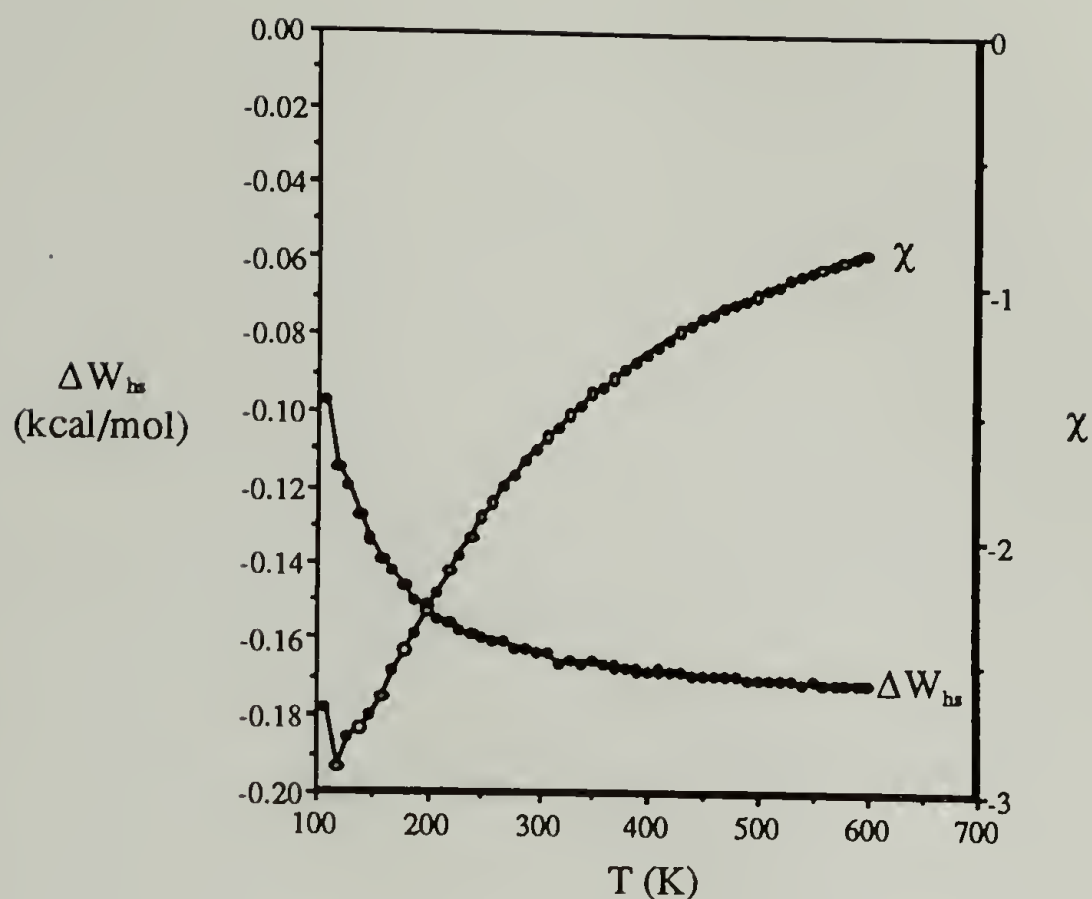


Figure 2.3 Simulated interaction energy  $\Delta W_{hs}$  and the  $\chi$  parameter for the M24M/PPG model system.

The theory for prediction of mixing behavior needs be modified to include the following:

1. Accommodate a mixture of rigid and flexible chains.
2. Include parameters which can be predicted by the molecular simulation method,  
and
3. Predict phase separation even with negative interaction parameters.

Consideration of the original formalism of Flory's liquid crystal theory to the isotropic-anisotropic transition appears relevant.<sup>29</sup> In that theory, upon increasing rod concentration beyond a critical value, the system phase separates into one isotropic and

one anisotropic phase even if favorable interactions exist between rod and solvent. The driving force arises not only from the enthalpic but also entropic term associated with relative chain orientation. When the solvent is replaced by the random coil, and if the coil length is sufficiently long, the connectivity between the hard and soft segment can be ignored and thermodynamic equations simplified to a rod-coil blend system.<sup>30,31</sup> It has also been shown that an anisotropic phase of pure rods can be formed if the coil length is sufficiently long.

Extending Flory's rod-coil theory, the chemical potentials for the hard segment unit, 2, and the soft segment unit, 3, in the isotropic phase (soft segment rich domains) and the ordered phase (hard segment rich domains) have been derived as shown below. In these expressions, it is assumed that the same  $\chi$  exists in the isotropic and anisotropic/ordered phases.

#### Anisotropic/ordered Phase

$$\frac{\mu'_2 - \mu_2^0}{RT} = \ln \left( \frac{\phi'_2}{N_2} \right) + \phi'_2 (y-1) + \phi'_3 N_2 \left( 1 - \frac{1}{N_3} \right) + 2 (1 - \ln y) + \chi N_2 \phi_3'^2 \quad (2.7)$$

$$\frac{\mu'_3 - \mu_3^0}{RT} = \ln \left( \frac{\phi'_3}{N_3} \right) + \phi'_2 \left( \frac{N_3}{N_2} \right) (y-1) + \phi'_3 (N_3 - 1) + 2 \left( \frac{N_3}{y} \right) - \ln Z_3 + \chi N_3 \phi_2'^2 \quad (2.8)$$

#### Isotropic Phase

$$\frac{\mu_2 - \mu_2^0}{RT} = \ln \left( \frac{\phi_2}{N_2} \right) + \phi_2 (N_2 - 1) + \phi_3 N_2 \left( 1 - \frac{1}{N_3} \right) - 2 \ln N_2 + \chi N_2 \phi_3^2 \quad (2.9)$$

$$\frac{\mu_3 - \mu_3^0}{RT} = \ln \left( \frac{\phi_3}{N_3} \right) + \phi_2 N_3 \left( 1 - \frac{1}{N_2} \right) + \phi_3 (N_3 - 1) - \ln Z_3 + \chi N_3 \phi_2^2 \quad (2.10)$$

where the disorder parameter,  $y$ , is determined by

$$\exp \left( -\frac{2}{y} \right) = 1 - \phi_2' \left( 1 - \frac{y}{N_2} \right) \quad (2.11)$$

In the above expressions,  $N_2$  is the axial ratio or number of rod subunits,  $N_3$  is the degree of coil polymerization,  $\phi$  is the volume fraction calculated in terms of the number of each subunit,  $Z_3$  is the internal configuration partition function for the coil,  $\mu$  is the chemical potential in the isotropic phase, and  $\mu'$  of the ordered phase.  $\chi$ 's can be calculated by using the molecular simulation method developed earlier. At equilibrium, the chemical potentials must be the same for each species in the two phases. It is then possible to derive the phase diagram using eqs.(2.7)-(2.11).

The chemical potentials as a function of composition for the M24M/PPG-2000 system are shown in Figure 2.4. The phase diagrams can be determined only by setting eq.(2.7) equal to eq.(2.9), and (2.8) to (2.10), and to seek a simultaneous solution, subject to the condition imposed by eq.(2.11). In our case, as found previously for rods mixed with long coils,<sup>30,31</sup> this is impossible. The only possible solution is for the ordered phase containing only hard segments to coexist with a phase of hard segments dispersed in the soft segments. Any phase composition falling within the heterogeneous phase region will separate into these two phases. The calculated phase diagram is shown in Figure 2.5. All the compositions falling within the isotropic phase region cannot exhibit phase separation and only a single phase can occur.



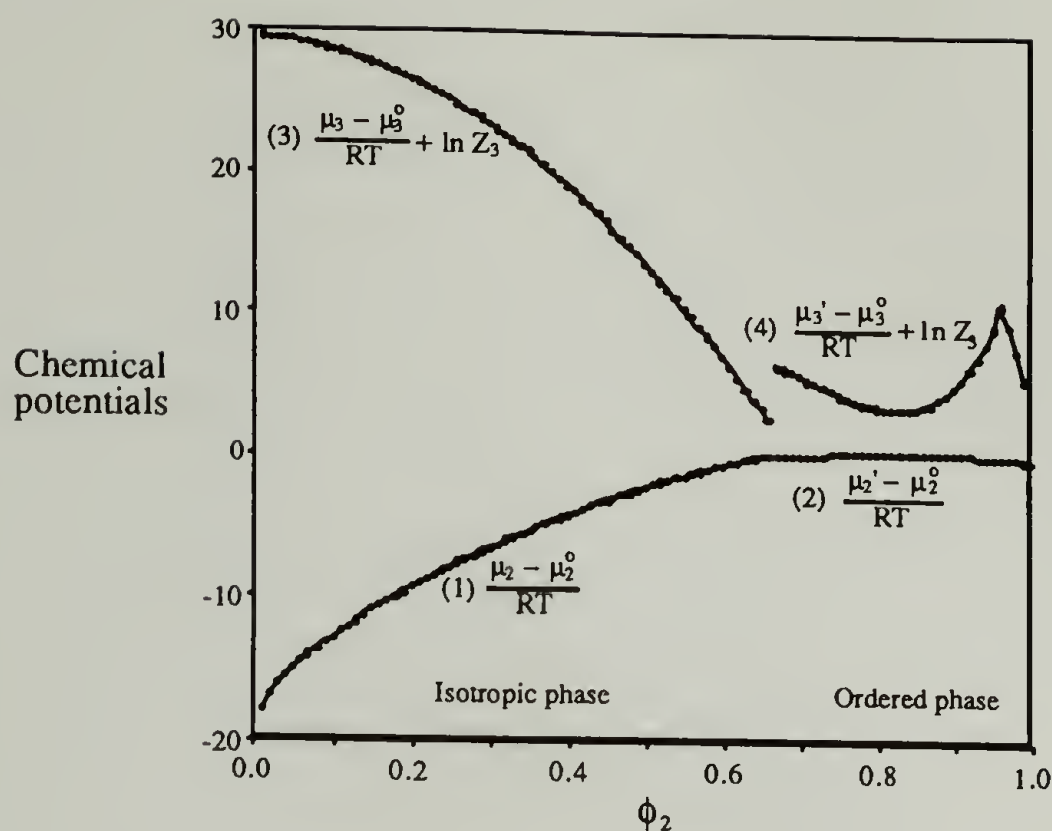


Figure 2.4 Simulated chemical potentials for the M24M/PPG model system by using Flory's rod-coil model; 1. Hard segments in the isotropic phase; 2. Hard segments in the anisotropic/ordered phase; 3. Soft segments in the isotropic phase; 4. Soft segments in the anisotropic phase.

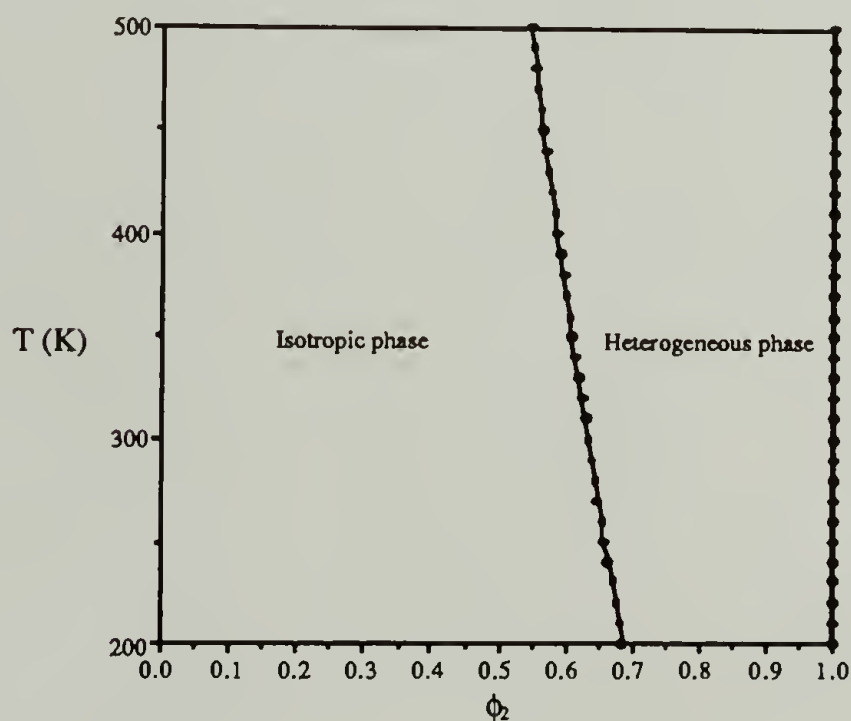


Figure 2.5 Simulated phase diagram for M24M/PPG-2000 model system.  $\phi_2$  is the number fraction of the hard segment subunits.

While this calculation successfully demonstrates the phase separation tendency for our model polyurethane with a negative  $\chi$ , the phase diagram indicates excessive phase mixing. For example, the calculation fails to predict phase separation for the M24M/PPG-2000 system ( $\phi_2 = 0.227$ ) at room temperatures when phase separated structures are known to occur. This is due to the fact that the  $\chi$  parameter used is inadequate to describe the enthalpic term for the ordered phase. As mentioned above, the  $\chi$  parameter is calculated by assuming random orientation for the chain segments. For the rigid hard segments in the hard segment rich domain, this approximation is incorrect. An obvious solution is to use an enthalpic expression which takes into consideration the relative hard segment orientation in this phase. In comparison to randomly oriented hard segments, the interactions between oriented segments are more specific and stronger and thus capable of shifting the phase boundary to lower values.

For a perfectly ordered state of hard segments,  $y = 1$ , and only varies in the isotropic phase reaching a maximum value of  $N_2$  for the completely disordered state. In Figure 2.4, the phase boundary is defined by the simultaneous solution of eqs.(2.7)-(2.11). If the solution for  $y$  is less than 1 for the perfectly ordered state, then  $y$  is taken to be 1. This is seen as the peak in curve 4. The chemical potentials for soft segments exhibit a large difference at the isotropic and anisotropic boundary because the phase with soft segments dispersed in the isotropic state is favorable. Conversely, for soft segments to be confined in the ordered phase is rather unfavorable. For hard segments, on the other hand, the crossover from a very imperfect ordered state to the completely random isotropic phase is smoother.

**D. Additional Considerations of Cohesive Energy of Hard Segments.** An interaction parameter,  $V$ , is introduced to describe the strong cohesive energy in the hard segment rich domain which further stabilizes these domains to

enhance phase separation. The enthalpic terms are derived from earlier studies on liquid crystalline polymers.<sup>32-34</sup> The modified expressions suitable for our system are shown below:

$$\frac{\mu'_2 - \mu_2^0}{RT} = \ln \left( \frac{\phi'_2}{N_2} \right) + \phi'_2 (y-1) + \phi'_3 N_2 \left( 1 - \frac{1}{N_3} \right) + 2 (1 - \ln y) - \left( \frac{\phi'_2 \langle P_2 \rangle}{\frac{RT}{V}} \right) \left( 1 - \frac{\phi'_2 \langle P_2 \rangle}{2} \right) \quad (2.12)$$

$$\frac{\mu'_3 - \mu_3^0}{RT} = \ln \left( \frac{\phi'_3}{N_3} \right) + \phi'_2 \left( \frac{N_3}{N_2} \right) (y-1) + \phi'_3 (N_3 - 1) + 2 \left( \frac{N_3}{y} \right) - \ln Z_3 + \frac{\phi_2'^2 \langle P_2 \rangle}{2 \left( \frac{RT N_2}{V} \right)} \quad (2.13)$$

with

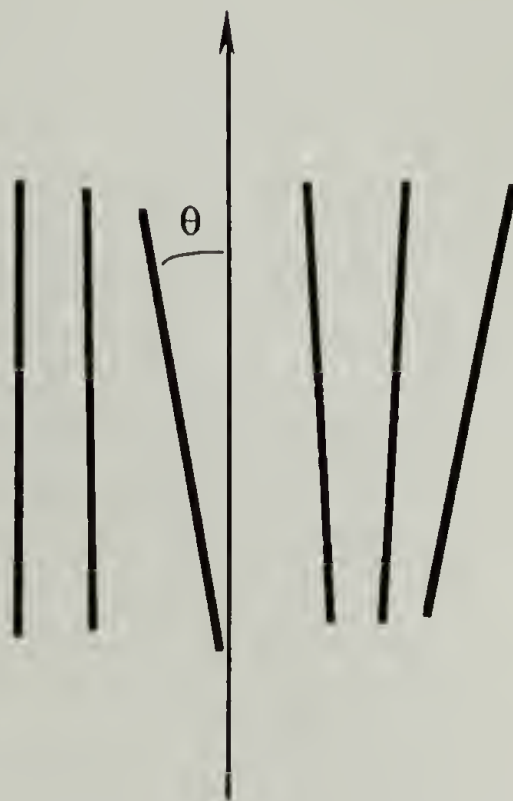
$$P_2 = \frac{1}{2} (3 \cos^2 \theta - 1) \quad (2.14)$$

$$y = N_2 \langle \sin \theta \rangle + 1 \quad (2.15)$$

$$\langle P_2 \rangle = 0.99972 - 0.9596 \left( \frac{RT}{V} \right) - 2.2413 \left( \frac{RT}{V} \right)^2 \quad (2.16)$$

where  $V$  is the cohesive energy term between hard segments packed in a parallel manner,  $P_2$  is the second-order Legendre polynomial,  $\langle P_2 \rangle$  is the order parameter, and  $\theta$  is the angle between the chain axis of one hard segment and the average orientational direction of the hard segments bundle (Figure 2.6).<sup>34</sup> In eqs.(2.12) and (2.13), following Flory's approach, the enthalpic terms of the ordered domains are determined only by hard/hard segment interactions while the soft/soft and soft/hard segment

interactions have been ignored. As described previously, coil penetration into hard segment rich domains is unlikely due to thermodynamic instability.



$$E(\cos \theta) = - V P_2(\cos \theta) \langle P_2 \rangle$$

Figure 2.6 Schematic drawing of the orientational order associated with hard segments.  $V$  is the Maier-Saupe interaction term between hard segments in the ordered phase.  $E(\cos\theta)$  is the mean cohesive energy associated with imperfect hard segment packing.  $\langle P_2 \rangle$  is the order parameter.

The interaction parameter,  $V$ , of two M24M segments has been approximated by using the average energy of 2 extremely different geometries. The first structure incorporates 2 molecules face-to-face thus minimizing the hydrogen bond contribution( 8.40 kcal/mol ), and a second geometry, with chains side-by-side with favorable hydrogen bonds(  $V = 21.46$  kcal/mol ). Based on our 2 calculations,  $V$  has been determined to be 15 kcal/mol for M24M, the average of the extreme values. The



V value has no relation to the  $W_{hh}$ , which is the average pair interaction between two subunits of the hard segment assuming no preferential orientation between them and that their contact points are randomly determined.  $W_{hh}$  is used for calculation of the  $\chi$  parameter in the isotropic phase while the V parameter is used for the ordered phase. The order parameter,  $\langle P_2 \rangle$ , in the ordered phase decreases with temperature. Eq.(2.16) is a sufficiently accurate approximation for  $RT/V < 0.1$ ,<sup>34</sup> which is typically the case. Phase diagrams of binary systems, including semi-rigid polymers, can be analyzed using such a formalism. We found that variation in the *coordination number*, Z, does not affect the phase diagrams calculated.

### 2.3 Results and Discussions

The re-calculated chemical potentials of hard segments in the two different phases at different temperatures are shown in Figure 2.7. Several points need to be emphasized:

- (1) For a sufficiently long coil and by solving eqs.(2.9)-(2.16), the only possible solution suggests the existence of a phase containing pure hard segments. Coils are quite unlikely to penetrate into the ordered phase decreasing the cohesive interactions between the hard segments and increasing their chemical potentials. The coil-rod interaction in the ordered phase and the existence of an interphase has been ignored.
- (2) As the ordered phase consists only of hard segments, based on Figure 2.7, the composition in the isotropic phase,  $\phi_2$ , can be determined by the condition

$$\mu_2(\phi_2) = \mu_2(\phi_2=1) \quad (2.17)$$

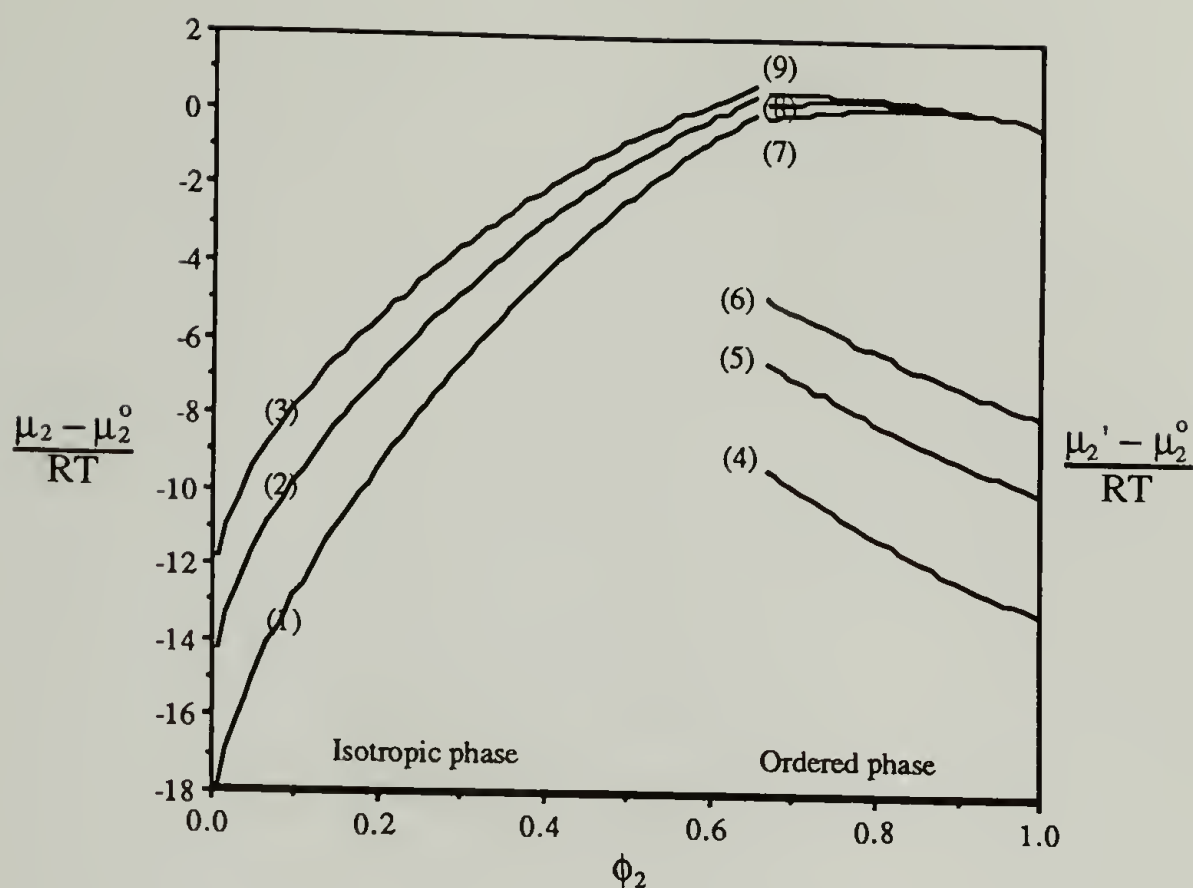


Figure 2.7 Simulated chemical potentials for the M24M/PPG-2000 system at different temperatures. For the isotropic phase at temperature of (1) 300K, (2) 400K, and (3) 500K; For the ordered phase at various temperatures (4) 300K, (5) 400K, and (6) 500K. The  $V$  interaction term is 15 kcal/mol; For the ordered phase at various temperatures; (7) 300K, (8) 400K, and (9) 500K, but without the Maier-Saupe modification.

Figure 2.8 shows the predicted phase diagram for M24M/PPG-2000 and M24M24M/PPG-2000 model systems.

If the overall hard segment concentration falls within the heterogeneous phase region, as in our case, it will phase separate into a pure hard segment phase coexisting with a soft segment rich phase. The composition is shown by curves 1 and 2 in Figure 2.8. By considering the orientation effect of the hard segments in the hard segment rich domain with the interaction term,  $V$ , the prediction of phase separation behavior in the

same temperature range has been improved in comparison to the result for the M24M/PPG-2000 system shown in Figure 2.4.

- (3) In this model, it is unnecessary for the ordered phase to form a crystalline structure to achieve phase separation. The driving force is the rigidity of the hard segment rather than crystallization. At best, most wide angle X-ray diffraction patterns obtained for polyurethanes exhibit relatively broad peaks.<sup>1,15,16</sup> Although crystallization of hard segments is not necessary for phase separation, it can enhance it.
- (4) If the hard and soft segments are chemically incompatible, i.e. with a positive  $\chi$ , curves 1-3 in Figure 2.7 will shift upwards, prohibiting phase mixing. Even for a negative  $\chi$ , phase separation can occur if the Maier-Saupe type interaction parameter,  $V$ , is sufficiently strong. Chemical incompatibility is not requisite for phase separation.
- (5) Details of the phase equilibrium diagram are determined by the temperature variation of the  $\chi$  term for the isotropic phase and the  $V$  term for the ordered phase.

#### *Effects of hard and soft segment size*

Phase diagrams for semi-rigid polyurethanes as a function of temperature, hard, and soft segments molecular weight are presented in Figures 2.8 and 2.9. Polyurethane phase behavior has been studied using most of the common characterization techniques such as mechanical spectroscopy, thermal analysis, electron microscopy, and infrared spectroscopy.<sup>1,2</sup> Even though it is accepted that phase separation occurs, only a few studies have quantitatively demonstrated the degree of phase separation and the exact parameters which can influence the phase behavior.<sup>13,14,35-38</sup> Quantitative interpretation of experimental data depends on the morphological model used, e. g. whether to include an interphase.<sup>36</sup> Temperature is known to have but a weak effect on the phase composition. There is no evidence that



the critical temperature lies within the 200-400 K temperature range.<sup>38,39</sup>

Furthermore, the measured composition of the 2 individual phases is very dependent on the techniques used.

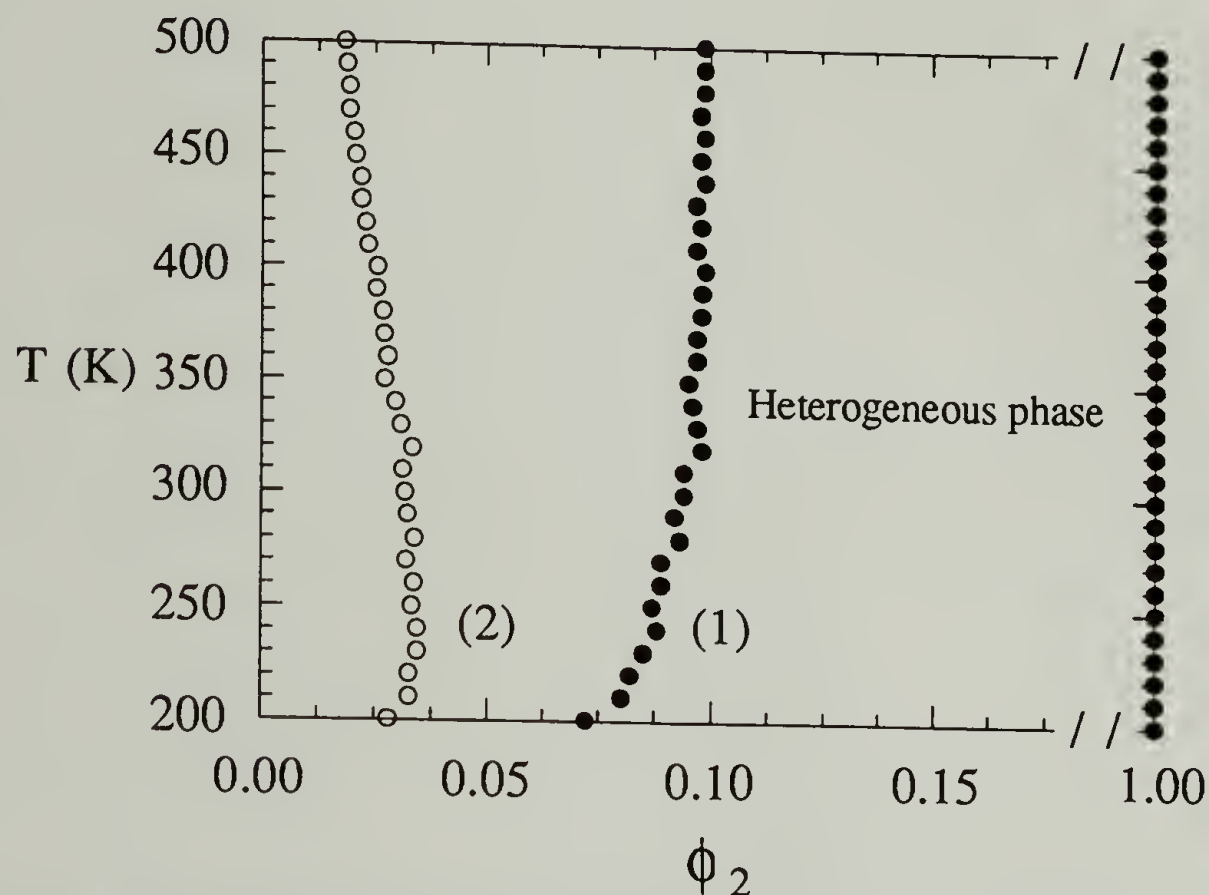


Figure 2.8 The effect of the hard segment length on the phase diagram. (1) M24M/PPG-2000 model system with  $V$  equal to 15 kcal/mol. (2) M24M24M/PPG-2000 model system with  $V$  equal to 24 kcal/mol.

Very limited experimental studies have been directed at polyurethanes incorporating hard segments containing diacetylene chain extenders, and only for polyurethanes containing short hard segments, usually 2 or 3 MDI units.<sup>15,40</sup> It is possible, however, to compare our calculations to similar systems containing more flexible hard segment chain extenders, butanediol (BD), for example. Even then, quantitative analyses are quite rare. One analysis of phase separated structure, more specifically a relatively pure hard segment rich domain coexisting with a soft segment rich domain mixed with hard segments, as well as an interphase, is based on scattering and changes in the glass transition temperature.<sup>36,38</sup> Other calculations utilize the association model



based on infrared results.<sup>39,19</sup> All of these studies show that the phase composition is virtually insensitive to temperature, at least in the range of interest. The generally accepted value of the degree of phase separation ranges from 30 to 90% for PPG-BD-MDI systems.<sup>36,37</sup>

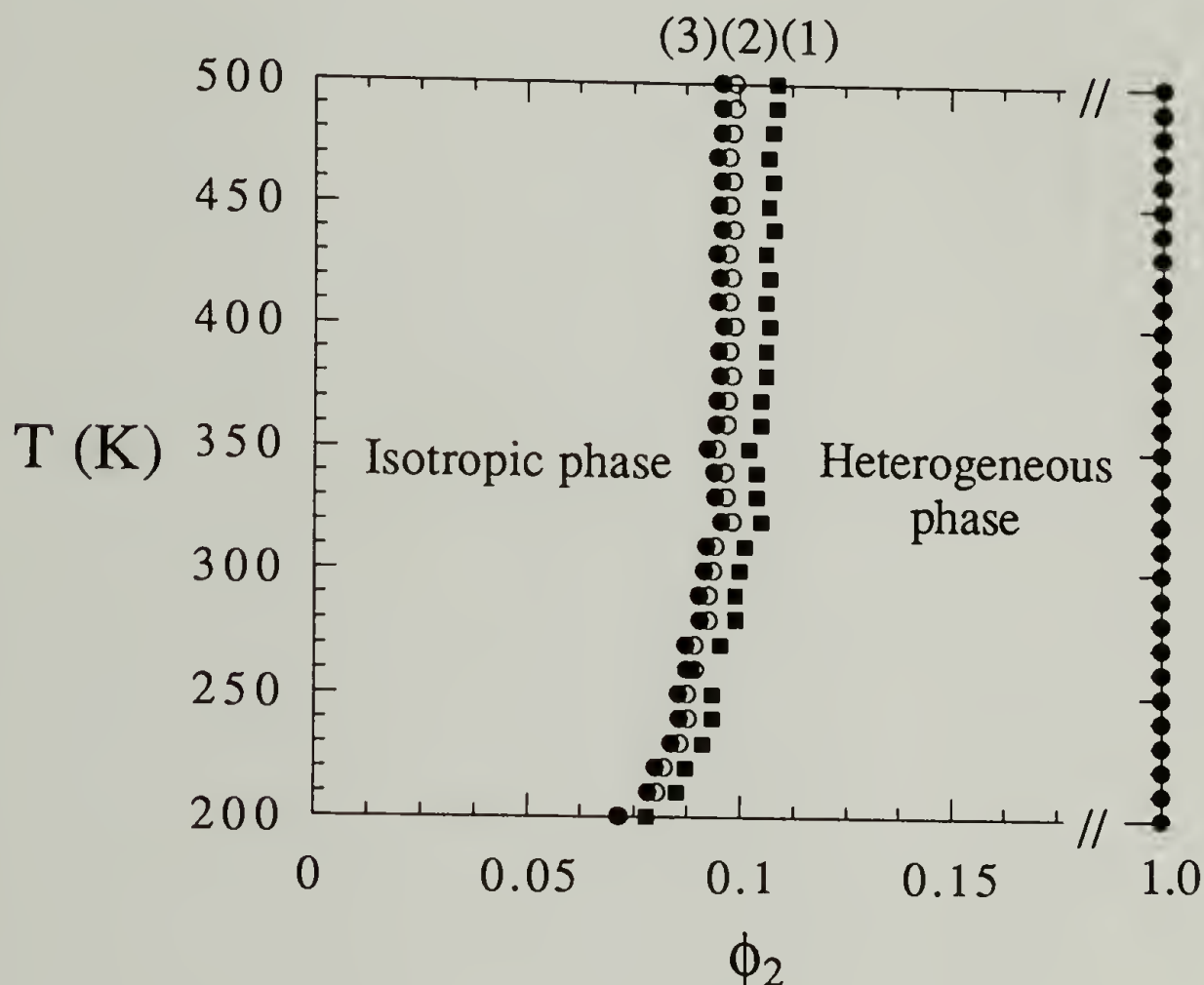


Figure 2.9 The effect of the soft segment length on the phase diagram. (1) M24M/PPG-1000; (2) M24M/PPG-2000; (3) M24M/PPG-3000. The Maier-Saupe  $V$  parameter is taken to be 15 kcal/mol for all cases.

For polyurethanes containing 30% hard segments, a system close to ours, the composition in hard segment rich domains is estimated to be 57% of hard segments by X-ray and 84% by DSC.<sup>36</sup> The purity of hard segment rich domain can never exceed 83% for longer hard segments by X-ray. NMR, however, shows that this domain can be virtually 100% hard segments for a model polyurethane with piperazine-based hard segment.<sup>13</sup> Thermal analysis data also indicate that with a change in hard segment

length from 3 to 4 MDI units, the purity of the hard segment rich domains increases significantly from 57% to 78%.<sup>36</sup> The composition of the soft segment rich phase is estimated to be about 10% to 30% of hard segments by weight using X-ray and about 20% to 28% by DSC.<sup>36</sup> Since, as previously noted, the exact phase composition determined by various experimental techniques differs considerably, simulation techniques in fact can provide a better understanding of phase composition in phase separated structures.

Our calculations are based on the model that hard segment rich domains are entirely pure hard segments. Our calculated results suggest that this phase coexists with another one containing both hard and soft segments. Generally speaking, our calculated results shown in Figures 2.8 and 2.9 show that longer hard segments or longer soft segments will cause lower hard segment concentration in the soft phase, as expected. From Figure 2.9, it is also possible to conclude that soft segment length has only a minor effect on phase composition. Conversely, hard segment length can significantly perturb phase composition. For polyurethanes containing 2 MDI units, we predict that soft segment domains contain approximately 10% of hard segments. This number decreases significantly to ~2.5 % when the hard segment length is increased to 3 MDI units (Figure 2.8). For polyurethanes containing 2 MDI units, changing PPG soft segment molecular weight from 1000 to 3000 does not significantly affect the phase diagram.

To quantitatively define the phase separated structure, it is most convenient to use the parameter associated with the fraction of overall hard segments in the hard segment rich domains,  $F_{HH}$ , which can be calculated using values derived from Figures 2.8 and 2.9.  $F_{HH}$  can be calculated using the following expression only with availability of the total number fraction of hard segment subunit in the whole system,  $\phi_{2T}$ , and the composition of the isotropic phase of the hard segment subunit.

$$F_{HH} = \frac{\phi_{2T} - \left( \frac{1 - \phi_{2T}}{1 - \phi_2} \right) \phi_2}{\phi_{2T}} \quad (2.18)$$

For our system, the  $\phi_{2T}$ 's are 0.227 and 0.320 for M24M/PPG-2000 and M24M24M/PPG-2000 respectively. The calculated temperature dependence of the phase separation for different hard segment lengths is summarized in Figure 2.10. Longer hard segments have higher  $F_{HH}$  values. Available DSC and X-ray experimental results at room temperature also show this trend.<sup>36</sup> The variation of  $F_{HH}$  values for different hard segment lengths, however, is not as large as our calculation which are based on semi-rigid diacetylene chain extenders (~65% for 2 MDI units and 95% for 3 MDI units). Previous experimental data using DSC indicate that  $F_{HH}$ 's for the more flexible BD chain extenders range from 30% (3 MDI units) to 89% (14 MDI units).<sup>36</sup>

This difference between predicted and experimental values derived from DSC may arise from inherent limitations associated with the thermal analysis technique. The degree of phase separation estimated by DSC is based on the  $T_g$  of the soft segments. Higher  $T_g$  values are usually correlated with lower degrees of phase separation.<sup>36</sup> It is, however, impossible to extract the exact phase composition from  $T_g$  changes as at least two factors contribute to changes in the  $T_g$  of polyurethane soft segments. First, the 'copolymer' effect due to the hard segments dissolved in the soft phase is the only contribution taken into account to calculate the phase composition.<sup>36</sup> Second, the 'crosslinking' effect associated with confinement of soft segment chain end by virtue of its connection to the phase separated hard domains will also increase  $T_g$ .<sup>41-43</sup> This effect is difficult to address quantitatively, however. Earlier measurements have, in fact, shown that it can be dominate.<sup>41-43</sup> In addition, our calculation for the diacetylene chain extender system involves a more rigid unit compared to butanediol chain extender. This factor could also influence the degree of phase separation.



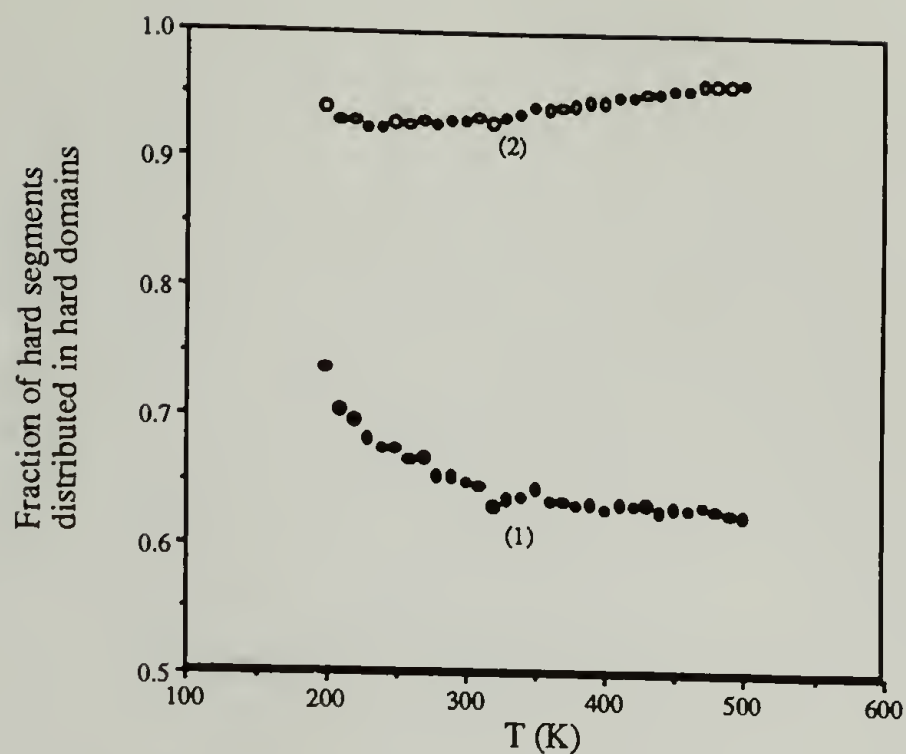


Figure 2.10 The effect of the hard segment length on the fraction of hard segments distributed in the hard segment rich domain,  $F_{HH}$ . (1) M24M/PPG-2000 model system with  $V$  equal to 15 kcal/mol; (2) M24M24M/PPG-2000 with  $V$  equals to 24 kcal/mol.

The effects of changing soft segment molecular weight are not clear. Although some thermal experiments measuring changes in  $T_g$  have been carried out for soft segments of different lengths, individual phase compositions have not been defined. Our calculated degree of phase separation for different soft segment lengths are summarized in Figure 2.11. We predict that samples containing longer soft segments have a lower degree of phase separation. Although the observed large decreases in  $T_g$  with increasing soft segment length might lead to the conclusion that phase separation increases with increasing soft segment length, such changes have been interpreted to arise from the crosslinking effect mentioned above.<sup>41-43</sup>



## Role of Various Secondary Forces

In our analysis, both the relative orientation of the hard segments and interchain interactions vary as a function of temperature. This is consistent with solid state NMR data obtained for the MDI-BD copolymer which showed that the BD chain extender librates within an angular deviation of 12 - 16 degrees in a temperature range from 62 to 83 °C.<sup>44</sup> At elevated temperatures, the degree of this librational motion for the hard segments increases causing  $\langle P_2 \rangle$  to decrease. This behavior is reflected by the apparent decrease of hydrogen bonds seen in infrared spectroscopy.<sup>15</sup> Variation in hydrogen bond strength with temperature for two M24M hard segments can be calculated utilizing simulation methods (eqs.(2.14) and (2.16)); results are presented in Figure 2.12.

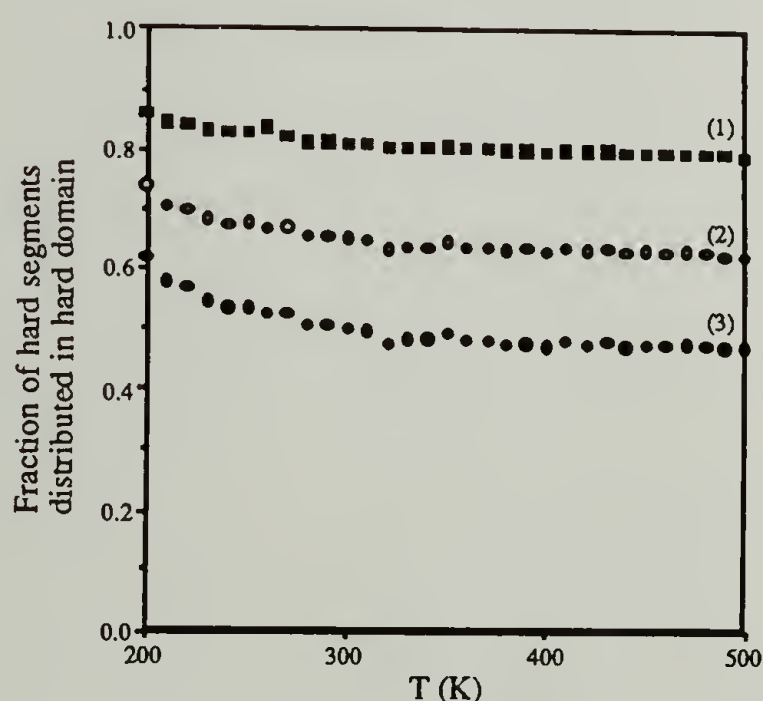


Figure 2.11 The effect of the soft segment length on the fraction of hard segments distributed in the hard segment rich domain,  $F_{HH}$ . (1) M24M/PPG-1000; (2) M24M/PPG-2000; (3) M24M/PPG-3000.  $V$  is taken to be 15 kcal/mol in all cases.

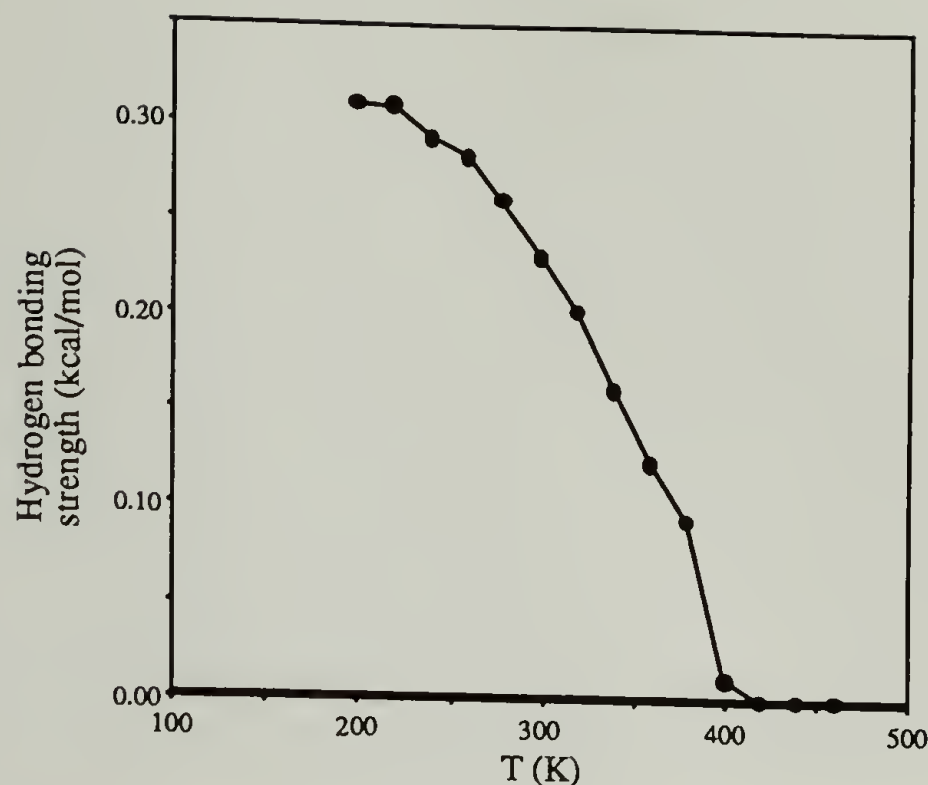


Figure 2.12 Simulated hydrogen bonding strength at different temperatures for two isolated M24M hard segments described by the Maier-Saupe model.

These results, consistent with experimental data,<sup>15</sup> are obtained for a simplified model since we assume that the entire hard segment librates as a rigid rod without considering the local functional group dynamics and segmental migrations. A new interpretation of infrared data is thus provided. The generally accepted explanation for the decrease in the amount of hydrogen bonds observed in infrared with increasing temperatures is attributed either to thermal expansion effects or increased phase mixing. We propose that an increase of hard segment libration can also possibly explain the reduction in the hydrogen bonded component with negligible contributions from phase mixing.

Hydrogen bonds are strong secondary forces, but of short range and highly directional.

Steric interactions between phenyl rings generally inhibit hydrogen bond formation.

Our simulation studies demonstrate that departures from the ideal linear state, even at very small angles, will significantly diminish the strength of the hydrogen bond.

Chemical immiscibility of the hard/soft segments has long been suggested as the most important factor in determination of polyurethane phase separation. More specifically, inter-urethane hydrogen bonds are regarded as stronger than hard/soft interactions, providing the driving force for phase separation. As mentioned in the Introduction, this hypothesis is inconsistent with spectroscopic data presented in the literature and illustrated as follows. The frequency of the infrared active N-H stretching band reflects the relative strength of the various possible hydrogen bonds between the hydrogen and other functional groups. It has been proposed that stronger hydrogen bonds are directly associated with larger shifts in the N-H stretching frequency relative to the free N-H vibration.<sup>8,9</sup> In polyurethanes, the free N-H stretching vibration is usually observed at  $3700\text{ cm}^{-1}$ . When hydrogen bonds to the ether oxygen, an N-H stretching vibration is observed at  $3290\text{ cm}^{-1}$ . In contrast, the N-H stretching associated with the inter-urethane hydrogen bond is observed at  $3350\text{ cm}^{-1}$ .<sup>4,8</sup> These results suggest that inter-urethane hydrogen bonds are not stronger than those between N-H and ether oxygen. Recently, *ab initio* calculations along with associated experimental studies have provided similar results.<sup>9-11</sup> In addition, other studies have concluded that the interaction parameter can be negative for phase separated polyurethanes.<sup>6,7</sup> More studies are required to reach definitive conclusions about the relative strength of these hydrogen bonds.

## 2.4 Conclusions

This simulation study suggests that phase separation behavior in polyurethanes is due to the chain rigidity effect of the hard segments. Strong cohesive interactions between hard segments if packed in favorable orientations will make the hard segments separate into a hard segment rich phase coexisting with a soft segment rich phase. In



many cases, with sufficiently long segment length, crystallization of hard segments further stabilize the phase separated structures. As expected, hard segment molecular weight greatly influences phase separation behavior. It is clear that samples containing longer hard segments exhibit a higher degree of phase separation. Although calculated values did not match experiments, the predicted trend was indeed verified. On the other hand, the effects of changing soft segment molecular weight are much more subtle. We predict that samples containing longer soft segments should contain a lower degree of phase separation, a suggestion consistent with infrared spectroscopic results. It is also our opinion that the thermal technique, particularly measurement of changes in  $T_g$ , cannot be used to measure phase composition of polyurethanes.

By deconvoluting the overall calculated internal energy of the system, the contribution of hydrogen bonding to the interaction term has been calculated to be <17% with the remainder arising from van der Waals forces. Even though the strength of each hydrogen bonding pair is stronger than van der Waals forces, the number of van der Waals interactions is much greater than the hydrogen-bonding contribution. Indeed, as mentioned before, studies have shown that polyurethanes without hydrogen bonds can also phase separate. Infrared spectroscopy is often cited to support the amount and extent of phase separation. For example, the relative intensity of hydrogen bonded free carbonyl stretching versus the hydrogen bonded component has been noted as primary evidence. Based on the present analysis, perhaps these spectroscopic analyses have provided only the characteristics of phase separated structures and cannot explain the driving force for phase separation. This simulation study provides an opportunity for further studies in this area.



## References

- (1) Petrovic, Z.S. ; Ferguson, J. *Prog. Polym. Sci.* **1991**, *16*, 695, and references therein.
- (2) Hepburn, C. *Polyurethane elastomers*, Applied Science Publishers, London, **1982**.
- (3) Culbertson, B.M. (Ed) *Multiphase Macromolecular Systems*, Plenum Publishing Corporation, New York, **1989**.
- (4) Lee, H.S. ; Hsu, S.L. ; *Macromolecules*, **1989**, *22*, 1100.
- (5) Chu, B.; Gao, T. ; Li, Y. ; Wang, J.; Desper, C.R. ; Byrne, C.A., *Macromolecules*, **1992**, *25*, 5724.
- (6) Hwang, K.K.S. ; Hemker, D.J. ; Cooper, S.L. *Macromolecules*, **1984**, *17*, 307.
- (7) Hwang, K.K.S. ; Lin, S.B.; Tsay, S.Y.; Cooper, S.L. *Polymer* , **1984**, *25*, 947.
- (8) Lee, H.S. ; Wang, Y.K.; Hsu, S.L. *Macromolecules*, **1987**, *20*, 2089.
- (9) Bandekar, J. ; Klima, S. *J. Molec. Struct.*, **1991**, *263*, 45.
- (10) Sun, H. *Macromolecules*, **1993**, *26* , 5924.
- (11) Bandekar, J.; Klima, S. *Spectrochim. Acta*, **1992**, *48A*, 1363.
- (12) Harrell, L.L., Jr. *Macromolecules*, **1969**, *2*, 607.
- (13) Kornfield, J.A.; Spiess, H.W.; Nefzger, H.; Eisenbach, C.D. *Macromolecules*, **1991**, *24*, 4787.
- (14) Christenson, C.P.; Harthcock, M.A.; Meadows, M.D.; Spell, H.L.; Howard, W.L.; Creswick, M.W.; Guerra, R.E.; Turner, R.B. *J. Polym. Sci., Polym. Phys. Ed.*, **1986**, *24*, 1401.
- (15) Rubner, M.F. *Macromolecules*, **1986**, *19*, 2114.
- (16) Blackwell, J.; Lee, C.D. *J. Polym. Sci., Polym. Phys. Ed.*, **1983**, *21*, 2169.
- (17) Paul, D.R.; Newman, S. (Eds) *Polymer Blends*, Academic Press, New York, **1978**.
- (18) Utracki, L.A. *Polymer Alloys and Blends*, Hanser Publishers, Munich, **1989**.
- (19) Coleman, M.M.; Graf, J.F.; Painter, P.C. *Specific Interactions and the Miscibility of Polymer Blends*, Technomic Publishing Co., Lancaster, **1991**.
- (20) Flory, P.J.; Abe, A. *Macromolecules*, **1978**, *11*, 1119.
- (21) Flory, P.J.; Ronca, G. *Mol. Cryst. Liq. Cryst.*, **1979**, *54*, 311.

- (22) Hølyst, R.; Cshick, M. *J Chem. Phys.*, **1992**, 96, 721; **1992**, 96, 730.
- (23) Liu, A.J.; Fredrickson, G.H. *Macromolecules*, **1992**, 25, 5551; **1993**, 26, 2817.
- (24) Fan, C.F.; Olafson, B.D.; Blanco, M.; Hsu, S.L. *Macromolecules*, **1992**, 25, 3667.
- (25) Flory, P.J. *Adv. Polym. Sci.*, **1984**, 59, 1, and references therein.
- (26) Stouch, T.R.; Jurs, P.C. *J. Chem. Inf. Comput. Sci.*, **1986**, 26, 4.
- (27) Mayo, S.L.; Olafson, B.D.; Goddard, W.A.,III *J. Phys. Chem.*, **1990**, 94, 8897.
- (28) Lu, X.; Weiss, R.A. *Macromolecules*, **1992**, 25, 3242.
- (29) Flory, P.J. *Proc. Royal Soc., London*, **1956**, A234, 73.
- (30) Matheson, R.R.,Jr.; Flory, P.J. *J. Chem. Phys.*, **1980**, 73, 6327.
- (31) Flory, P.J. *Macromolecules*, **1978**, 11, 1138.
- (32) Warner, M.; Flory, P.J. *J. Chem. Phys.*, **1980**, 73, 6327.
- (33) Maier, W.; Saupe, A.Z. *Naturforschg.*, **1959**, 14A, 882 ; **1960**, 15A, 287.
- (34) Priestley, E.B.; Wojtowicz, P.J.; Sheng, P. *Introduction to Liquid Crystals*, Plenum Press, NY and London, **1975**, Chap 3.
- (35) Koberstein, J.T.; Galambos, A.F.; Leung, L.M. *Macromolecules*, **1992**, 25, 6195.
- (36) Koberstein, J.T.; Leung, L.M. *Macromolecules*, **1992**, 25, 6205.
- (37) Dumais, J.J.; Jelinski, L.W.; Leung, L.M.; Gancarz, I.; Galambos, A.; Koberstein, J.T. *Macromolecules*, **1985**, 18,116.
- (38) Leung, L.M.; Koberstein, J.T. *Macromolecules*, **1986**, 19, 706.
- (39) Hu, J.; Park, Y.; Painter, P.C.; Coleman, M.M. *Polym. Prepr. (Am. Chem. Soc. , Div. Polym. Chem.)* **1988**, 29(1), 321.
- (40) Hu, X.; Stanford, J.L.; Day, R.J.; Young, R.J. *Macromolecules*, **1992**, 25, 672.
- (41) Andrady, A.L.; Sefcik, M.D. *J. Polym. Sci., Polym. Phys. Ed.*, **1983**, 21, 2453.
- (42) Feger, C.; MacKnight, W.J. *Macromolecules*, **1985**, 18, 280.
- (43) Petrovic, Z.S.; Javni, I. *J. Polym. Sci., Polym. Phys. Ed.*, **1989**, 27, 545.

- (44) Kintarnar, A.; Jelinski, L.W.; Gancarz, I.; Koberstein, J.T. *Macromolecules*, **1986**, *19*, 1876.

## CHAPTER 3

### A SPECTROSCOPIC STUDY AND THERMAL ANALYSIS OF PHASE SEPARATION BEHAVIOR IN DIACETYLENE-CONTAINING MODEL POLYURETHANES

#### 3.1 Introduction

Segmented polyurethane elastomers are multiblock copolymers consisting of soft segments and hard segments. It is generally agreed that these copolymers undergo microphase separation resulting in hard-segment-rich domains (hard domains), soft-segment-rich domains (soft domains) and interfaces between them.<sup>1,2</sup> The formation of hard domains as the physical crosslinking points between flexible soft segments are responsible for its thermoplastic elastomer feature. Despite of the similarity to the chemical crosslinking elastomers, their physical properties deviate widely from each other due to the distortion of hard domains under mechanical deformation which is related to the morphological features such as degree of phase separation, size and perfection of hard domains, and the interfaces. It is essential, therefore, to understand the controlling factors associated with the phase separation behavior.

Various models have been suggested but a consentaneous interpretation, which may even not exist, is still absent. Chemical immiscibility, reflected by the substantial Flory-Huggins  $\chi$  parameter, of hard/soft segments due to the strong interurethane hydrogen-bondings between hard segments is one of the most popular picture.<sup>1,2</sup> Experimental<sup>3,4</sup> as well as theoretical<sup>5</sup> study, nevertheless; indicate that it is not a necessary condition. Furthermore, the role of interurethane hydrogen-bondings between hard segments is found



to be overrated.<sup>5-9</sup> On the other hand, crystallization of hard segments is another possible driving force. A critical chain length model, for example, was proposed along with this point of view.<sup>10</sup> But again experimental evidences<sup>11,12</sup> clearly show that crystallization of hard segments is still not necessary for phase separated structure. Kinetic argument associated with the hard-segment mobility is an alternative model.<sup>13,14</sup> Hard segments with more flexibility is believed to result in higher phase separation than the rigid ones according to this hypothesis and the experimental result.<sup>14</sup> However, the evaluation of degree of phase separation based on the hard-domain crystallinity together with the glass transition temperature of soft segments is disputable in those study.

In our previous study, we proposed that the chain rigidity of hard segments can influence phase separation behavior significantly.<sup>5</sup> Using molecular simulation technique, we showed that phase separation can be achieved when chains are rigid even when crystallization or chemical immiscibility are lacking. This contribution is complementary to other factors and sometimes can be the predominant one. The influence of hard/soft segment length on the phase separation behavior has been calculated with this rigid rod model. In this work, we would like to compare experimental results with those predictions.

Several hard domain models have been suggested depending on the systems,<sup>2,5,15-22</sup> but the hard/soft segment length effect on hard-domain packing for poorly crystallized systems has rarely been investigated. The cross-polymerization reaction of diacetylenes can be used as a probe for this aspect. It is well known that diacetylenes can undergo cross-polymerization and its reactivity is very sensitive to the local ordering.<sup>23-25</sup> This unique feature has been utilized to study the ordering in the hard domains for diacetylene-containing polyurethanes<sup>12,21,22</sup>. With the same approach, we performed a systematical comparison of the hard/soft segment length effect on the hard-domain packing for various diacetylene-containing polyurethane elastomers.

## 3.2 Experimental Section

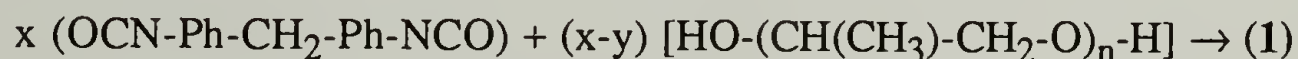
### A. Synthesis of Diacetylene-Containing Segmented Polyurethane Elastomers.

**1. Purification of Reactants.** 4,4'-methylenebis(phenyl isocyanate), MDI (Eastman Kodak), was vacuum distilled at 120°C (10  $\mu$ m) and stored under dry argon at -20°C. 2,4-Hexadiyne-1,6-diol (Fluka) was recrystallized from toluene at about 70°C and vacuum dried for 4 h prior to use. Monodisperse poly(propylene glycols), PPG (Scientific Polymer Products), with molecular weights of 1000, 2000 and 3000 were dried under vacuum (1 mm) at 80°C for 3 days to remove water. N,N-Dimethylformamide, DMF (Aldrich), was dried by Linde type 4Å molecular sieves followed by distillation under reduced pressure. All of the reagents were stored under dry argon.

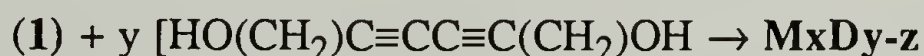
**2. Synthesis of the Linear Diacetylene-Containing Segmented Polyurethane Elastomers via Two-Step Method.** A series of diacetylene-containing segmented polyurethane elastomers with various average lengths in the hard/soft segments were prepared by the same procedure (Scheme I)

#### Scheme I

Step 1



Step 2



where  $z = 1000, 2000, \text{ and } 3000$  for  $n = 17, 34, \text{ and } 52$ , respectively.

To a three-neck round-bottom flask equipped with a magnetic stirrer and nitrogen purge was added the required amounts of solid MDI. The MDI was stirred and degased under reduced pressure at 50°C for 5 min then the system was purged by argon. PPG with required weight was added into the flask and stirred with the molten MDI. System was degased for 5 min at 50°C again then purged by argon with vacuum-line techniques. Reaction proceeded at 85°C for 2 h under inert atmosphere. The resultant solution was then cooled to room temperature. A 2% solution of 2,4-hexadiyne-1,6-diol in DMF was transferred into the system by cannulation. Reaction continued at 50°C for 1 h then at 25°C for another hour. When the reaction was complete, the mixture was precipitated and washed in deionized water for 12 h. Finally, the products were vacuum dried for 48 h at room temperature under dark condition. All the products were stored under inert atmosphere at -20°C in the dark to prevent cross-polymerization. The compositions and the physical characteristics of these copolymer are summarized in Table 3.1. For all of the copolymerizations, the stoichiometric equivalence of NCO and OH groups associated with MDI, PPG and 2,4-hexadiyne-1,6-diol are maintained. In this work, MxDy-z stands for the polyurethane with x units of MDI's and y units of diacetylenes in the hard segment, while z is the molecular weight of soft segment.

## **B. Characterization of Copolymers.**

**1. Molecular Weight Determinations.** Molecular weights and their distributions were determined by gel permeation chromatography (GPC). Results are listed in Table 3.2. A Waters Model 590 equipped with Waters Model 730 Data Module and two PL-Gel Mixed C columns was used. The eluent was THF at a flow rate of 1mL/min at 30.0°C. Samples were detected with a Waters 410 Differential Refractometer. The GPC was calibrated by polystyrene standards of known molecular weights. Universal calibration for the hydrodynamic volume effect, however, had not been conducted,



therefore; the molecular weights listed in Table II are more useful for comparative purposes rather than as absolute values. The measured molecular weights and their polydispersities are within the range for typical polyurethane elastomers<sup>11,12,19</sup> so the differences in properties of these materials cannot be attributed to the molecular weight effect.

Table 3.1 Characteristics of As-Prepared Segmented Diacetylene-Containing Polyurethane Elastomers.

sample	hard segment <sup>a</sup> (wt%)	physical state
M2D1-1000	38	dry elastomer
M2D1-2000	23	sticky elastomer
M2D1-3000	17	sticky elastomer
M3D2-2000	33	dry elastomer
M5D4-2000	46	dry elastomer

a. MDI+diacetylene.

Table 3.2 Molecular Weights and Molecular Weight Distributions of As-Prepared Segmented Diacetylene-Containing Polyurethane Elastomers.

sample	$\bar{M}_n$	$\bar{M}_w$	$\bar{M}_w/\bar{M}_n$
M2D1-1000	14,472	31,172	2.15
M2D1-2000	18,585	42,002	2.26
M2D1-3000	20,803	44,102	2.12
M3D2-2000	15,364	34,571	2.25
M5D4-2000	15,277	36,207	2.37



**2. Thermal Analysis.** Thermogravimetric analysis (TGA) was carried out using Perkin Elmer -7, purged with nitrogen. Samples of about 15 mg were used for each run. The heating rate was 20°C/min from room temperature to 450°C. For all of the samples the onset of gradual weight loss started at about 230°C then followed by a dramatic drop at about 370°C. Differential scanning calorimetry (DSC) was performed with a TA Instruments 2910 from -100°C to 300°C at 10°C/min, purged with nitrogen. The temperature was calibrated at -87°C and 156.6°C by cyclohexane and indium. 20 mg and 10 mg samples were used for the glass transition temperature ( $T_g$ ) and the melting point ( $T_m$ ) together with the thermal cross-polymerization study, respectively. Glass transition temperatures were determined by inflection points of the step change in the thermograms. No distinct endothermic peaks corresponding to the melting of hard domains had been observed for all the samples by DSC below 150°C.

**3. Infrared Spectroscopy.** Infrared spectra were recorded on a IBM IR 38 Fourier transform infrared spectrophotometer (FTIR) equipped with a deuterated triglycine sulfate (DTGS) detector. Generally, 200 scans were collected at 2 cm<sup>-1</sup> resolution. Heating experiments from 30°C to 150°C were performed with a heating block which can be controlled to within 1°C using an Omega temperature controller and a copper-constantan thermocouple sensor. The equilibrium time for each temperature range is 15 min for 30-50°C, 10 min for 60-80°C, and 5 min for above 80°C, respectively. Degree of phase separations were determined by the relative heights of the two Amide I bands in 1700-1740 cm<sup>-1</sup> region. Inherent extinction coefficients for these two bands were taken to be the same.

**4. Raman Spectroscopy.** Raman spectra were obtained on a Bruker 88 Fourier transform Raman bench (FT-Raman) excited by Nd:Yag laser (1064 nm) in the near-infrared region. Incident laser power was maintained at 300mW. Typically, 2000

scans were coadded to achieve an acceptable single-to-noise ratio. The excitation/collection geometry was  $180^\circ$  and the spectral resolution was  $4\text{ cm}^{-1}$ . Because of the long wavelength for the excitation laser used in the FT-Raman, fluorescence-free spectra were obtained even for the dark-purple, cross-polymerized samples which were prepared by heating the as-prepared copolymers at  $100^\circ\text{C}$  for 9 h. There was no indication of any weight loss for all of the samples measured by TGA under similar conditions.

### 3.3 Results and Discussion

**1. Thermal Analysis.** Glass transition temperatures and the corresponding heat capacity jumps, together with the thermograms of the as-prepared samples are shown in Table 3.3 and Figure 3.1, respectively.

Table 3.3 Thermal Properties (DSC) of As-Prepared Segmented Diacetylene-Containing Polyurethane Elastomers.

sample	$T_g$ ( $^\circ\text{C}$ ) <sup>a</sup>	$T_m$ ( $^\circ\text{C}$ ) <sup>b</sup>	$\Delta C_p/(\Delta C_p^\circ W_s)$ (%) <sup>c</sup>	$T_{\text{exo}}$ ( $^\circ\text{C}$ ) <sup>d</sup>	relative area of exotherm <sup>e</sup>
M2D1-1000	-12.30	none	89.9	196	1.12
M2D1-2000	-42.78	none	93.2	209	1.00
M2D1-3000	-54.70	none (75)	96.2	217	0.81
M3D2-2000	-39.05	none	89.6	189	1.06
M5D4-2000	-35.11	none	80.7	182	1.24

a. Determined by the inflection point.

b. Value in parentheses represents a weak endotherm.

c.  $\Delta C_p$ ,  $W_s$  and  $\Delta C_p^\circ$  are the heat capacity jump for the polyurethane elastomers at the glass transition temperature of soft segment, the weight fraction of the soft segment in the elastomer, and the heat capacity jump for the uncrosslinked neat soft segment at its  $T_g$ , respectively

d. Peak position of exotherm.

e. Area under the onset of exotherm to its peak position. Normalized by the area of M2D1-2000.

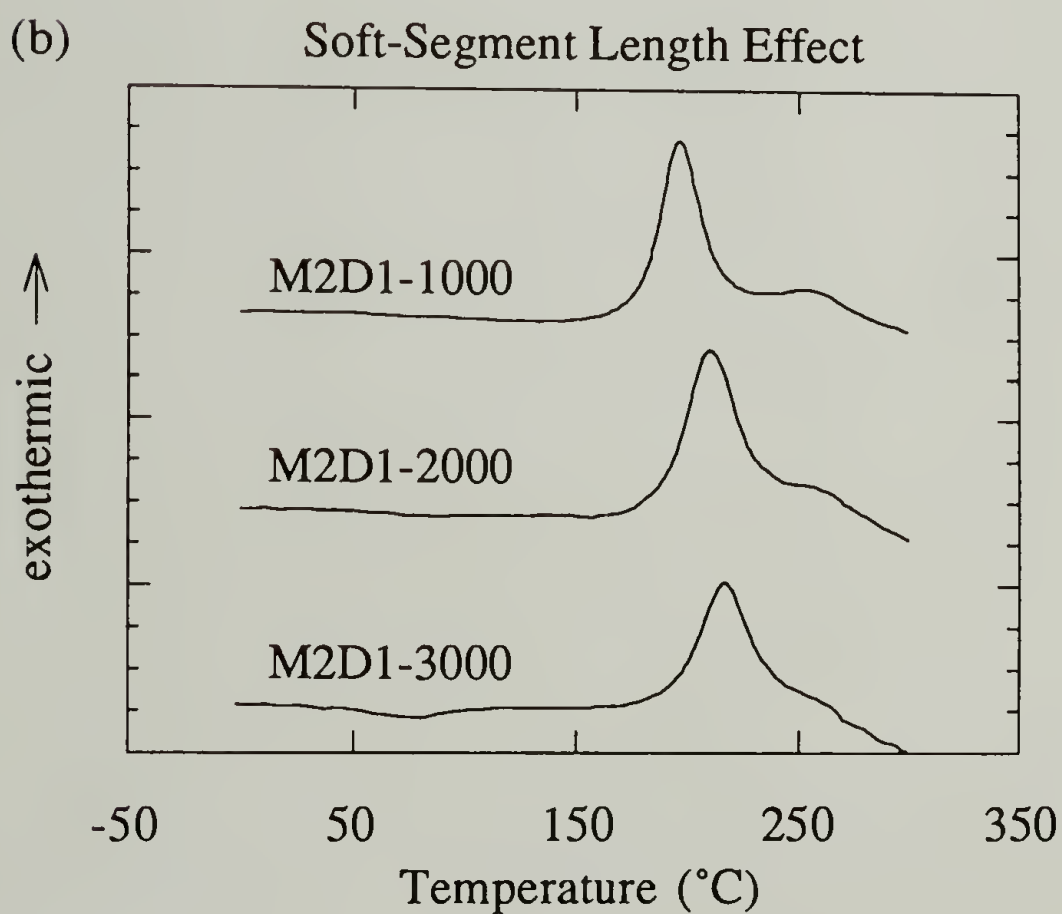
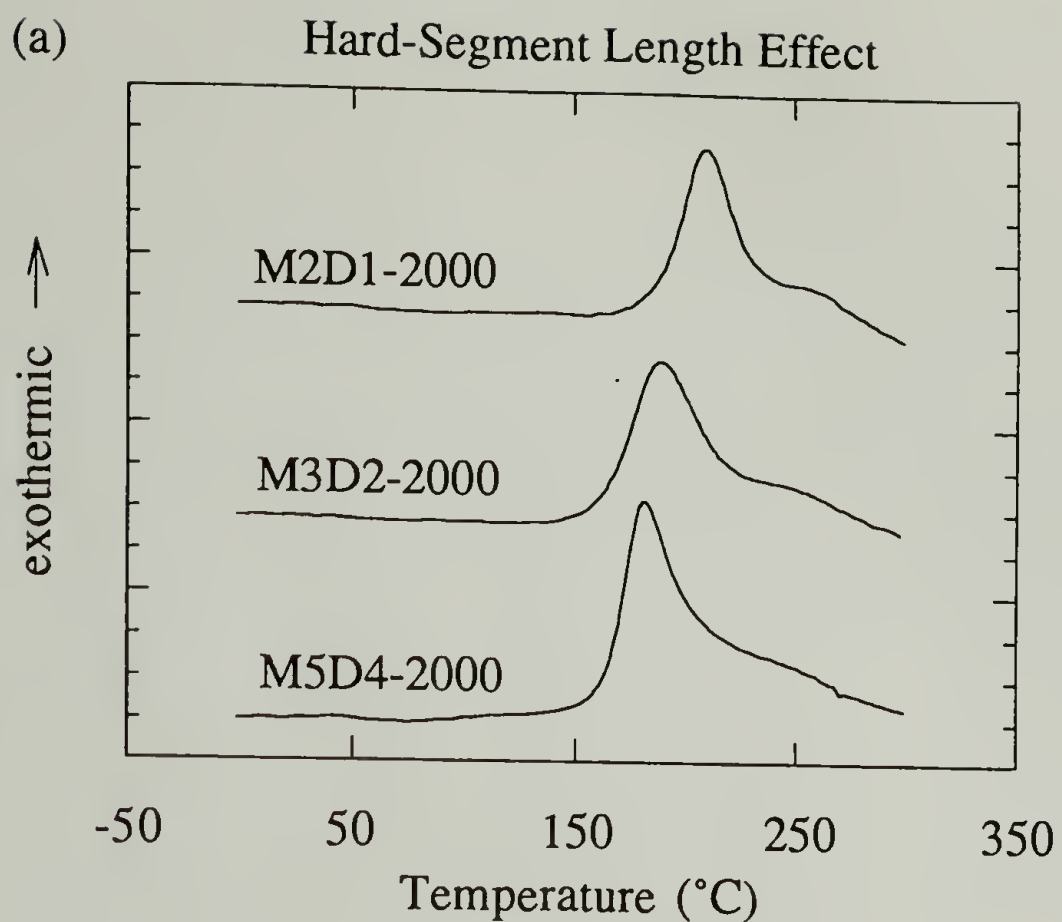


Figure 3.1 DSC traces for as-prepared diacetylene-containing polyurethanes : (a) Hard-segment length effect, and (b) soft-segment length effect. All of the traces have been normalized to the unit mass of hard-segment.

The absence of melting endotherm for all of our samples is not unusual compared with other phase-separated polyurethanes.<sup>11,12,19</sup> It is known that steric hindrance associated with the MDI units prohibits the crystallization in hard domains. Notwithstanding this scarcity of three dimensional long range ordering, the existence of local ordering in hard domains is clearly manifested by their capability of undergoing cross-polymerization as reflected by the exothermic peaks in Figure 3.1. The solid state topochemical cross-polymerization of diacetylenes is one of the most well characterized reaction<sup>23-26</sup>. In the monomer matrix, cross-polymerization proceeds by successive tilting of diacetylene segments until they approach each other within a distance  $R \leq 4\text{\AA}$  (Figure 3.2).

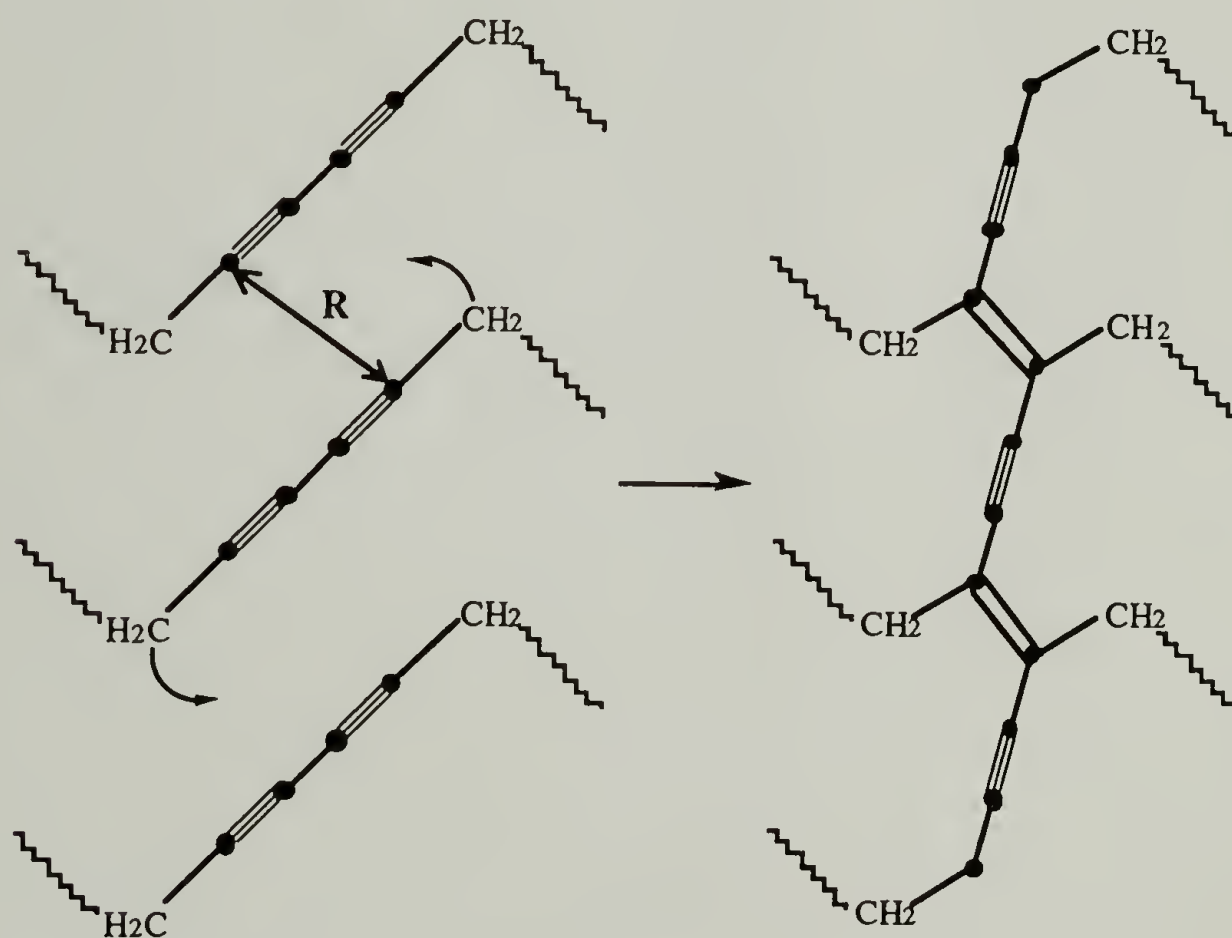


Figure 3.2 Schematic representation of the cross-polymerization of diacetylenes : Tilting of diacetylene units so as to reach each other by  $R \leq 4\text{\AA}$  is required to proceed this reaction.



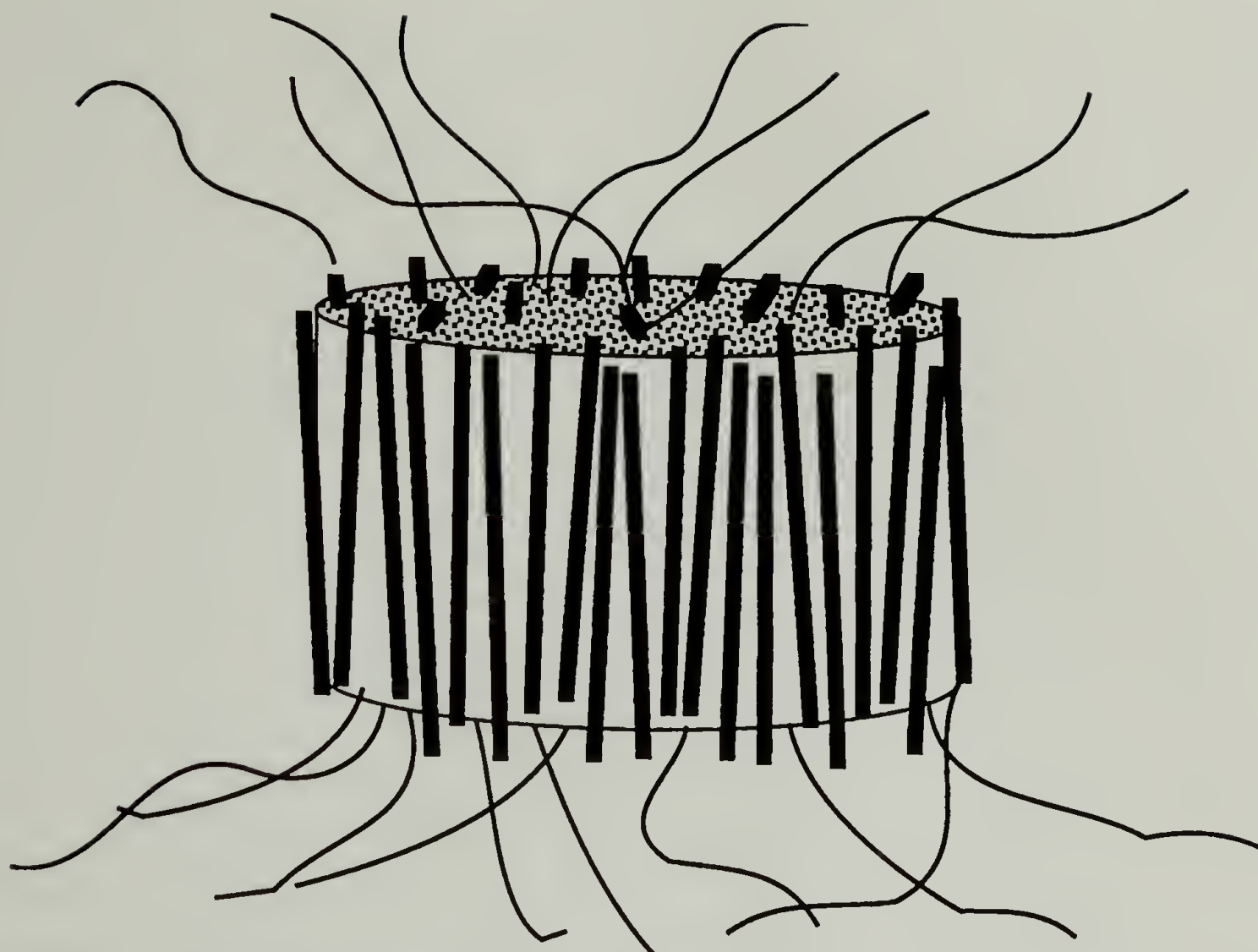


Figure 3.3 Schematic representation of the non-crystalline hard-domain structure proposed by our previous study : The occurrence of phase separation and local ordering in the hard domains are attributed to the chain rigidity of hard segments. The ordering is a function of cohesive energy between hard segments and the temperatures. The solid rods represent hard segments while the curves represent soft segments.

The required activation energy for the rotational, and sometimes translational, motion is provided by thermal treatment, photoradiation, or by high-energy radiation. The reactivity is controlled by the packing of monomers instead of the chemical nature of substituents. In spite of the fact that most documented reactions were conducted by monomer single-crystals, the cross-polymerization can also be accomplished in other imperfectly organized phases; for example, as in Langmuir-Blodgett films<sup>27</sup>, in surfactants<sup>28</sup>, in thermotropic liquid-crystals<sup>29</sup> or in others<sup>12,19,22</sup>. Consequently, there is no contradiction between the non-crystalline nature of hard domains and their cross-polymerizing ability. In our

previous study, we proposed a morphological model for the phase-separated structure of non-crystalline polyurethanes<sup>5</sup> The driving force, in this case, can be attributed to the chain rigidity of hard segments and to a varying degree local ordering can be obtained (Figure 3.3). Our DSC result successfully verifies this picture. Furthermore, it also clearly shows the inadequacy by regarding hard-domain crystallinity as a measure of the degree of phase separation.

Additionally, Figure 3.1 reveals that the exothermic peak position depends on hard/soft segment lengths. Polyurethanes with longer hard segment or shorter soft segment exhibit lower exothermic peaks. Even though this result demonstrates that hard/soft segment lengths do affect the hard-domain packing, it is difficult to conjecture their relationship by the DSC alone. Spectroscopy, on the other hand, can provide more information about this aspect .

As is quite well-known, DSC is frequently used to evaluate the phase composition as well as the degree of phase separation of polyurethane elastomers in many cases.<sup>1,2,30-32</sup> The degree of phase separation is defined as the fraction of hard segments dispersed in the hard domains. The associated methodology is to use Fox equation, or its modified form, together with the heat capacity jump to calculate the phase composition. Nevertheless, phase compositions remain inaccessible without taking explicitly into account the crosslinking effect of soft segments. It has been documented that the confinement of polymer chain ends will dramatically change its glass transition temperature<sup>33,34</sup> and the heat capacity jump<sup>33-35</sup> (crosslinking effect). For instance, the glass transition temperatures of crosslinked poly(propylene glycols) deviate from their linear forms by 56.15°C and 27.4°C for molecular weight 1000 and 3000, respectively.<sup>33</sup> Since the soft segments in phase-separated structure possess similar chain-confinement behavior, the applicability of thermal analysis for this purpose deserves more elaborate consideration; for example, it is inadequate to conclude that longer soft segments exhibit higher degree of

phase separation according to their lower  $T_g$ 's and higher heat capacity jump values (Table 3.3). On the other hand, even if quantitative evaluation of phase compositions is not feasible by DSC, comparison on the relative degree of phase separation for various hard-segment lengths based on the same soft-segment length is still possible. From the  $T_g$ 's and heat capacity jump values listed in Table 3.3, we can conclude that longer hard-segment will introduce higher degree of phase separation. Finally, our previous calculation predicted that longer soft-segment should generate a lower degree of phase separation, which is contradictory to the intuitive judgement from the DSC data (Table 3.3). Our prediction has been confirmed by spectroscopic results shown as follows.

**2. Infrared Analysis.** It is well accepted that free carbonyl groups have higher stretching frequency ( $\sim 1735\text{ cm}^{-1}$ ) than the hydrogen-bonded ones ( $\sim 1700\text{ cm}^{-1}$ ).<sup>8,36</sup> For our systems, only hard segments possess carbonyl groups which can bond to the N-H groups of other hard segments. In other word, presumably hard segments dissolved in the soft-segment-rich phase should have higher carbonyl stretching frequency than in the hard domains, hence degree of phase separation can be estimated by Amide I region via the relative amount of hydrogen-bonded carbonyl groups. Curve deconvolution technique can be used to resolve these two peaks but the result is very sensitive to the selection of parameters chosen. Therefore we only use the peak heights instead of the resolved areas to calculate the degree of phase separation. The FT-IR spectra in Amide I region are depicted in Figure 3.4 together with their corresponding degree of phase separation in Table 3.4 which clearly show that longer hard segments or shorter soft segments do have higher degree of phase separation as what we predicted.<sup>5</sup>



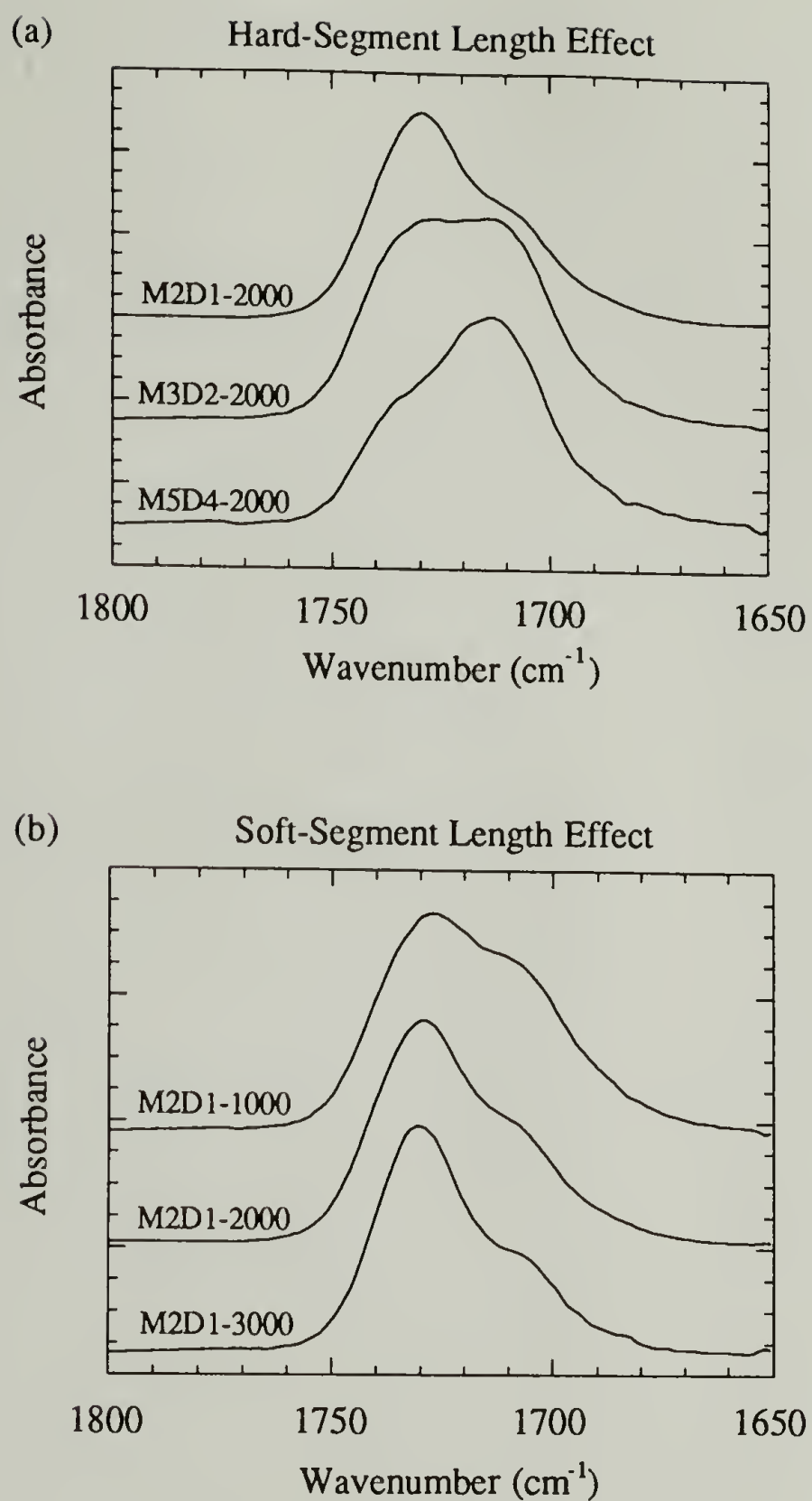


Figure 3.4 Infrared spectra of as-prepared diacetylene-containing polyurethanes in Amide I region : (a) Hard-segment length effect, and (b) soft-segment length effect. The higher bands and lower bands are corresponding to free C=O and hydrogen-bonded C=O, respectively.



Table 3.4 Infrared Results for As-Prepared Segmented Diacetylene-Containing Polyurethane Elastomers : Peak Positions of N-H Stretching and C=O Stretching, and Fraction of Hydrogen-Bonded Carbonyl Groups.

sample	peak position of N-H stretching hydrogen- bonded to C=O (cm <sup>-1</sup> )	peak position of hydrogen-bonded C=O stretching (cm <sup>-1</sup> )	fraction of hydrogen-bonded C=O (%)
M2D1-1000	3304	1705	42.6
M2D1-2000	3302	1705	34.9
M2D1-3000	3300	1705	30.7
M3D2-2000	3315	1711	50.3
M5D4-2000	3318	1713	63.8

This result reveals that phase compositions calculated by the DSC data are strongly biased by the crosslinking effect as shown by the opposite trend for different soft segment lengths. The measured degree of phase separation for all of our samples are much lower than our simulated values. Also, the variation is not so significant as what we predicted. Direct comparison between these two results, however, is difficult because our samples are supposed to a great deal of isolated MDI units and a broad distribution in hard-segment lengths as a consequence of the synthesis procedure, while our calculations were based on monodisperse hard-segment length. Furthermore, uncertainty also exist in the degree of phase separation obtained by infrared method. For example, the degree of phase separation measured by infrared is only about 70% for B4 polymer which is a highly phase-separated polyurethane elastomer consisting of monodisperse hard segments.<sup>37,38</sup> Chain packing in the hard domains is a possible reason for this discrepancy.<sup>38</sup> Nevertheless, comparison of relative degree of phase separation by infrared is still feasible due to the lack of complexity

from crosslinking effect. Finally, we have assumed that the cohesive energy between hard segments in hard domains is proportional to the hard segment length and is independent of the soft segment length in our previous calculation. This assumption may also lead to some errors.

The entire phase diagrams are determined by the chemical potential variation of hard domains and soft domains. Decrease in the degree of phase separation at elevated temperatures is not necessary based on the rigid rod model.<sup>5</sup> Our previous calculations predicted that the phase compositions do not change much in the temperature range of 200-500°K.<sup>5</sup> The degree of phase separation at various temperatures measured by infrared is depicted in Figure 3.5. Because the threshold of cross-polymerization is ~90°C under the thermal process employed, only the results from 30 to 80°C are shown. Figure 3.5 shows that there is only minor change in the fraction of hydrogen-bonded carbonyl groups and, for some samples, this value may increase with temperatures. Both findings are consistent with our prediction. We should be very cautious about the quantitative interpretation on Figure 3.5 though. It is known that variation in the ordering of hard domains at different temperatures will also affect the carbonyl region even without any change in the phase composition which can be seen in the N-H stretching and Amide II regions.<sup>5</sup> It is difficult to separate these two effects from infrared measurements.

The degree of order in hard domains may be revealed by the peak position of hydrogen-bonded N-H or hydrogen-bonded carbonyl groups (Table 3.4). Infrared spectra of N-H stretching region for the as-prepared polyurethanes are shown in Figure 6. It has been proposed that the bands near 3420, 3320, and 3295 cm<sup>-1</sup> correspond to the free N-H, N-H hydrogen-bonded to carbonyl groups, and N-H hydrogen-bonded to ether, respectively.<sup>8,9</sup> It is also well known that stronger hydrogen bonding is associated with larger shift in hydrogen-bonded N-H or C=O.<sup>39</sup> Therefore, the relative degree of order in hard domains can be revealed these quantities. General speaking, the better packing in hard

domains presumably possesses lower frequency in the carbonyl-bonded N-H and hydrogen-bonded C=O. The soft-segment effect on the domain packing is difficult to tell due to the minor difference in those frequencies, but significant differences for various hard segments are shown in Figure 3.6 and Table 3.4.

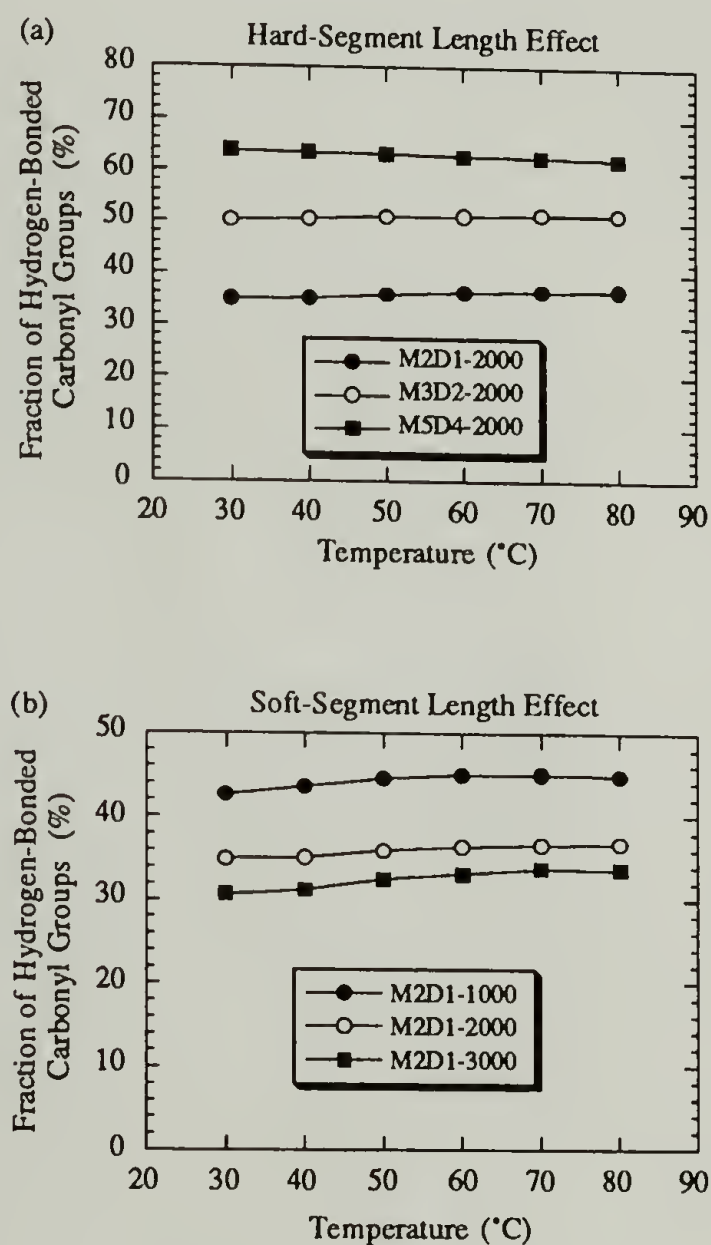


Figure 3.5 Variation of fraction of hydrogen-bonded C=O for as-prepared diacetylene-containing polyurethanes as a function of temperatures : (a) Hard-segment length effect, and (b) soft-segment length effect. Values are determined by the relative peak heights in infrared Amide I region.



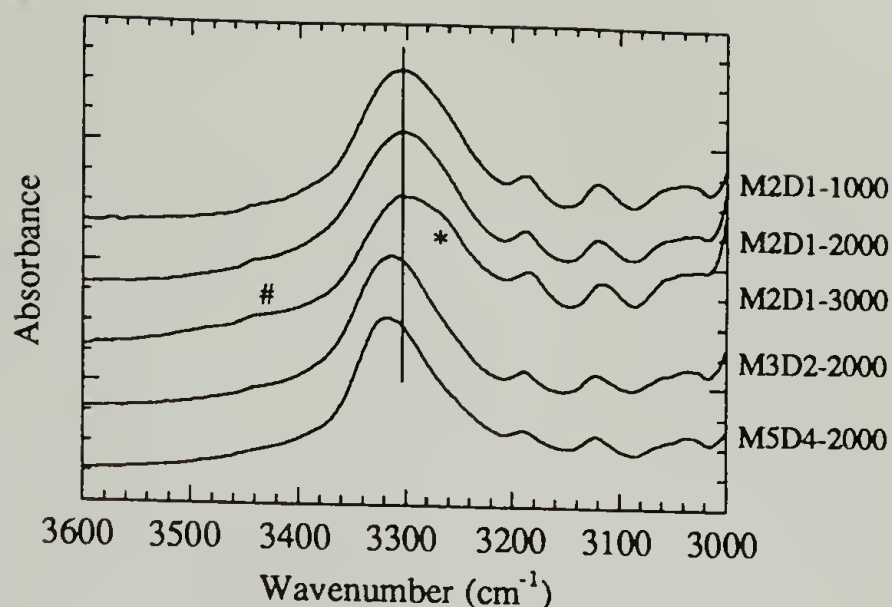


Figure 3.6 Infrared spectra of as-prepared diacetylene-containing polyurethanes in N-H region : The symbols # and \* indicate the band positions of free N-H and hydrogen-bonded N-H via ether groups. Solid line indicates the peak location of hydrogen-bonded N-H via C=O for M2D1-2000 for comparison purpose.

From the lower positions of the carbonyl-bonded N-H and hydrogen-bonded C=O bands for shorter hard-segment, we can conclude that shorter hard-segment will introduce better packing in hard domains. It is very interesting to examine the  $3295\text{ cm}^{-1}$  bands assignable to the N-H  $\cdots$  ether interaction. In the M2D1-1000, 2000, and 3000 samples, we found that the M2D1-3000 has the strongest  $3295\text{ cm}^{-1}$  peak height. This feature can be interpreted as the lower degree of phase separation for M2D1-3000 which results in more N-H  $\cdots$  ether interactions. This interpretation not only is consistent with our previous prediction, it also provides another evidence for the assignment of  $3295\text{ cm}^{-1}$  attributed to the N-H  $\cdots$  ether interactions. Finally, the broader band width for the N-H bands compared with well-defined polypeptide crystalline suggests that the structure in hard domains is far from perfect crystalline.

**3. FT-Raman.** A very unique application of FT-Raman is to study hard domain order by investigating the capability of diacetylene segments to undergo cross-polymerization. The FT-Raman spectra for all of the samples before and after cross-



polymerization are shown in Figure 3.7. Assignments for some major bands in the region of 2500 - 1400  $\text{cm}^{-1}$  are summarized in Table 3.5. The characteristic bands for cross-polymerized samples are 2093  $\text{cm}^{-1}$   $\text{C}\equiv\text{C}$  stretching and 1480  $\text{cm}^{-1}$   $\text{C}=\text{C}$  stretching, respectively. All of our samples clearly demonstrate the capability of cross-polymerization between diacetylenes even though none of them exhibits crystalline features. This result once again proves that crystallization is not necessary for phase-separated structure while hard domains still can possess varying degree of local ordering due to the chain rigidity effect.

The extent of cross-polymerization can be monitored by comparing the intensities of 2093  $\text{cm}^{-1}$  or 1480  $\text{cm}^{-1}$  bands to the 2260  $\text{cm}^{-1}$  bands.<sup>22</sup> Raman spectra in Figures 3.7 clearly show that longer soft-segment or shorter hard-segment has higher degree of cross-polymerization under the same thermal history. The extent of cross-polymerization is determined by the degree of phase separation, the order in the hard-domain packing, and the thermal history. Because we already know that longer soft-segment or shorter hard-segment has a lower degree of phase separation, we infer that the packing in the hard domains is better for longer soft-segment or short hard-segment. To verify this conjecture, we can examine the bandwidths as well as the positions of conjugated  $\text{C}\equiv\text{C}$  and  $\text{C}=\text{C}$  stretching bands for cross-polymerized samples (Figure 3.8). It is well accepted that for longer polydiacetylene chains the conjugated  $\text{C}\equiv\text{C}$  and  $\text{C}=\text{C}$  bands will shift to lower frequencies due to an increase in the polymer of  $\pi$  electron delocalization. These bandwidths provide the information about the polydiacetylene length distribution.<sup>22</sup> Figure 8 shows that longer soft-segment or shorter hard-segment has narrower bandwidth for the conjugated  $\text{C}\equiv\text{C}$  and  $\text{C}=\text{C}$  bands which indicates that the packing is more uniform for these cases. Figure 3.8 also shows that polyurethane with longer hard-segment has higher frequency which indicates that it has smaller length of polydiacetylene. This result can be

(a) Hard-Segment Length Effect

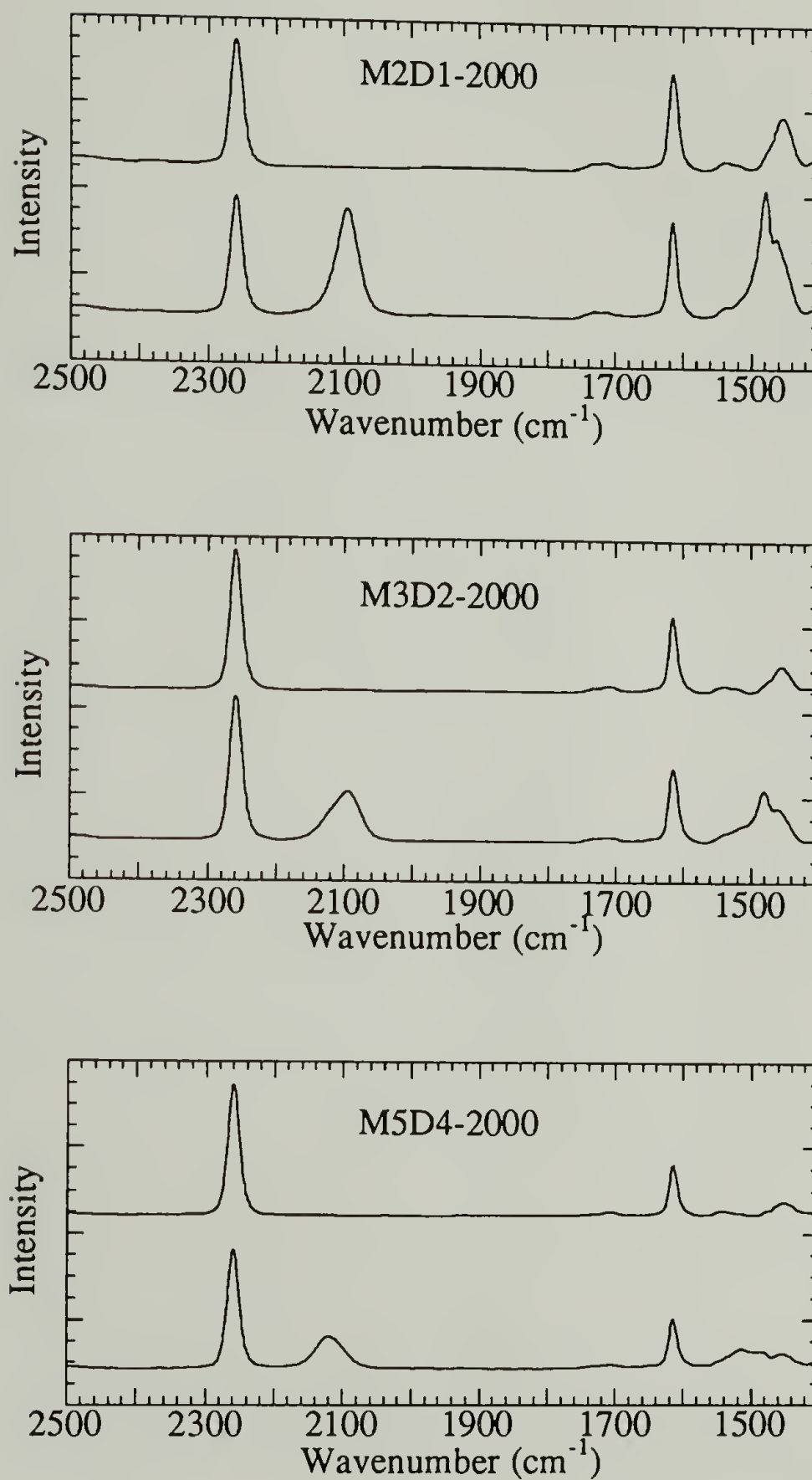


Figure 3.7 FT-Raman spectra of as-prepared and cross-polymerized diacetylene-containing polyurethanes : (a) Hard-segment length effect, and (b) soft-segment length effect. For each compound, the upper spectrum is for as-prepared sample and the lower one is for cross-polymerized one. Cross-polymerization was conducted under the thermal treatment of  $100^{\circ}\text{C}$  for 9 h.  
(Continued, next page)

(b) Soft-Segment Length Effect

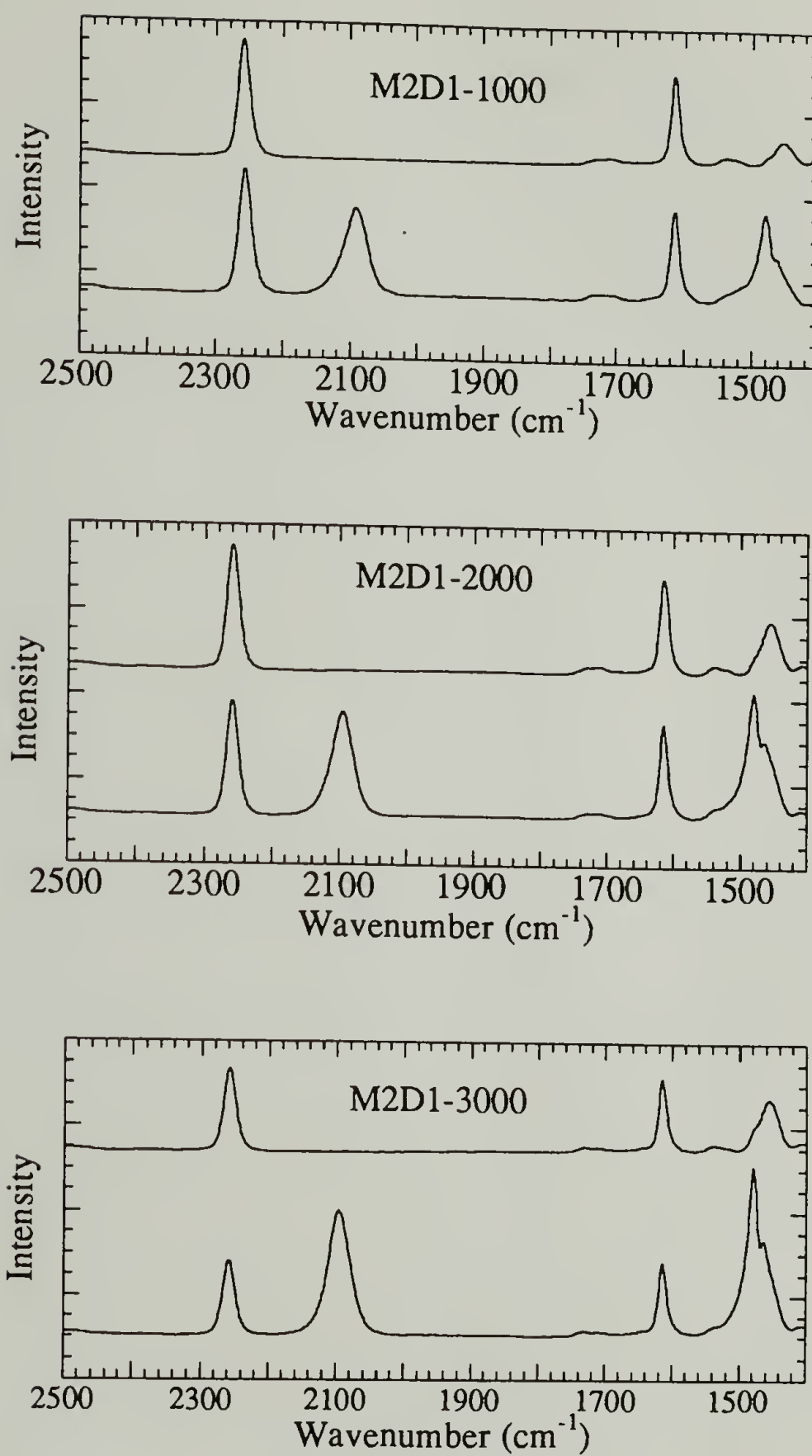


Figure 3.7 (continued)

Table 3.5      Assignments of the Major Bands in Raman Spectra (2500-1400  $\text{cm}^{-1}$ ) for As-Prepared and Cross-Polymerized Segmented Diacetylene-Containing Polyurethane Elastomers

wavenumber ( $\text{cm}^{-1}$ )	band assignment
2260	uncross-polymerized $\text{C}\equiv\text{C}$ stretching
2093	conjugated $\text{C}\equiv\text{C}$ stretching in cross-polymerized structure
1728	Amide I, mostly free $\text{C}=\text{O}$ stretching
1711	Amide I, mostly hydrogen-bonded $\text{C}=\text{O}$ stretching
1615	phenyl ring stretching in the hard segments
1530	Amide II, mostly N-H in-plane deformation and C-N stretching
1480	conjugated $\text{C}=\text{C}$ stretching in cross-polymerized structure
1454	$\text{OCH}_2$ deformation from soft segments



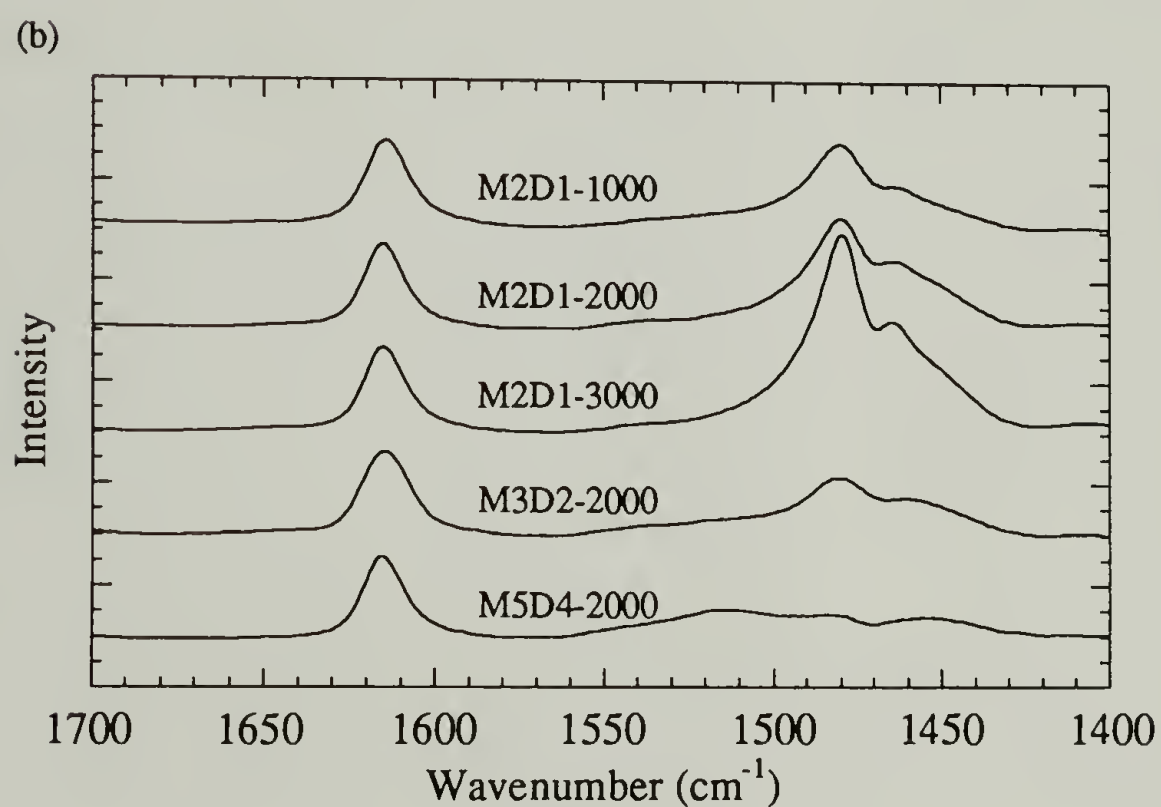
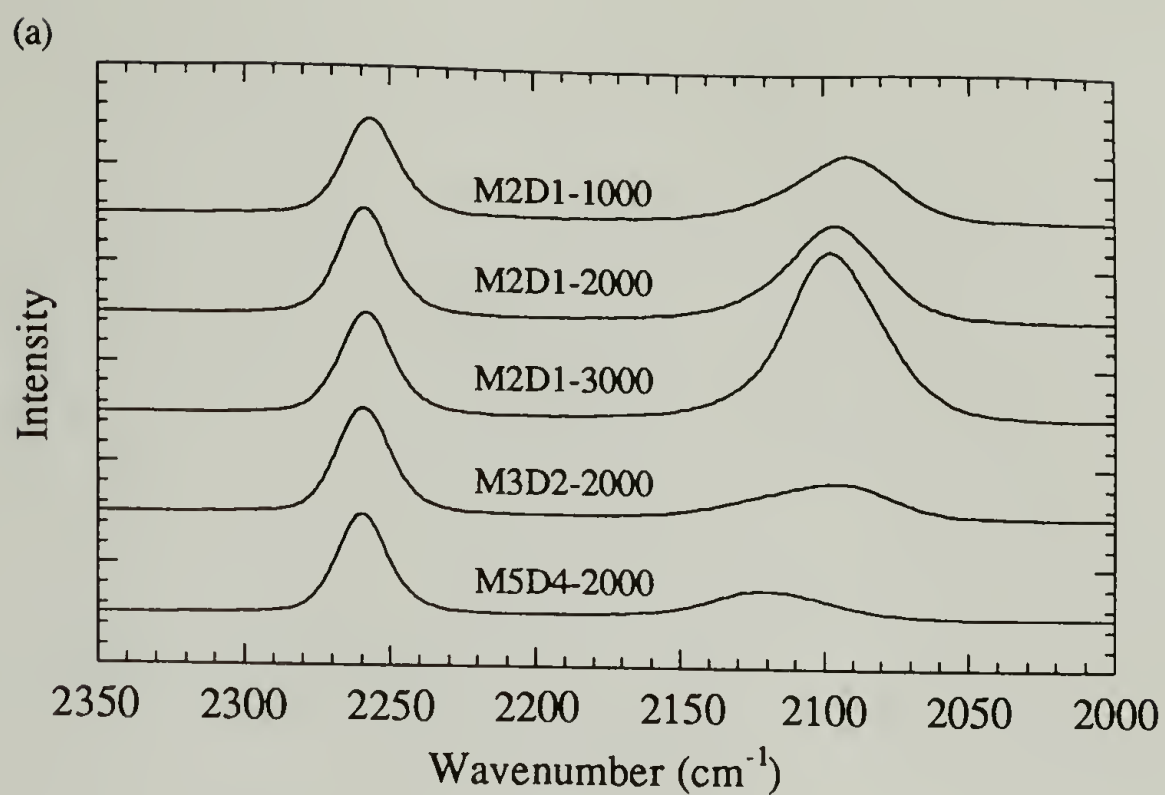


Figure 3.8 FT-Raman spectra of cross-polymerized diacetylene-containing polyurethanes : (a)  $\text{C}\equiv\text{C}$  stretching region, and (b)  $\text{C}=\text{C}$  stretching region.

interpreted by its less ordered structure. Very interestingly, shorter soft-segment (M2D1-1000) shows a lower stretching frequency of conjugated  $C\equiv C$  than a longer one (M2D1-3000) by  $6\text{cm}^{-1}$ . In our opinion, the length of polydiacetylene is determined not only by the order in acetylene matrix, it is also determined by the domain size. The higher conjugated  $C\equiv C$  stretching frequency for longer soft segment can be interpreted by its smaller domain size instead of the less ordering in packing.

In our previous simulation, we assumed that soft-segment length has no effect on the ordering of hard-domain, and the packing in hard domains is better for longer hard-segment according to the idealized rigid rod model. From the FT-Raman result we know that some modifications should be made with this assumption to get better predictions. This implies that there is a chance for longer hard-segment to be lower of hard-segment concentration in the soft-segment-rich phase than shorter ones. One possible reason for shorter soft-segment making more disorder in hard domains is that shorter soft-segment is always associated with higher  $T_g$  in the phase-separated structure which in turn leads to less mobility for hard segments to accommodate the most favorable packing. On the other hand, in our previous calculation we treated the hard-segment as a rigid rod with linear shape. It is known, however, that there is a kink for every MDI segment so the steric effect will deteriorate the packing of hard domains for longer hard-segment.

Cross-polymerized diacetylene-containing segmented polyurethane elastomers have been proposed to be used in non-linear optical applications<sup>12</sup> and photographic applications<sup>21</sup>. Its optical properties depend on how order the hard domains can be and how high the degree of phase separation can be achieved. Their ultimate performance is decided by their mechanical properties, the degree of packing order in hard domains, and the conversion of cross-polymerization of diacetylene segments. The best candidate is

determined by a balance of these factors. From our experience, M2D1-1000 is the best choice in this series.

We would like to re-examine the DSC result with the knowledge of order in hard domains. Figure 3.1 reveals that longer hard-segment or shorter soft-segment exhibits lower exothermic peak temperature. This observation is in direct contradiction to the expectation that higher ordered hard-segment domains leads to higher exothermic peak. This hypothesis is not generally true for the reason as follows. A kinetic model for the cross-polymerization of diacetylenes has been proposed by Kollmar and Sixl.<sup>40</sup> In that case, the energy barriers of molecular translation, rotation, as well as the mismatch of diacetylenes in the crystal matrix have all been taken into consideration. The activation energy in the addition stage has been shown to increase with the chain length of polydiacetylenes. Furthermore, the activation energy is also a function of conversion, temperature, and the crystal packing. The DSC and FT-Raman results show a systematic trend that better packing in hard domains exhibits lower exothermic peak. Possible reasons are that either better packing leads to longer polydiacetylene chains which in turn results in higher activation energy, or is due to the higher translational and rotational energy barrier for better packing structure. Finally, it is also necessary to reconsider interpretation of data. In Figure 3.1, all traces are normalized to the hard-segment weight. The degree of phase separation may reflect on the exothermic peak area if cross-polymerization is presumably completed in hard domains. But thermal degradation and imperfectness in hard-domain packing prohibit the applicability of using entire exothermic peak area to calculate the degree of phase separation. A relative value can be estimated, however, by comparing the half peak areas from the onset to the peak position so as to minimize the degradation effect. The results are listed in Table 3.3. Those data correlate to the Amide I result well, again showing that longer hard-segment or shorter soft-segment possesses higher degree of phase separation. Quantitative evaluation about the degree of phase separation by this



method, nevertheless, is still difficult due to the complexity of different degree of ordering in hard domains.

### 3.4 Conclusions

In this study, we demonstrated that crystallization of hard domains is not necessary for the formation of phase-separated structure. Even in this case, hard domains still can possess varying degrees of local ordering. Chain rigidity of hard-segment is presumably responsible for this behavior according to our rigid rod model. Most of the main features of our previous predictions have been verified by this spectroscopic study. Amide I region are used to estimate the degree of phase separation which shows that longer hard-segment or short soft-segment exhibits higher degree of phase separation. Thermal analysis, on the other hand, will lead to invalid result on the phase composition due to the crosslinking effect. FT-Raman was used to study the ordering of hard domains. and we conclude that longer soft-segment or short hard-segment has better packing in hard domains by this study.



## References

- (1) Hepburn, C. *Polyurethane elastomers*; Applied Sciences Publishers: London, 1982.
- (2) Petrovic, Z. S.; Ferguson, J. *Prog. Polym. Sci.* **1991**, *16*, 695.
- (3) Hwang, K. K. S.; Hemker, D. J.; Cooper, S. L. *Macromolecules* **1984**, *17*, 307.
- (4) Hwang, K. K. S.; Lin, S. B.; Tsay, S. Y.; Cooper, S. L. *Polymer* **1984**, *25*, 947.
- (5) Tao, H.-J.; MacKnight, W. J.; Hsu, S. L. *Macromolecules* **1994**, in press.
- (6) Harrell, L. L. ; J. *Macromolecules* **1969**, *2*, 607.
- (7) Kornfield, J. A.; Spiess, H. W.; Nefzger, H.; Hayen, H.; Eisenbach, C. D. *Macromolecules* **1991**, *24*, 4787.
- (8) Lee, H. S.; Wang, Y. K.; Hsu, S. L. *Macromolecules* **1987**, *20*, 2089.
- (9) Sun, H. *Macromolecules* **1993**, *26*, 5924.
- (10) Koberstein, J. T.; Stein, R. S. *J. Polym. Sci., Polym. Phys. Ed.* **1983**, *21*, 1439.
- (11) Miller, J. A.; Lin, S. B.; Hwang, K. K. S.; Wu, K. S.; Gibson, P. E.; Cooper, S. L. *Macromolecules* **1985**, *18*, 32.
- (12) Rubner, M. F. *Macromolecules* **1986**, *19*, 2114.
- (13) Li, Y.; Ren, Z.; Zhao, M.; Yang, H.; Chu, B. *Macromolecules* **1993**, *26*, 612.
- (14) Li, Y.; Kang, W.; Stoffer, J. O.; Chu, B. *Macromolecules* **1994**, *27*, 612.
- (15) Meuse, C. W.; Tao, H.-J.; Hsu, S. L.; MacKnight, W. J. *Polym. Prepr. (Am. Chem. Soc., Div. Polym. Chem.)* **1993**, *34*(2), 266.
- (16) Blackwell, J.; Gardner, K. H. *Polymer* **1979**, *20*, 13.
- (17) Eisenbach, C. D.; Nefzger, H. In ; B. M. Culbertson, Ed.; *Multiphase Macromolecular Systems*; Plenum Publishing Corp.: New York, 1989; pp 339.
- (18) Eisenbach, C. D.; Heinemann, T.; Ribbe, A.; Stadler, E. *Die Angewandte Makromolekulare Chemie* **1992**, *202/203*, 221.
- (19) Hu, X.; Stanford, J. L.; Day, R. J.; Young, R. J. *Macromolecules* **1992**, *25*, 672.
- (20) Lee, H. S.; Wang, Y. K.; MacKnight, W. J.; Hsu, S. L. *Macromolecules* **1988**, *21*, 270.
- (21) Liang, R.-C.; Lai, W.-Y. F.; Reiser, A. *Macromolecules* **1986**, *19*, 1685.
- (22) Nitzsche, S. A.; Hsu, S. L.; Hammond, P. T.; Rubner, M. F. *Macromolecules* **1992**, *25*, 2391.

- (23) Wegner, G. *Makromol. Chem.* **1971**, *145*, 85.
- (24) Baughman, R. H.; Yee, K. C. *Macromol. Rev.* **1978**, *13*, 219.
- (25) Enkelmann, V. *Adv. Polym. Sci.* **1984**, *63*, 91.
- (26) Schott, M.; Wegner, G. In ; M. S. Chemla and J. Zyss, Ed.; *Nonlinear Optical Properties of Organic Molecules and Crystals*; Academic Press: Orlando, 1987; Vol. 2, chapter III-1; pp 3.
- (27) Day, D. R.; Lando, J. B. *J. Appl. Polym. Sci.* **1981**, *26*, 1605.
- (28) Schoen, P. E.; Yager, P.; Priest, R. G. In ; D. Bloor and R. R. Chance, Ed.; *Polydiacetylenes : Synthesis, Structure and Electronic Properties*; Martinus Nijhoff Publishers: Dordrecht, The Netherlands, 1985; pp 223.
- (29) Schen, M. A.; Kotowski, K.; Cline, J. *Polymer* **1991**, *32*, 1843.
- (30) Koberstein, J. T.; Leung, L. M. *Macromolecules* **1992**, *25*, 6205.
- (31) Koberstein, J. T.; Galambos, A. F.; Leung, L. M. *Macromolecules* **1992**, *25*, 6195.
- (32) Leung, L. M.; Koberstein, J. T. *Macromolecules* **1986**, *19*, 706.
- (33) Andrady, A. L.; Sefcik, M. D. *J. Polym. Sci., Polym. Phys. Ed.* **1983**, *21*, 2453.
- (34) Feger, C.; MacKnight, W. J. *Macromolecules* **1985**, *18*, 280.
- (35) Chang, S.-S. *Polymer* **1992**, *33*, 4768.
- (36) Coleman, M. M.; Graf, J. F.; Painter, P. C. *Specific Interactions and the Miscibility of Polymer Blends*; Technomic Publishing Co.: Lancaster, PA, 1991.
- (37) Christenson, C. P.; Harthcock, M. A.; Meadows, M. D.; Spell, H. L.; Howard, W. L.; Creswick, M. W.; Guerra, R. E.; Turner, R. B. *J. Polym. Sci.: Part B: Polym. Phys.* **1986**, *24*, 1401.
- (38) Meadows, M. D.; Christenson, C. P.; Howard, W. L.; Harthcock, M. A.; Guerra, R. E.; Turner, R. B. *Macromolecules* **1990**, *23*, 2440.
- (39) Pimentel, G. C.; McClellan, A. L. *The Hydrogen Bond*; Reinhold Publishing Corp.: New York, 1959.
- (40) Kollmar, C.; Sixl, H. *J. Chem. Phys.* **1987**, *87*, 5541.

## CHAPTER 4

# INVESTIGATION ON THE PHASE SEPARATION BEHAVIOR OF POLYURETHANE ELASTOMERS BY TWO-DIMENSIONAL WIDELINE-SEPARATION NUCLEAR MAGNETIC RESONANCE SPECTROSCOPY

### 4.1 Introduction

It is well known that polyurethane elastomers exhibit phase separated structure.<sup>1</sup> Various techniques have been used to assess the phase composition but quantitative evaluation is hard to achieve.<sup>2</sup> For example, DSC measurement associated with Fox equation or its modified form is commonly utilized to determine the phase composition based on the changes in glass transition temperature ( $T_g$ ) and the heat capacity change of the soft segments. The phase compositions, however, remain inaccessible by this method without taking explicitly into account the crosslinking effect. It is well documented that the confinement of polymer chain ends will dramatically change its glass transition temperature<sup>3,4</sup> and the heat capacity jump<sup>3-5</sup> (crosslinking effect). For instance, the glass transition temperature of crosslinked poly(propylene glycol) deviates from its linear form by 56.15°C and 27.4°C for molecular weight 1000 and 3000, respectively.<sup>3</sup> The soft segments in phase separated structure possess similar behavior, therefore the application of thermal analysis for this purpose deserves more elaborate consideration about this notable effect.

Several kinds of methods associated with solid state NMR have been used to investigate the phase separation behavior of polyurethane elastomers.<sup>6-12</sup> The recently developed method of two-dimensional wideline-separation nuclear magnetic resonance spectroscopy (WISE-NMR)<sup>13</sup> provides us an alternative tool in determining the phase composition of polyurethane elastomers. In this experiment, a correlation between



chemical structure and segmental mobility is established as reflected in the  $^{13}\text{C}$  chemical shifts and the  $^1\text{H}$  line shapes, respectively. Segments dispersed in the hard-segment-rich domain are immobilized resulting in broad components in the  $^1\text{H}$  spectra. It is therefore possible to calculate the fraction of hard/soft segment distributed in each phase from resolved  $^{13}\text{C}$  spectrum.

In this chapter, we present the results of our investigation on the phase separation behavior of a polyurethane elastomer by two-dimensional wideline-separation nuclear magnetic resonance spectroscopy. Comparison of our finding with other techniques is also provided.

## 4.2 Experimental Section

**A. Materials.** To avoid the complexity arising from the polydispersity in hard segments, we employed a model polyurethane with monodisperse hard segment length, B4 polymer, which was kindly supplied by Dow Chemical Corporation<sup>14</sup>. The hard segment of B4 polymer contains five MDI's [4,4'-methylenebis(phenyl isocyanate)] and four BD's (butanediol) units. The soft segment is monodisperse PPG [poly(propylene glycol)] with molecular weight of 2000. B4 polymer consists of 45 wt% hard segments. The structure is shown in Figure 4.1.

**B. Measurements.** The basic version of WISE-NMR measurement<sup>13</sup> has been adopted in this study without the incorporation of TOSS sequence<sup>15,16</sup> for suppressing  $^{13}\text{C}$  spinning sidebands. Detail description about its principle, pulse sequence and the applications have been published previously.<sup>13,17</sup> Spectra were taken at 25°C by a Bruker MSL-300 spectrometer with magic angle spinning at 4.0 kHz. Sample of about 200 mg was prepared by grinding under liquid nitrogen and then was packed into a sapphire rotor with KelF end caps. A cross polarization time of 1000  $\mu\text{s}$  and 128  $t_1$  increments with a



dwel time  $t_1$  of 4  $\mu$ s were used(Figure 4.2). Curve deconvolution was carried out with the software *LAB CALC* (Galactic Ind. Corp.).

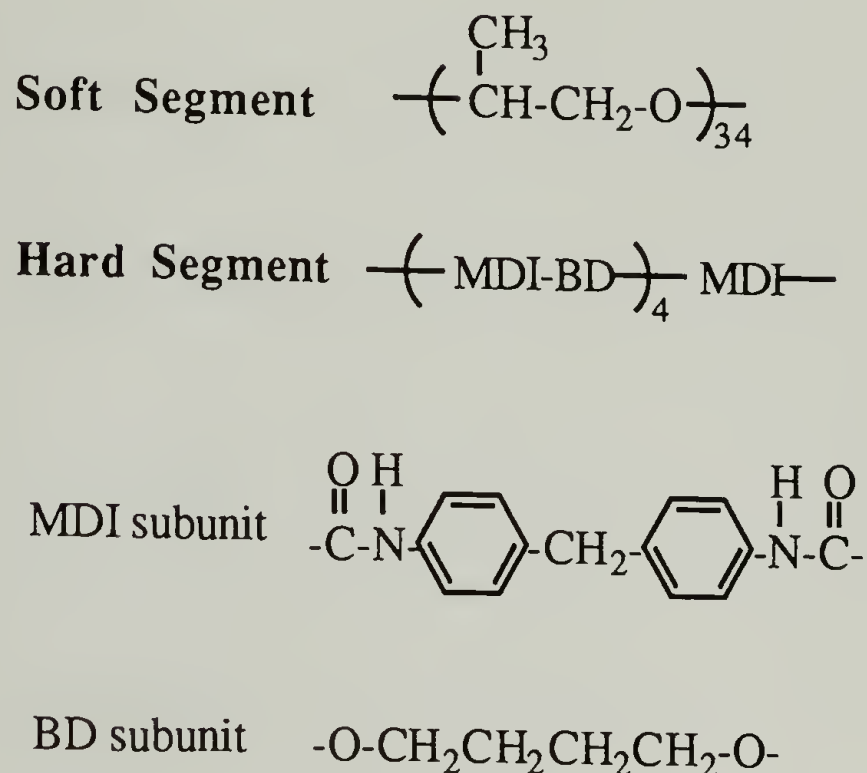


Figure 4.1 Structures of the soft segment and hard segment for B4 polymer.

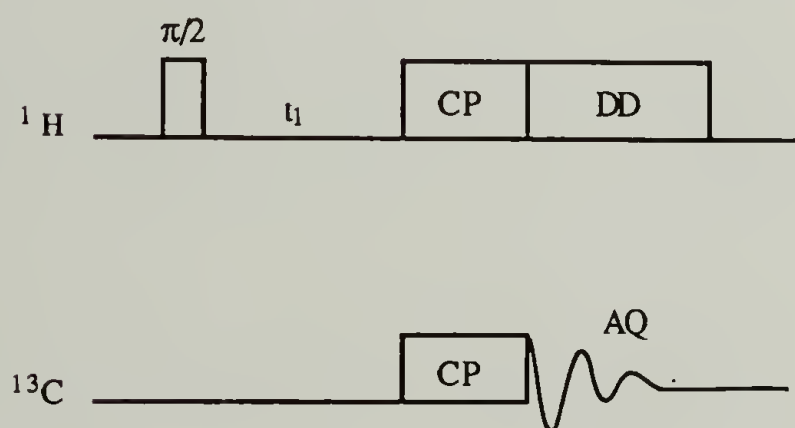


Figure 4.2 Pulse sequence of WISE-NMR experiment used in this work with proton evolution, cross polarization (CP), and  $^{13}\text{C}$  acquisition (AQ) with dipolar decoupling (DD) of protons.

Heat capacity change measurement was performed by a TA Instruments DSC-2910 purged with dry nitrogen. Runs were conducted on polymer samples of about 10 mg at a heating rate of 10°C/min from -100°C to 30°C. The temperature has been calibrated by cyclohexane at -87°C associated with its crystal-crystal transformation.

#### 4.3 Results and Discussion

The WISE spectrum for B4 polymer at 25°C is shown in Figure 3a. The  $^{13}\text{C}$  chemical shifts associated with soft segments are 18 ppm and 75 ppm corresponding to the PPG methyl groups and methylene groups, respectively. For the hard segments, the chemical shifts of the phenyl rings are located in the 115-140 ppm region, butandiol methylenes located at 25 and 66 ppm, and 155 ppm for the carbonyl.<sup>10</sup> To evaluate the fraction of mobile soft segments, the cross section of WISE spectrum along the 75 ppm for methylenes of soft segment is shown in Figure 3b. We find out that there is only a mobile component with a bandwidth (FWHH, full width at half height) of 3.2 kHz. Because the dipolar line width for the immobile CH or  $\text{CH}_2$  is known to be 50kHz, therefore we conclude that the soft segments are rarely dissolved into the hard domains according to the absence of this immobile component. This result is consistent with the finding for piperazine-based polyurethane with monodisperse hard segment length by deuterium NMR measurement.<sup>9</sup> On the other hand, the  $(\Delta C_p/W_s)/\Delta C_p^0$  value by thermal analysis is 78% which is frequently referred to the fraction of soft segments dispersed in the hard-segment-rich domains<sup>2,18</sup>, where  $\Delta C_p$ ,  $W_s$  and  $\Delta C_p^0$  are the heat capacity change for the polyurethane elastomers at the glass transition temperature of soft segment, the weight fraction of the soft segments in the elastomers, and the heat capacity change for the uncrosslinked neat soft segments at its  $T_g$ , respectively. The  $(\Delta C_p/W_s)/\Delta C_p^0$  value is lower than the WISE result probably due to the extra contribution from crosslinking effect which can also decrease the heat capacity change.<sup>4,5</sup> It is inadequate, therefore, to take the

heat capacity change value as the fraction of soft segments dispersed inside the hard domains or in the interfaces without extracting the crosslinking effect explicitly.

The exact distribution of the hard segments in two phases is difficult to estimate due to the very weak intensity in the region of 115-140 ppm.<sup>10</sup> We can see, however, from Figure 3a that there is no sizable amount of mobile hard segment component which is detectable (Figure 3a). We believe that the degree of phase separation is very high for B4 polymer according to this result. The  $T_{1\rho}^C$  measurement of the B4 polymer was investigated previously which indicated that the B4 polymer is very likely to phase separate completely.<sup>10</sup> Our WISE measurement is consistent with this conjecture. Further work on enhancing the WISE signal in the region of 115-140 ppm will be conducted in the near future.

Glass transition temperature change and infrared measurement have also been used to estimate the degree of phase separation for B4 polymer previously.<sup>14</sup> Here, the degree of phase separation is defined as the fraction of hard segments distributed in the hard domains. The reported degree of crystallinity of B4 polymer is 73% by DSC measurement.<sup>14</sup> Because the hard domains are not necessarily composed of perfect crystalline structure, the actual degree of phase separation should be higher than the degree of crystallinity. On the other hand, the composition of the soft-segment-rich phase was previously proposed to be estimated by the following generalized Fox equation<sup>18</sup>

$$\frac{w_1 + (1-w_1)k}{T_g} = \frac{w_1}{T_{g1}} + \frac{k(1-w_1)}{T_{g2}} \quad (4.1)$$

where  $T_g$ ,  $T_{g1}$ , and  $T_{g2}$  are the glass transition temperatures for the soft segments in the phase-separated structure, for the pure linear soft segments, and for the hard domains, respectively.  $w_1$  in eq 1 is the weight fraction of soft segments in the soft-segment-rich

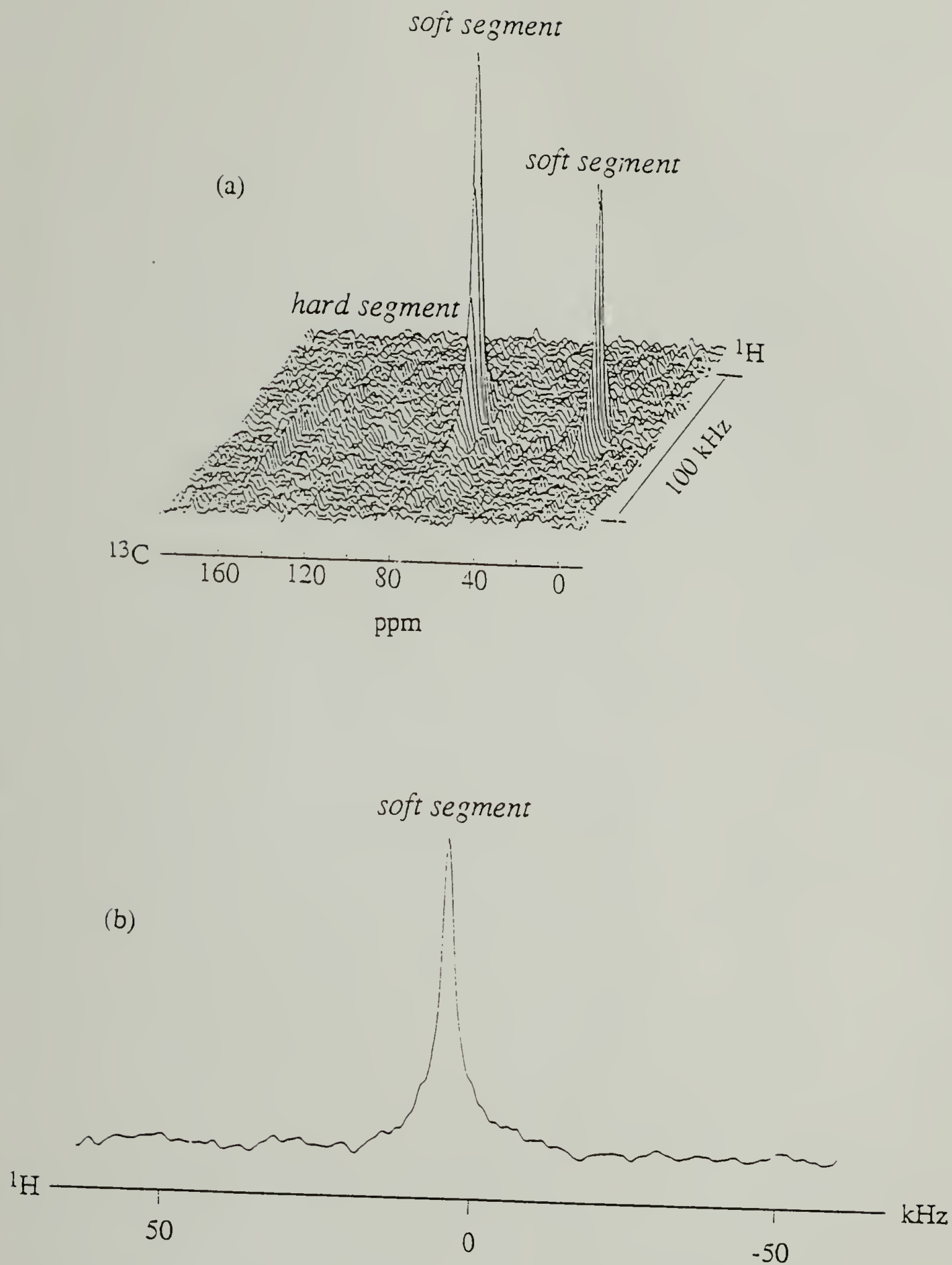


Figure 4.3 WISE-NMR spectrum of B4 polymer (a), and its cross section along 75ppm (b).



phase. The parameters used in this calculation are  $T_g = -32^\circ\text{C}$ ,  $T_{g1} = -69^\circ\text{C}$ ,  $T_{g2} = 109^\circ\text{C}$  and  $k = 1.18$ .<sup>14,18</sup> The soft-segment-rich phase consists of 29% of the hard segments according to this calculation and the associated degree of phase separation is unreasonably low. It is believed that the crosslinking effect on  $T_g$  prohibits its applicability to the phase composition determination. Finally, the degree of phase separation estimated by the carbonyl region of infrared is about 70%<sup>14</sup> assuming that the carbonyl groups in the hard domains are all hydrogen-bonded and they are free from hydrogen-bonding outside the hard domains. The crosslinking effect will not affect the carbonyl stretching region, nevertheless, the degree of phase separation determined by the infrared method still might be less than its true value due to two reasons. First, the carbonyl groups in the interfaces might not show hydrogen-bonded feature. Besides, because the hard domains are not necessarily composed of perfect crystalline structure, or even they do, some carbonyl groups still cannot form hydrogen-bonding according to Blackwell's model.<sup>10,19,20</sup>

#### 4.4 Conclusions

Our finding by the WISE-NMR measurements indicates that the B4 polymer is likely to phase separate completely and forms relatively pure hard-segment-rich phase and soft-segment-rich phase. Thermal analysis is difficult to calculate the phase composition explicitly due to the complexity of crosslinking effect. Even though the degree of phase separation measured by infrared cannot reflect its true value, it is a more reliable tool to determine the relative degree of phase separation for different chain lengths in hard/soft segments than the thermal analysis method because the infrared method is free from the complication of the crosslinking effect.

## References

- (1) Hepburn, C. *Polyurethane elastomers*; Applied Sciences Publishers: London, 1982.
- (2) Petrovic, Z. S.; Ferguson, J. *Prog. Polym. Sci.* **1991**, *16*, 695 and references therein.
- (3) Andrady, A. L.; Sefcik, M. D. *J. Polym. Sci., Polym. Phys. Ed.* **1983**, *21*, 2453.
- (4) Feger, C.; MacKnight, W. J. *Macromolecules* **1985**, *18*, 280.
- (5) Chang, S.-S. *Polymer* **1992**, *33*, 4768.
- (6) Assink, R. A. *J. Polym. Sci., Polym. Phys. Ed.* **1977**, *15*, 59.
- (7) Dickinson, L. C.; Shi, J.-F.; Chien, J. C. W. *Macromolecules* **1992**, *25*, 1224.
- (8) Dumais, J. J.; Jelinski, L. W.; Leung, L. M.; Gancarz, I.; Galambos, A.; Koberstein, J. T. *Macromolecules* **1985**, *18*, 116.
- (9) Kornfield, J. A.; Spiess, H. W.; Nefzger, H.; Hayen, H.; Eisenbach, C. D. *Macromolecules* **1991**, *24*, 4787.
- (10) Meadows, M. D.; Christenson, C. P.; Howard, W. L.; Harthcock, M. A.; Guerra, R. E.; Turner, R. B. *Macromolecules* **1990**, *23*, 2440.
- (11) Nierzwicki, W. *J. Appl. Polym. Sci.* **1984**, *29*, 1203.
- (12) Okamoto, D. T.; Cooper, S. L.; Root, T. W. *Macromolecules* **1992**, *25*, 1068.
- (13) Schmidt-Rohr, K.; Clauss, J.; Spiess, H. W. *Macromolecules* **1992**, *25*, 3273.
- (14) Christenson, C. P.; Harthcock, M. A.; Meadows, M. D.; Spell, H. L.; Howard, W. L.; Creswick, M. W.; Guerra, R. E.; Turner, R. B. *J. Polym. Sci.: Part B: Polym. Phys.* **1986**, *24*, 1401.
- (15) Dixon, W. T. *J. Magn. Reson.* **1980**, *44*, 220.
- (16) Dixon, W. T. *J. Chem. Phys.* **1982**, *77*, 1800.
- (17) Tekely, P.; Palmas, P.; Mutzenhardt, P. *Macromolecules* **1993**, *26*, 7363.
- (18) Koberstein, J. T.; Leung, L. M. *Macromolecules* **1992**, *25*, 6205.
- (19) Blackwell, J.; Gardner, K. H. *Polymer* **1979**, *20*, 13.
- (20) Blackwell, J.; Nagarajan, M. R. *Polymer* **1981**, *22*, 202.

## CHAPTER 5

### A SPECTROSCOPIC ANALYSIS OF PHASE SEPARATION BEHAVIOR OF POLYURETHANE IN RESTRICTED GEOMETRY\*

#### 5.1 Introduction

Segmented polyurethane elastomers are alternating block copolymers consisting of flexible soft segments and more rigid hard segments. A variety of techniques have revealed a phase separated morphology, with hard segments mainly residing in hard segment rich domains.<sup>1,2</sup> This relatively pure phase coexists with one containing mainly soft segments with some hard segments dispersed in it.<sup>3</sup> Formation of hydrogen bonds, crystallization of hard segments, chain folding, excluded volume effect, and kinetics arguments have all been proposed as possible explanations for this phase separation behavior.<sup>1-6</sup> In our previous study, we proposed that the excluded volume effect associated with the stiffness of the hard segment is an important factor for phase separation for the [methylene bis(phenyl isocyanate)] (MDI) based system.<sup>6</sup> The phase diagrams calculated for the system containing MDI extended by diacetylenes as hard segment mixed with poly(propylene glycol) (PPG) as the soft segment are consistent with experimental results.<sup>7</sup>

The basic assumption in our past studies is that if the excluded volume effect of the hard segments is important, the hard segments will phase separate into disk-like domains with nematic-like structure due to the strong lateral interactions between them.<sup>6,7</sup>

---

\* The experimental part was conducted by Dr. Curtis W. Meuse.



It is most convenient to characterize the phase separation behavior by following the relative intensity of the 2 components generally seen in the C=O stretching(  $\sim 1700\text{ cm}^{-1}$  ) region. The higher frequency component is assigned to the carbonyl stretching free from hydrogen bonding. The lower frequency component is characteristic of hydrogen bonded carbonyls in phase separated domains. The phase separation kinetics can be determined from the change in the relative intensity of the 2 components as a function of time.<sup>8</sup> In some cases, segmental orientation needs to be taken into account.<sup>8</sup> Our previous spectroscopic analyses have shown that a spinodal decomposition mechanism does not fit the data well.<sup>9</sup> Instead a model forming disk-like domains can be used to explain the kinetics observed. An *Avrami-like* analysis yielded a coefficient  $\sim 2$ .<sup>9</sup>

In a follow-up study, we used the external reflectance technique to monitor the relative intensity of the 2 carbonyl stretchings in the  $1700\text{ cm}^{-1}$  region for polyurethanes on various substrates. Our data suggested a high degree of segmental orientation on the substrate.<sup>8</sup> After taking this structural anisotropy into account, we have been able to demonstrate that the ultimate degree of phase separation is also highly dependent on film thickness. In this current study, we have carried out kinetics experiments similar to the ones we conducted in the past. We found, most surprisingly, that the phase separation kinetics measured in extremely thin polyurethane films, in the order of 10's or 100's angstroms thick, are quite different, i.e. much slower, as compared to the ones measured for the bulk state.<sup>9</sup> The factors governing the structure formation in a restricted geometry, e.g. an ultra-thin film on a substrate, are unknown and the transition from the bulk to the thin film structure is unclear. Intuitively, the degree of phase separation and the orientation of the phase separated domains are expected to be dependent on the length of the hard segments. Theory predicts that the orientation caused by the surface would only affect the first three or four layers from the interface between the air and the polymer.<sup>10-13</sup>



It is our hypothesis that the slow phase separation kinetics and the lowering of the degree of phase separation in extremely thin films are directly related to the constraints of the air-solid interface.<sup>14-16</sup> Intuitively, semi-rigid hard segments simply lack the translational freedom to form hard-segment rich domains in extremely thin films as compared to the bulk state. In this current study, based on the spectroscopic data obtained, we have formulated and solved the mass transport equation to form hard-segment rich domains with the boundary conditions defined by the air-solid interfaces. Using the model developed, we were able to analyze this aspect as well. There is little doubt that chain rigidity influences strongly the formation of phase separated structure in thin films. Our results are reported here.

## 5.2 Experimental Section

The polyurethane (B2 polymer) used in these experiments has been described previously.<sup>17</sup> The monodisperse hard segment consists of 3 MDI units extended by 2 butanediol linkages. The soft segment is a 2000 molecular weight poly(propylene glycol) (PPG). The gold surfaces for infrared external reflection experiments are 200 nm thick of 99.999% gold coated on microscope slides prepared by the Brysen Optical Company of Safety Harbor, Florida. The 16 nm thick B2 polymer films are formed by casting one drop of 2.5 mg/ml polyurethane in tetrahydrofuran (THF) solution directly onto the surface of glycerin. The glycerin is then heated to ~60 °C and the film is transferred by placing the gold surface face down onto the film. In this fashion it is possible to attach the polyurethane to the gold substrate. Since glycerin is soluble in water, any residual glycerin in the sample is removed by rinsing the sample in water heated to ~60 °C. Other film thicknesses are produced by spin casting (using a Headway Research Inc. spin coater at 3000 rpm for 30 seconds) directly onto the gold surfaces from 0.01 to 0.5% (weight per

volume) solutions in THF. The continuity and film thicknesses were checked by contact angle and ellipsometry methods as described previously.<sup>8</sup>

The infrared spectra are obtained with a Nicolet 60SXB spectrometer equipped with a narrow-band MCT detector using an external reflection cell purchased from Specac Ltd. of Milford, Connecticut. All spectra were collected at 2 cm<sup>-1</sup> resolution. The external reflection cell holds the sample in a horizontal position that allows it to be easily modified to incorporate a heating block beneath the sample in order to obtain spectra at variable temperatures. The temperature of the heating block could be controlled to within 1 °C using an Omega programmable temperature controller and a copper-constantin thermocouple sensor. In order to conduct the phase separation experiment, the molten sample can be cooled to a desired temperature in the sampling chamber of this reflection cell. We have built another heating unit immediately adjacent to the reflectance cell to melt the sample. It is possible to transfer the sample from the molten state to the reflectance unit set at the desired phase separation temperature without opening the sample chamber. The temperatures can be controlled sufficiently well, so that data collection can be started within 10 seconds after the sample is transferred into the reflectance cell.

In order to obtain spectra as a function of time, a program was written that initially collects 10 sets of 64 scans and later collects 109 sets of 512 scans. Once the kinetic experiment is completed, all 119 files are Fourier transformed and ratioed against a constant background. Changes in the infrared spectra for a 16 nm B2 polymer films are shown in Figure 5.1. The kinetics data for the much thicker film, >2 μm, of B2 polymer have been published earlier.<sup>9</sup>

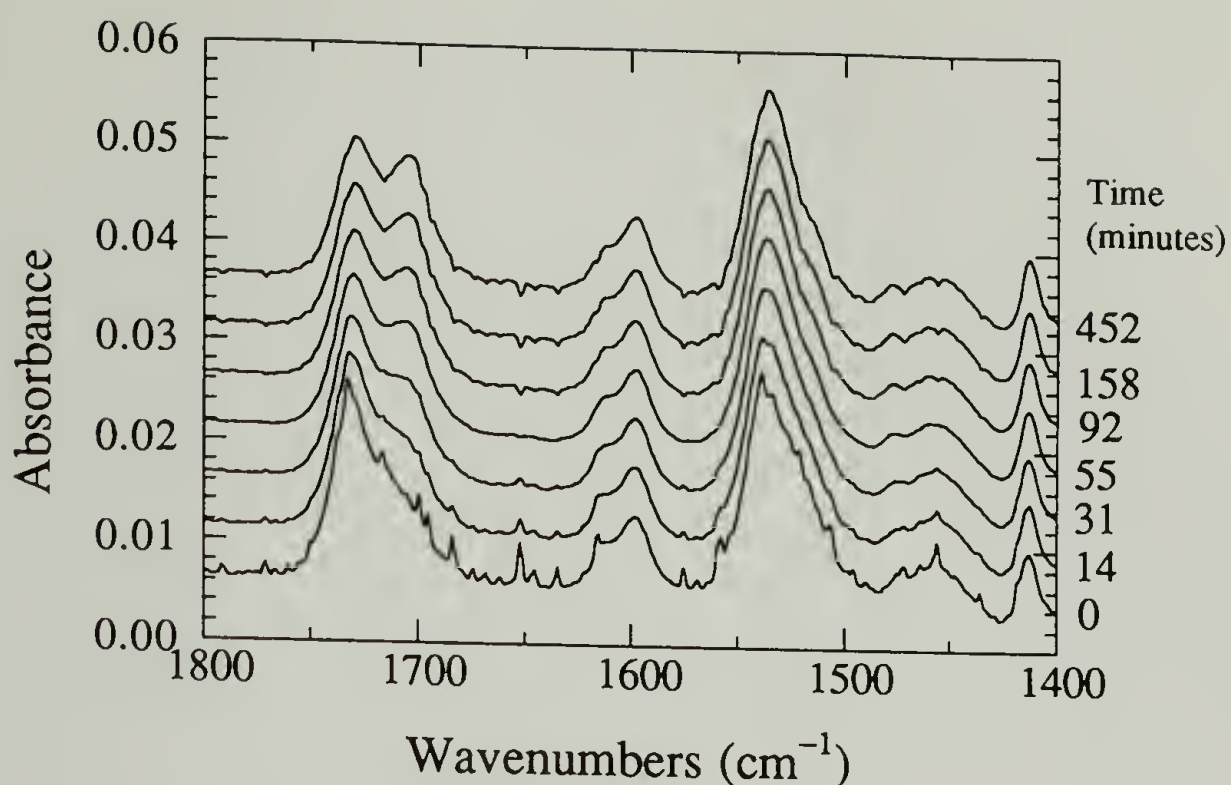


Figure 5.1 Infrared external reflection spectra for the phase separation process of a 16 nm B2 polymer film on gold at 23°C.

### 5.3 Experimental Results

Phase separation kinetics of model polyurethanes have been characterized by infrared spectroscopy using two different carbonyl bands in the Amide I region. The higher frequency band at  $1730\text{ cm}^{-1}$  is assignable to hard segments that are surrounded by soft segments ( free from hydrogen bonding ) and the lower frequency band at  $1700\text{ cm}^{-1}$  is associated with hard segments hydrogen bonded to each other. The relative intensity of these two bands is usually indicative of the degree of phase separation. If the sample is heated to above its phase mixing point then quenched to a temperature below the phase mixing temperature to begin the phase separation process, isothermal phase separation kinetics can be determined by analyzing the Amide I band changes as a function of temperature and time. This type of kinetics experiment has been carried out in previous studies to study the phase separation behavior in thick films (considered to be bulk-like).<sup>9</sup> In that case, because the signal available is sufficiently strong, infrared spectroscopy was



easily carried out using the standard transmission mode. In cases when the samples are thin, on the order of 10's nm, the most convenient method is to use the reflectance technique.<sup>8</sup> Figure 5.1 is an example of the isothermal phase separation spectra for a 16 nm B2 polymer film. Unlike the transmission experiment, however, the degree of phase separation of a ultra-thin film cannot be simply determined by the relative intensity of the two Amide I bands obtained with the reflectance technique, since preferential orientation usually is present.<sup>8</sup> The boundary conditions associated with reflections from a dielectric film on a metallic substrate are such that only vibrations with transition moments in the scattering plane ( p-polarization ) can be observed. Therefore, the apparent relative intensity of the bands seen in the Amide I region can be associated either with differences in the degree of phase separation or in the orientation of molecules on the surface. It is possible, though, to separate these two effects and obtain the degree of phase separation at different times.<sup>8</sup>

After correcting for spectroscopic anomalies, an *Avrami-type* analysis has been applied to characterize the phase separation kinetics of polyurethanes as described previously.<sup>9</sup> In this model, the volume fraction of phase separated domains,  $X(t)$ , is expressed as

$$X(t) = 1 - \exp ( - kt^n ) \quad (5.1)$$

where  $k$  is the rate constant and  $n$  is described as the Avrami exponent. The value of the exponent has been used to suggest different types of phase transformation mechanisms.<sup>18</sup>

Data presented in Figure 5.2 for a 16 nm film show an initial slope of 1.25 changing to ~0.6 at later stages. The change in the slope can be interpreted as due to the decrease in concentration of hard segments in the isotropic phase.<sup>9</sup> Growth of the phase separated domains can only be continued when other hard segments diffuse to the domain surface. This exponent is considerably smaller than the one we found for the bulk state. In



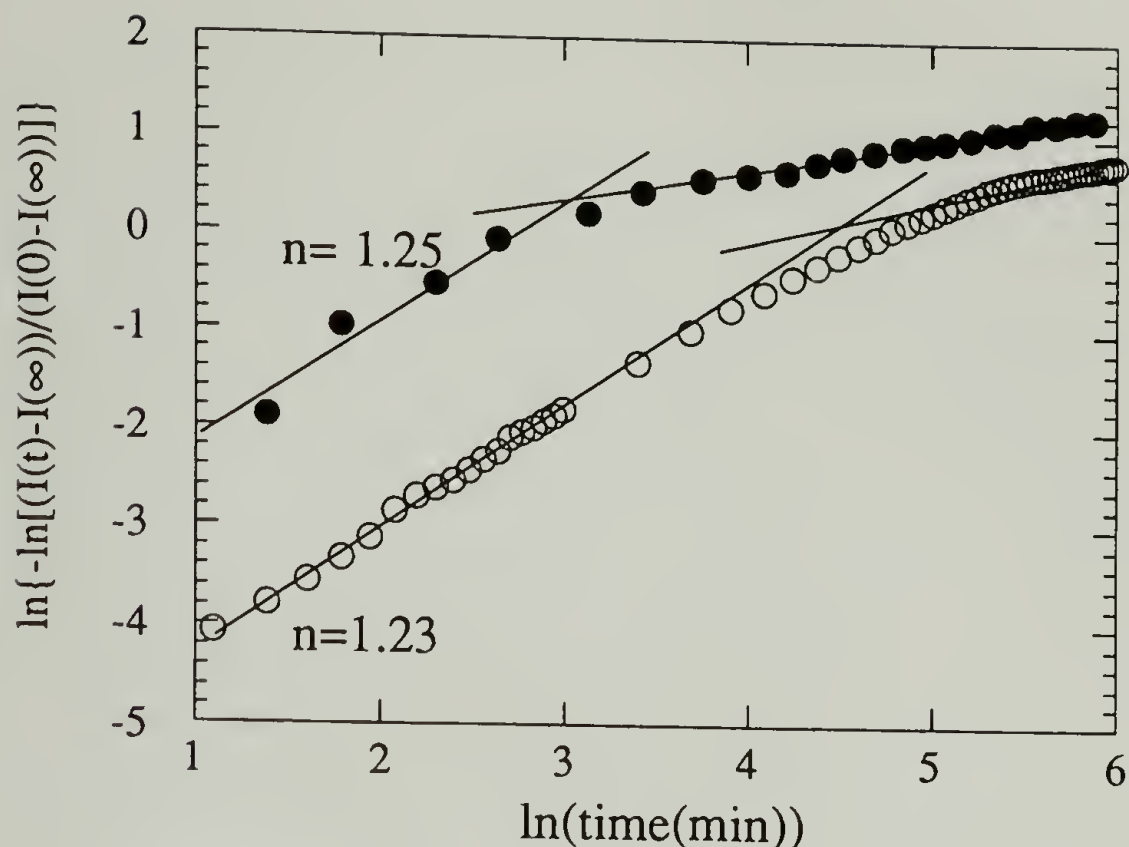


Figure 5.2 Avrami plots of isothermal phase separation kinetics for a 16 nm thick film on gold at 23°C; Experimental results(●); Simulated results (o) using a disk model.

that case, the value is in the range of 1.8-2.0 in the initial stage changing over to 0.6 at later stages. In addition, in this study we found that the value of the first exponent strongly depends on film thickness. It decreases with decreasing film thickness. In addition, we found the ultimate degree of phase separation achievable, i. e. the degree of phase separation at extremely long time, also decreases with film thickness. These results are summarized in Figures 5.3 and 5.4.

#### 5.4 Model Used to Analyze Phase Separation Kinetics

In our study we hypothesize that geometric effects associated with chain stiffness and strong lateral intermolecular interactions should be considered. If the hard segment is

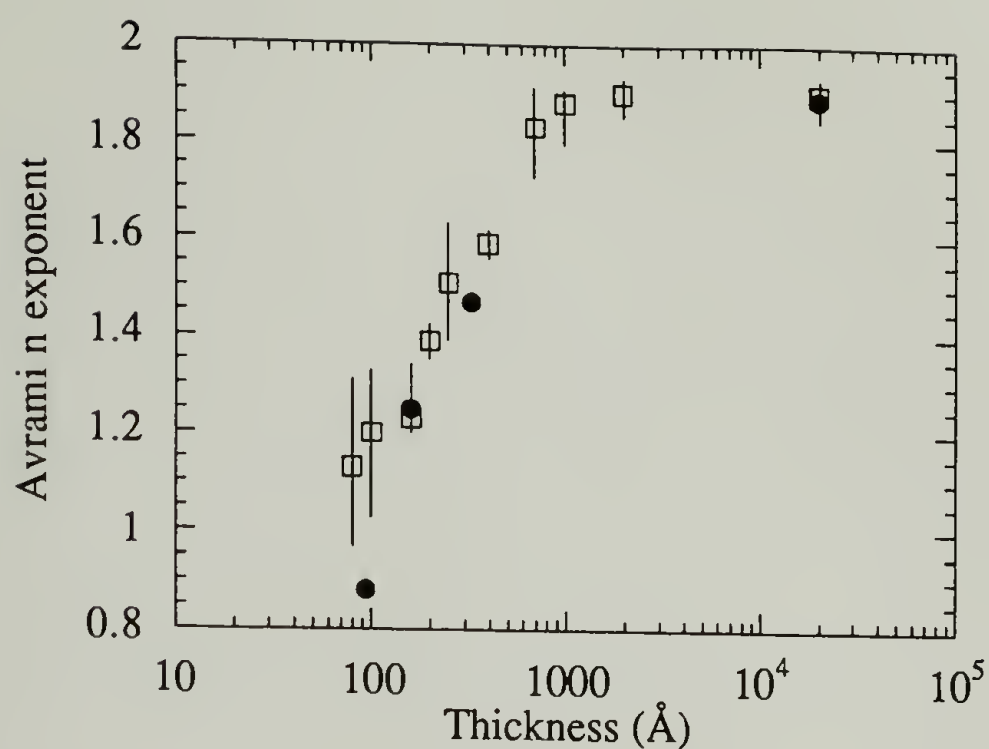


Figure 5.3 Comparison of Avrami exponents as a function of film thickness for B2 polymer at 23°C; Experimental results(●); Simulated results(□) based on a disk model.

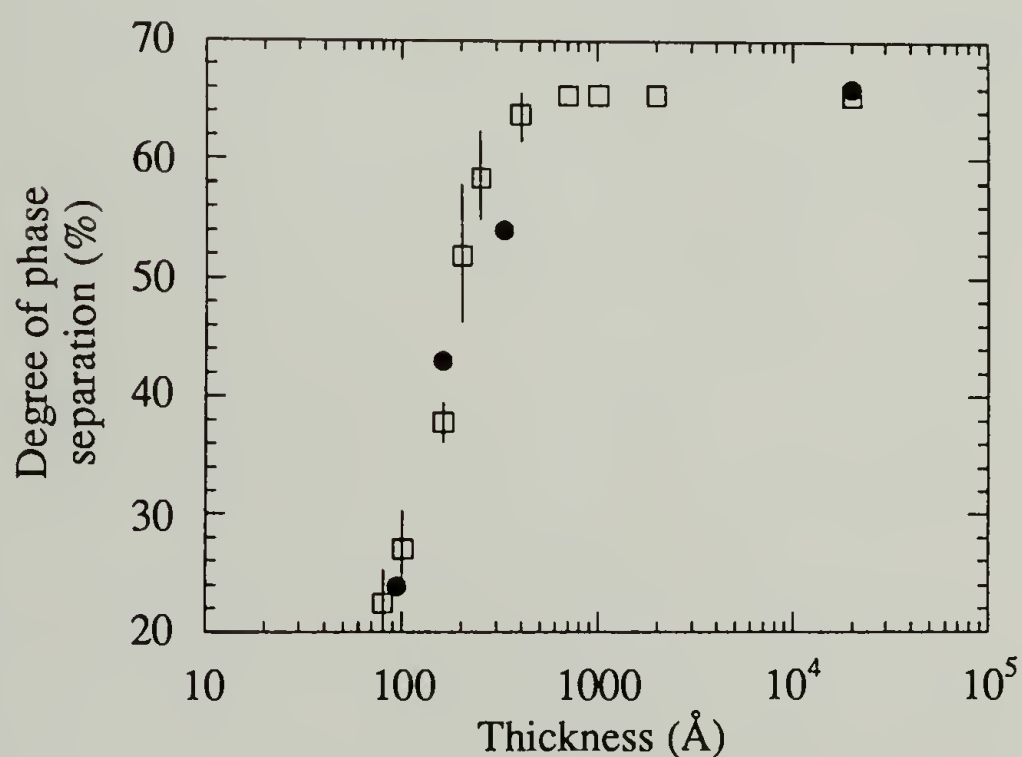


Figure 5.4 Comparison of ultimate degree of phase separations as a function of film thickness for B2 polymer at 23°C; Experimental results(●); Simulated results(□) based on disk model.

fairly flexible, the hard segment rich domains are expected to form isotropic structures such as spheres. In contrast, if the chains are rigid and coupled with strong intermolecular interactions, then disk-like hard segment rich domains are favored to form as suggested earlier.<sup>6</sup> The type of domains formed will result in different kinetics. This is particularly so for phase separation in restricted geometry such as in air-solid interface. It is important to develop a model to explain in a quantitative fashion the kinetics as shown in Figures 5.2 and 5.3. In addition, the dramatic change in the degree of phase separation in ultra-thin film region (Figure 5.4) also needs explanation. Lastly, the anisotropic property of the film formed is an extremely important factor and should be incorporated in the model.

Analytical calculation is difficult to take into account the experimental data described above, therefore a nucleation and growth process incorporating the *Monte Carlo* method is used for simulating the phase separation process. The simulation is off-lattice type and is assumed to proceed in a box with a lateral dimension of 1.5  $\mu\text{m}$  and a variable thickness ranging from 8 nm to 2  $\mu\text{m}$ . The hard segment is taken to be 5 nm in length based on our simulation studies. The domain growth is assumed to be heterogeneous. The chain rigidity of the hard segment is taken into consideration so the disk-like model has been adapted for the growing entity. The location and orientations of *nuclei* are determined by the *Monte Carlo* method. Because these hard segments are assumed to be rigid, not all positions or orientations of the nuclei obtained by the *Monte Carlo* method are acceptable. Given the initial position and orientation of the nuclei at  $t = 0$ , i.e. the first segment, it is possible to monitor concentric cylindrical growth with the center axis being the orientation of the first segment. The sizes of the concentric cylinders at various time are determined by the growth rate constant,  $G$ , and the hard segment concentration in the isotropic phase. There are two parameters,  $G$  and the number of nuclei per unit volume, necessary for our analysis which are determined from the data obtained for the 2  $\mu\text{m}$  and 16 nm thick films. Initial estimates for these two values are fitted to the two exponents measured for a 2  $\mu\text{m}$

thick film. Then the best fit is used to calculate the exponents and the ultimate degree of phase separation for the 16 nm thick film at 20° C. Iterative calculations were carried out until the 2 parameters fit the kinetics data for both the 2  $\mu\text{m}$  and 16 nm films. The determined G value is 25 nm/min and the number of nuclei per unit volume is 1080  $(\mu\text{m})^{-3}$ .

The phase separated domains are allowed to *grow* when additional 10,000 probing points are placed randomly into the box. The volume fraction of phase separated domains,  $X(t)$ , is determined by the fraction of probing points which are located within the domains at a particular cylinder (Figure 5.5).

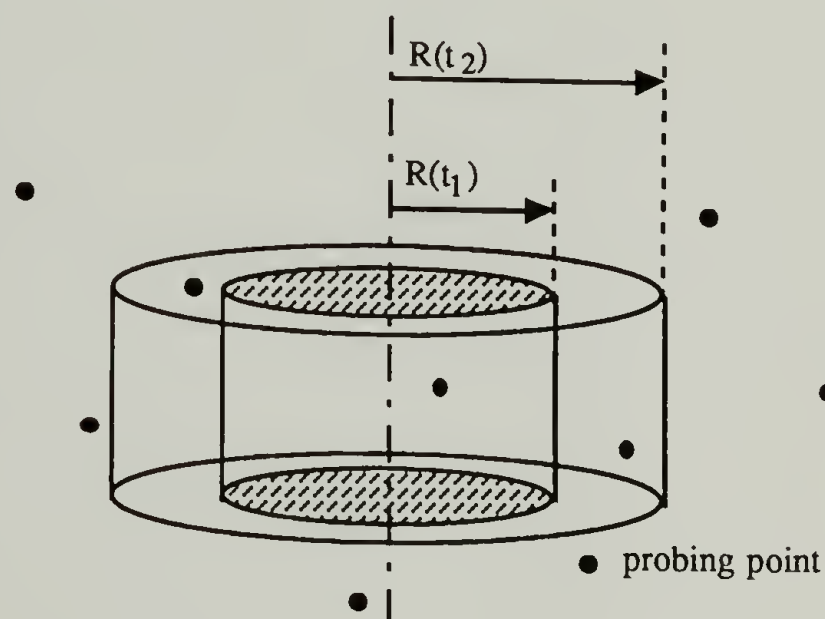


Figure 5.5 Schematic illustration of the domain growth at various time and the measurement of  $X(t)$  by the probing points.

To test whether a probing point falls inside growing entities in order to measure  $X(t)$ , the following algorithms have been used for disk like domain. If the distance from a probing point to the center line of a disk is smaller than the disk radius, and this probing point falls between the two surfaces of the disk, then the probing point is accepted. It is immediately evident that the phase separation rate and Avrami exponent will decrease significantly if the growing domains are on the same order of size as the film thickness because many points



are excluded from further consideration as a function of time. This is shown schematically in Figure 5.6. This factor is extremely important in thin films but negligible for a thick film. In this fashion we have satisfied the experimental observation that high anisotropy has been observed for these films particularly in extremely thin samples.

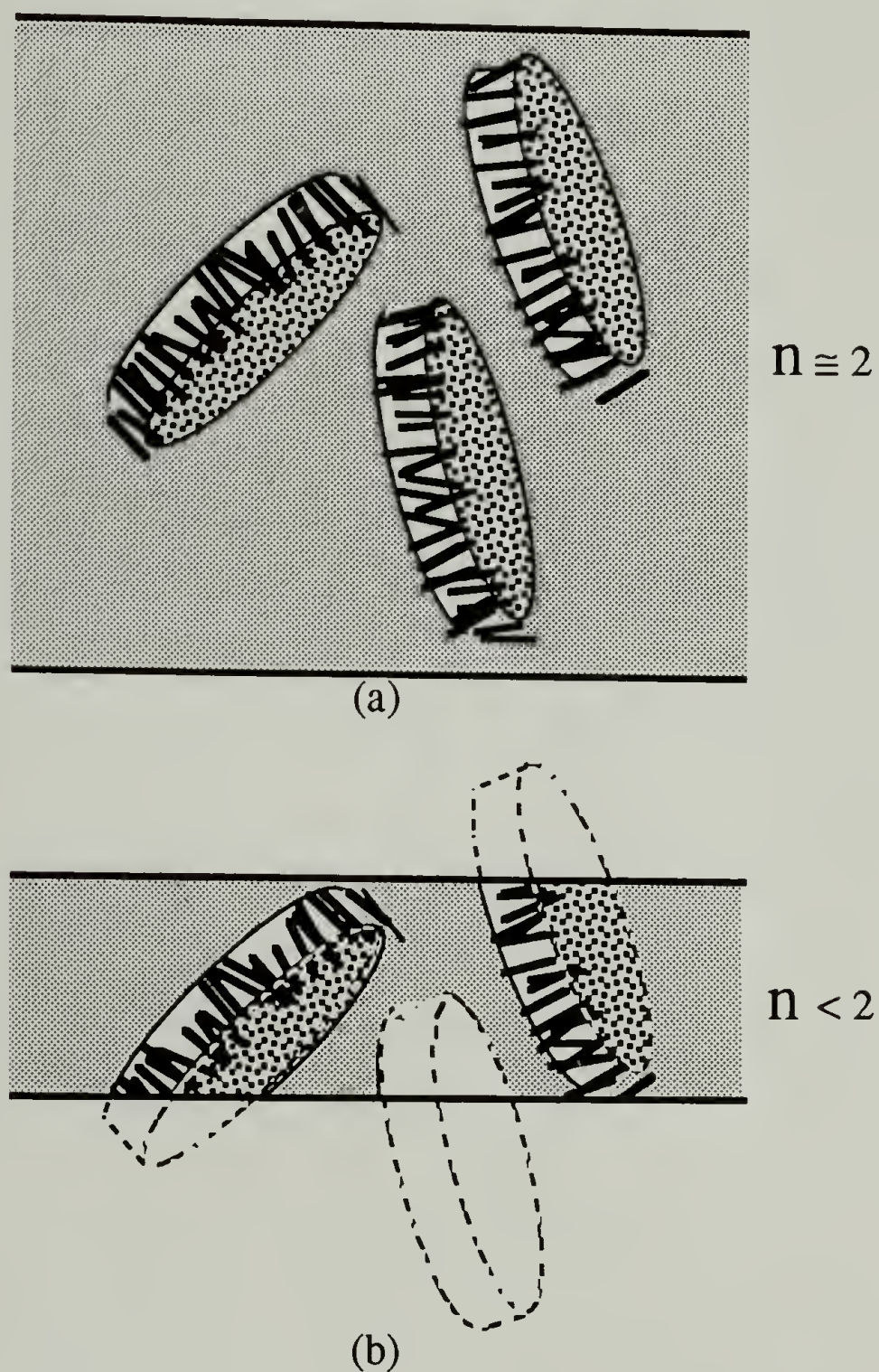


Figure 5.6 Schematic illustration of film thickness effect on phase separation kinetics; (a) Thick film; (b) Thin film which has smaller  $n$  and lower degree of phase separation due to the void part.

Our experimental data whether for bulk or in thin films have always suggested a changing kinetics as a function of time. The phase separation slows significantly at long time. In all cases involving linear growth, the rate only depends on the concentration profile of hard segments in the isotropic phase. This changing kinetics can be seen as follows:

Assuming  $R_g$  is the growth rate of hard domains

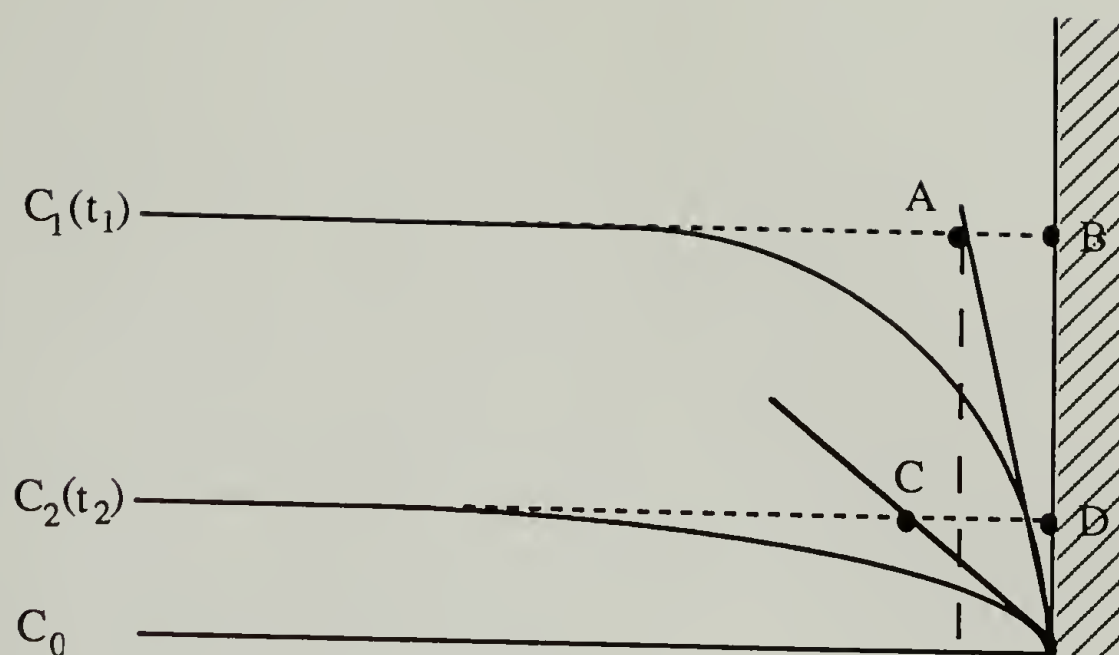
$$R_g(t) = \frac{dV}{dt} = \frac{A(t) \cdot \Delta R(t)}{\Delta t} \quad (5.2)$$

where  $A(t)$  is the active surface area at time  $t$ , and  $\Delta R$  is the hard domain size increment within a small time interval  $\Delta t$ . The driving force for hard segments diffusing toward the hard segment rich domains is the hard segment concentration gradient near the domain surface, which can be expressed as

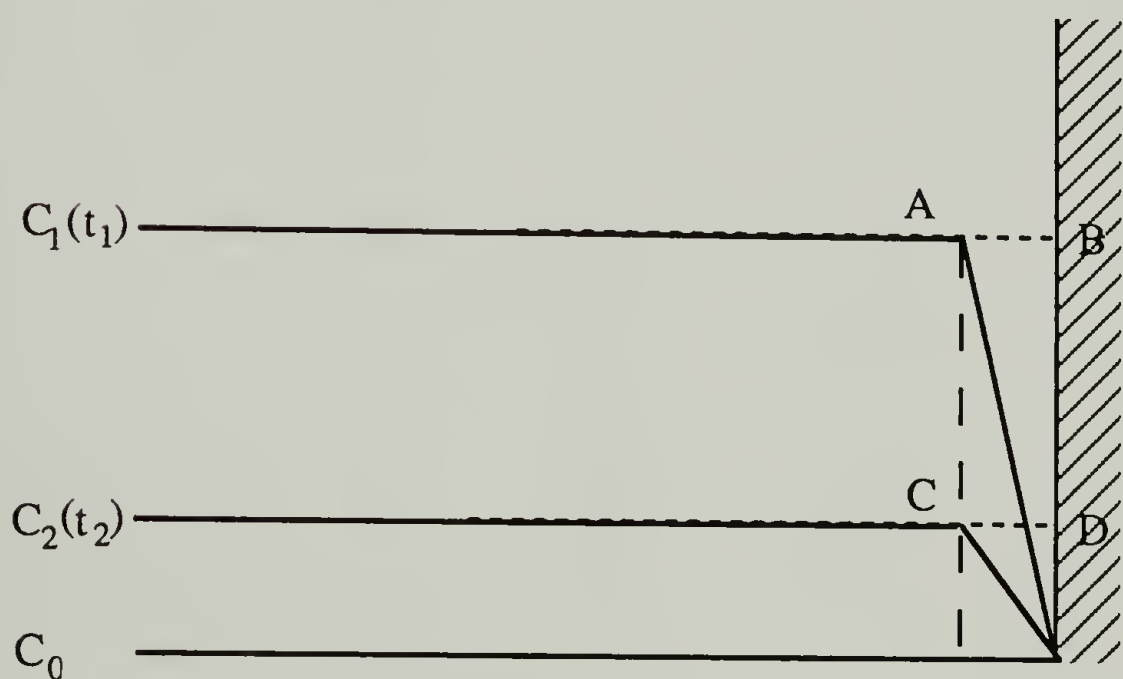
$$R_g = -k \nabla C \big|_{\text{surface}} \quad (5.3)$$

The hard segment concentration profile is shown in Figure 5.7.  $C_0$  is the hard segment equilibrium concentration near the hard domain surface while  $C_1$  and  $C_2$  are the hard segment concentrations in the isotropic phase. Length AB and CD in Figure 5.7 can be defined as the diffusion boundary layer thicknesses at time  $t_1$  and  $t_2$  which increase as the isotropic concentration decreases. To simplify the calculation, the diffusion boundary layer thicknesses AB and CD are assumed to be constant (Figure 5.7b). This assumption is a good one for at least the early stage of phase separation. The phase separation rate can then be expressed as

$$R_g(t) \cong G [ C(t) - C_0 ] A(t) \quad (5.4)$$



(a)



(b)

Figure 5.7 Schematic illustration of the hard segment concentration profile from the hard domain surface to the isotropic phase; (a) Actual profile; (b) Linear concentration profile in the diffusion boundary layer as an approximation used in this simulation.



where  $C(t)$  is the hard segment concentration in the isotropic phase and  $G$  is the rate constant that is assumed to be independent of time. From eqs(5.2) and (5.4), we have

$$\Delta R(t) = G \cdot F_c \cdot \Delta t \quad (5.5)$$

$F_c$  is a concentration factor defined as

$$F_c(t) = C(t) - C_0 \quad (5.6)$$

By definition,  $C(t)$  is the mass of hard segments in the isotropic phase divided by the volume of the isotropic phase at time  $t$ . Then

$$C(t) = \frac{C_T - X(t)}{1 - X(t)} \quad (5.7)$$

where  $C_T$  is the overall hard segment concentration. Combining eqs.(5.6) and (5.7), the concentration factor can be expressed as

$$F_c(t) = \frac{C_T - X(t)}{1 - X(t)} - C_0 \quad (5.8)$$

which can be determined by  $X(t)$  if  $C_0$  and  $C_T$  are known. As can be seen below, the dramatic decrease of  $F_c(t)$  at the later stages of phase separation may cause the changing slope as seen in Figures 5.8 and 5.9.  $C_T$  of B2 polyurethane is 0.32.  $C_0$  is estimated to be 0.14 taken as the hard segment concentration in isotropic phase of a 2  $\mu\text{m}$  B2 polymer film by infrared spectroscopy. This estimation is based on the assumption that hard domains consist of pure hard segments.<sup>6, 19</sup> The exact  $C_0$  value may be slightly different from the ones used in our analysis. Our predictions, however, will not be affected. The impingement effect has been considered but the hindrance of the disk lateral growth blocked by other disk surfaces are ignored due to the low  $C_T$  value. The blocking effect



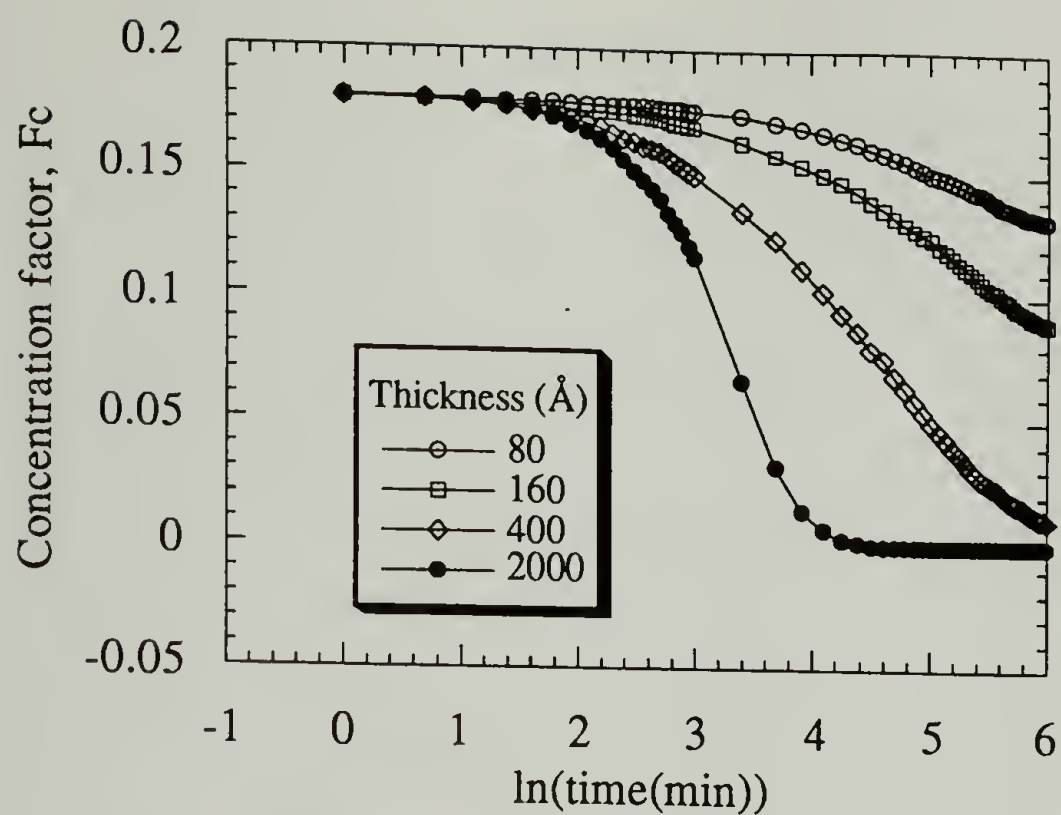


Figure 5.8 Changes in the concentration factor  $F_c$  for different film thicknesses simulated by disk model.

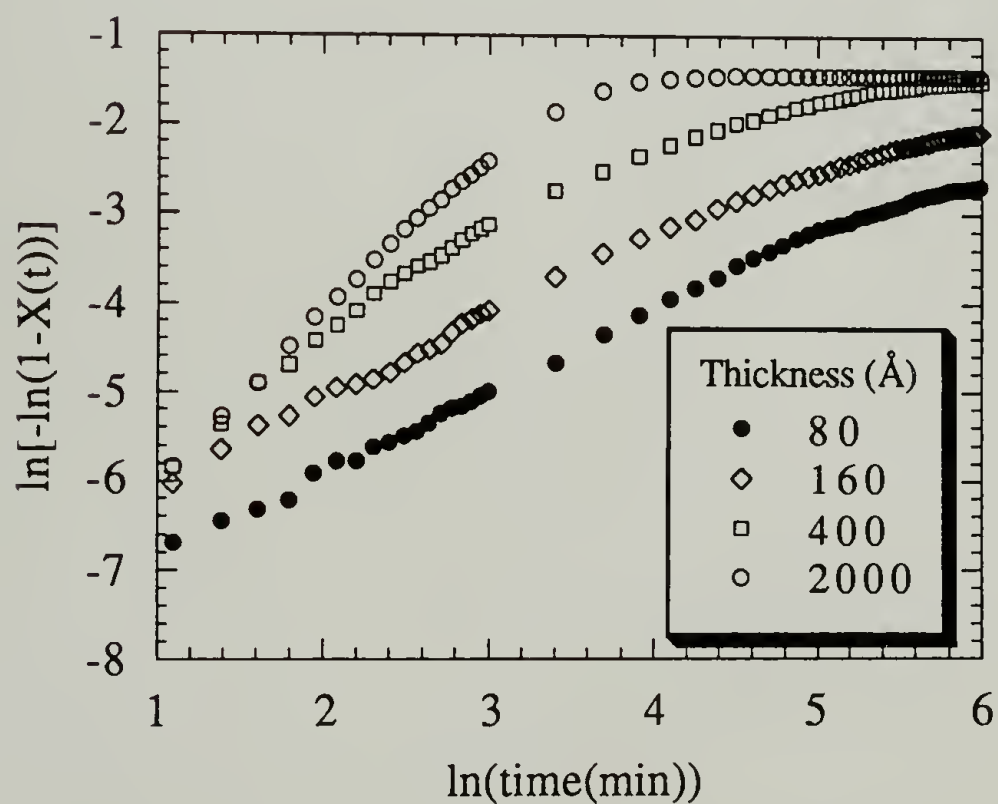


Figure 5.9 Simulated Avrami plots for several film thicknesses for disk model.

will further decrease the exponent  $n$  and the ultimate degree of phase separation. Finally, specific interactions or adsorption of polyurethanes to the supporting surface are neglected.

### 5.5 Comparison of Simulation to Experiment

The simulated kinetics curves of the entire series of films with varying thicknesses are shown in Figure 5.9. All the important features observed in our experiment, i.e. changing kinetics and the degree of phase separation as a function of film thickness, have been reproduced with accuracy. The calculated exponents are summarized in Figure 5.3. The error bars are associated with different random number sequences. These simulated results show that the exponent,  $n$ , starts to deviate from the one measured for the bulk state at a film thickness of  $\sim 10$  times the hard segment length ( $\sim 50$  nm) due the restriction effect of the air/solid interface. The final degree of phase separation is determined by the plateau  $X(t)$  value and is plotted in Figure 5.4. Decrease in the final degree of phase separation is well reproduced by our simulation. We have also clearly shown that having an air/solid interface starts to affect the degree of phase separation if the film thickness is smaller than 10 times the hard segment length. The voids within the film as shown in Figure 5.6b cannot be filled by the growing domains and will result in a lower degree of phase separation and Avrami exponent compared with the thick film case (Figure 5.6a). Obviously, the decrease in the degree of phase separation for thin polyurethane films is kinetically controlled and is a consequence of chain rigidity.

The principal difference between simulation and experiment is that slope change occurs at later time in the calculations than in the experiment (Figure 5.2). This deviation is attributed to the approximation of a constant diffusion boundary layer thickness. Using this approximation will result in a higher diffusion rate in the later stages than the actual case. To obtain better agreement between simulation and experiment, a more exact concentration profile describing the boundary layer thickness change needs to be included.

The initial exponent or the final degree of phase separation calculated will not be affected by this approximation.

## 5.6 Analysis of Structural Anisotropy

Because of chain rigidity, the growth of the hard segment rich domain is restricted to the lateral direction due to the strong cohesive interactions between hard segments. When domains reach to the interface, either air/solid or solid/substrate, no more growth can occur. In thinner films there are fewer possible orientations (virtually all the segments need to be oriented parallel to the surface) for hard segments to be located in the film. Based on the spectroscopic data obtained, we found a very high degree of chain orientation for thin polyurethane films, if the film thickness is of the same order as the hard segment length. Our infrared external reflection experimental data have shown the hard segments of B2 polymer begin to exhibit preferential orientation for films thinner than 32.8 nm, which is ~6 times the hard segment length. We have rationalized this observation as shown below.

Assuming  $L$  is the rigid rod length and  $D$  is the film thickness (Figure 5.10), if the center of the rod is located within a distance  $x$  of the surface which is smaller than  $(L/2)$ , then there exists a minimum  $\theta$  for this rod to be confined within the film with an angle

$$\theta_{\min} = \cos^{-1}\left(\frac{x}{(L/2)}\right) \quad (5.8)$$

With the rod center in this location, the averaged  $\cos^2\theta$  with all allowed orientations is



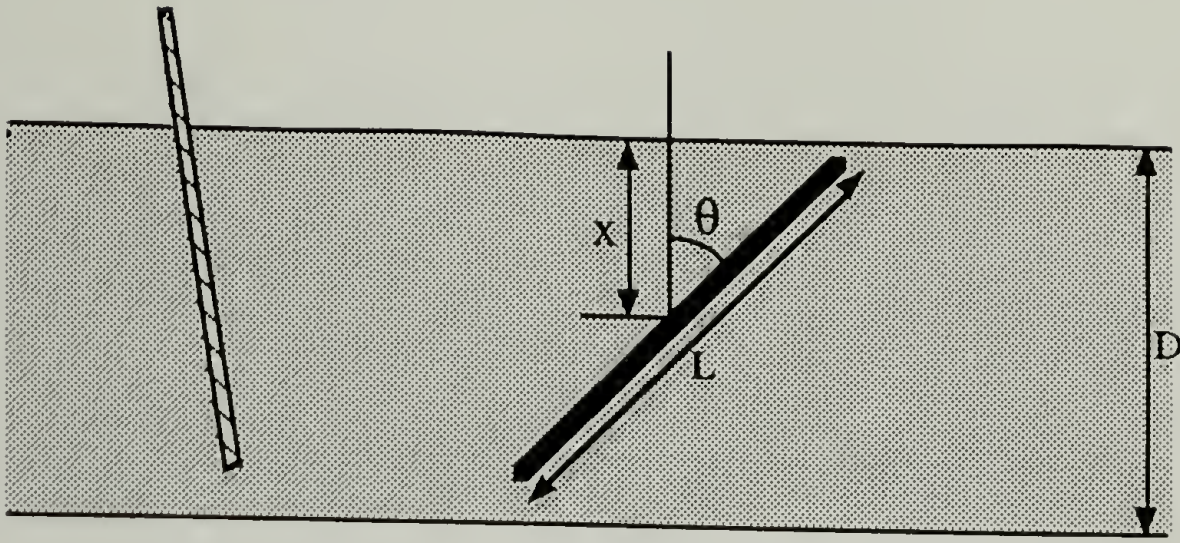


Figure 5.10 Schematic illustration of the preferential orientation effect of hard segment in a ultra-thin film; Dashed rod- forbidden orientation; Solid rod- allowed orientation with geometric variables used in the text.

$$\begin{aligned}
 \langle \cos^2 \theta \rangle &= \frac{\int_{\theta_{\min}}^{\pi/2} 2\pi(L/2)^2 \sin \theta \cos^2 \theta d\theta}{\int_{\theta_{\min}}^{\pi/2} 2\pi(L/2)^2 \sin \theta d\theta} \\
 &= \frac{1}{3} \cos^2 \theta_{\min} \\
 &= \frac{4}{3} \left( \frac{x}{L} \right)^2
 \end{aligned} \tag{5.9}$$

For a film with thickness smaller than the rod length with rod centers randomly distributed inside the film, we have

$$\begin{aligned}
 \langle \cos^2 \theta \rangle &= \frac{\int_0^{D/2} \frac{4}{3} \left( \frac{x}{L} \right)^2 dx}{D/2} \\
 &= \left( \frac{D}{3L} \right)^2
 \end{aligned} \tag{5.10}$$

(  $L \geq D$  )

With eq.(5.10), we can calculate the orientation distribution function,  $f$  as



$$f = \frac{3\langle \cos^2 \theta \rangle - 1}{2}$$

$$= \frac{\frac{1}{3}(D/L)^2 - 1}{2} \quad (L \geq D)$$
(5.11)

For a film thicker than the rod length, we have

$$\langle \cos^2 \theta \rangle = \frac{\frac{1}{9}L + \frac{1}{3}(D-L)}{D}$$

$$= \frac{1}{3} - \frac{2}{9}\left(\frac{L}{D}\right) \quad (D \geq L)$$
(5.12)

which is based on the fact that  $\langle \cos^2 \theta \rangle$  is 1/9 if D equals L (eq.(5.10)) and is 1/3 for the isotropic case. Using eq.(5.12), the orientation function for a film thicker than the hard segment length is

$$f = -\frac{1}{3}\left(\frac{L}{D}\right) \quad (D \geq L)$$
(5.13)

Figure 5.11 clearly shows that for rigid rods confined within two surfaces the preferential orientation of hard segments is high when the film thickness is smaller than 10 times the rod length. This prediction is consistent with our experimental data and *Monte Carlo* simulation results. We can also *safely* define a 'thick film', i.e. a film absent of effects from having constraints from surfaces or interfaces, as having a thickness much greater than 10L. Direct comparison of the orientation functions derived from infrared spectra to the calculated ones is difficult, though, because the exact transition dipole moment direction of the carbonyl groups and the precise hard segment structures need to be determined. These two results, however, show quite consistent trends if we assume that the carbonyl transition dipole moment direction is approximately perpendicular to the chain axis.

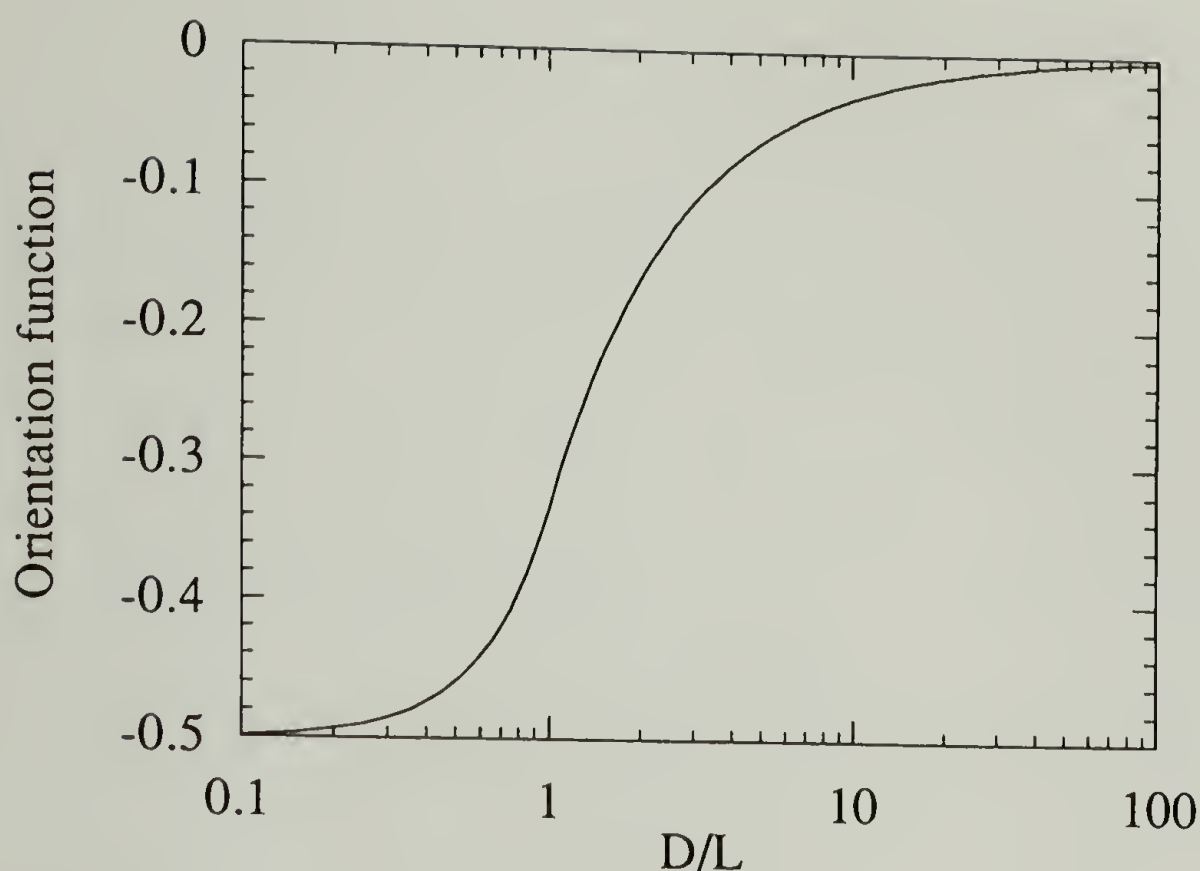


Figure 5.11 Calculated orientation function of rods confined within two surfaces.  $D$  is the film thickness and  $L$  is the rod length.

## 5.7 Conclusions

The relatively slow rate of phase separation, the ultimate degree of phase separation, and the observed high value of chain orientations on the substrate are consequences of having a polyurethane with semi-rigid hard segments. Our reflectance infrared measurements have been used to analyze the phase separated structures in thin films. The phase separation obeys an *Avrami* type rate process. From this, the growth rate constant can be obtained. Then using a *Monte Carlo* simulation method to fix the location and orientation of the points, the process can be modeled using two parameters, the growth rate alluded to above, and the number density of nuclei. We conclude that the hard segment rigidity is very important and it might be the dominating driving force for phase separation

for the B2 polymer. For longer hard segments it may not be able to keep the whole chain from bending but the chain rigidity should still dominate the phase separation process. Finally, this work clearly demonstrates that the phase separation behavior and the domain size of polyurethanes in the ultra-thin film region differ significantly from its bulk state. Their differences in other physical properties are also expected.

## References

- (1) Petrovic, Z. S.; Ferguson, J. J. *Prog. Polym. Sci.* **1991**, *16*, 695.
- (2) Hepburn, C. *Polyurethane elastomers*; Applied Sciences Publishers: London, 1982.
- (3) Koberstein, J. T.; Leung, L. M. *Macromolecules* **1992**, *25*, 6205.
- (4) Koberstein, J. T.; Stein, R. S. *J. Polym. Sci., Polym. Phys. Ed.* **1983**, *21*, 1439.
- (5) Li, Y.; Ren, Z.; Zhao, M.; Yang, H.; Chu, B. *Macromolecules* **1993**, *26*, 612.
- (6) Tao, H.-J.; Hsu, S. L.; MacKnight, W. J. *Polym. Prepr., (Am. Chem. Soc., Div. Polym. Chem.)* **1992**, *33*(2), 575.
- (7) Tao, H. J.; MacKnight, W. J.; Hsu, S. L., *Macromolecules*, in press.
- (8) Meuse, C. W.; Yang, X.; Yang, D.; Hsu, S. L. *Macromolecules* **1992**, *25*, 925.
- (9) Lee, H. S.; Wang, Y. K.; MacKnight, W. J.; Hsu, S. L. *Macromolecules* **1988**, *21*, 270.
- (10) Helfand, E. *J. Chem. Phys.* **1975**, *63*, 2192.
- (11) Yoon, D. Y.; Flory, P. J. *Macromolecules* **1984**, *17*, 868.
- (12) Theodoro, D. N. *Macromolecules* **1988**, *21*, 1411.
- (13) Theodoro, D. N. *Macromolecules* **1988**, *21*, 1422.
- (14) Stein, R. S.; Powers, J. J. *Polym. Sci.* **1962**, *56*, S9.
- (15) Escleine, J. M.; Monasse, B.; Wey, E.; Haudin, J. M. *Colloid Polym. Sci.* **1984**, *262*, 363.
- (16) Billon, N.; Escleine, J. M.; Haudin, J. M. *Colloid Polym. Sci.* **1989**, *267*, 668.
- (17) Christenson, C. P.; Harthcock, M. A.; Meadows, M. D.; Spell, H. L.; Howard, W. L.; Creswick, M. W.; Guerra, R. E.; Turner, R. B. *J. Polym. Sci., Polym. Phys. Ed.* **1986**, *24*, 1401.
- (18) Wunderlich, B. *Macromolecular Physics*; Academic Press: New York, 1976; pp chapter 6 .
- (19) Kornfield, J. A.; Spiess, H. W.; Nefzger, H.; Eisenbach, C. D. *Macromolecules* **1991**, *24*, 4787.



## CHAPTER 6

### SPECTROSCOPIC STUDY OF THE CHAIN CONFORMATION CHANGES OF A BIO-DEGRADABLE POLYESTER ELASTOMER, POLY( $\beta$ -HYDROXYOCTANOATE), DURING THE PHASE TRANSFORMATION AND MECHANICAL DEFORMATION PROCESSES.\*

#### 6.1 Introduction

Poly( $\beta$ -hydroxyoctanoate) (PHO) is a polyester produced by bacteria *Pseudomonas oleovorans* which grow on sodium octanoate or octane as the carbon source under limited nutrient or a lack of oxygen condition.<sup>1-3</sup> The polymer is accumulated as intracellular granules as the energy storage materials in response to this sort of environmental stress making them inherently biodegradable. The resultant polyester is a random copolymer rather than a homopolymer because the metabolism of the bacteria can either add or cleave off two carbons from the food source molecules. The structure and composition of PHO are shown in Figure 6.1. This polymer is isotactic due to the absolute [R] configuration of the chiral carbons (Figure 6.1) making them to be crystallizable. However, the degree of crystallinity is only about 30% due to the random copolymer nature.<sup>4</sup> These crystalline domains act as physical crosslinks for the rest of non-crystalline, low  $T_g$  ( $-35^\circ\text{C}$ ) chains resulting in its thermoplastic elastomer feature.

---

\* PHO was prepared by Dr. K. D. Gagnon.

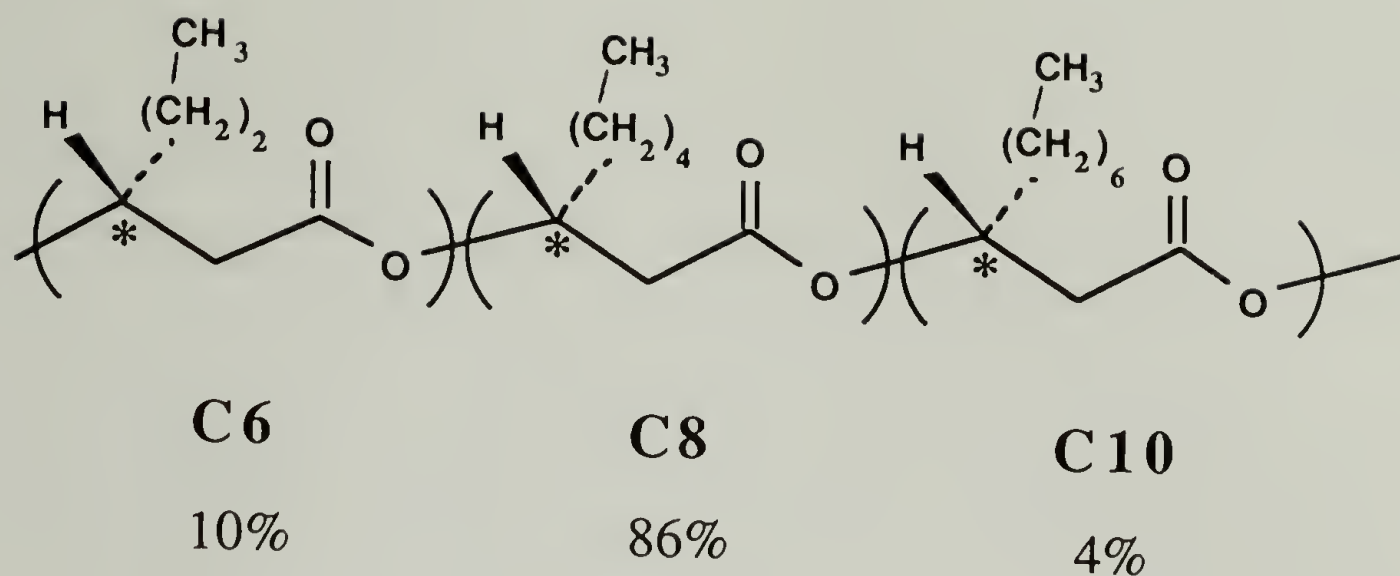


Figure 6.1 Chemical structure of bacterially produced poly( $\beta$ -hydroxyoctanoate), PHO, random copolyester. Carbons with \* are the chiral centers.

PHO will crystallize as a  $2_1$  helix in an orthorhombic lattice with two molecules per unit cell.<sup>4</sup> The side chains were proposed to form ordered sheets with extended conformation in the crystalline structure.<sup>4</sup> The fiber repeat is 4.55Å which is smaller than poly( $\beta$ -hydroxybutyrate) (PHB), 5.96Å, and poly( $\beta$ -hydroxyvalerate) (PHV), 5.56Å. This collapse in c dimension has been postulated to be driven by changes in side chain packing.<sup>4</sup> The crystallization rate of PHO is extremely slow.<sup>1-5</sup> The low degree of crystallinity and the slow crystallization rate are directly attributable to the random nature of the main chain sequence as well as the long side chains.

PHO possesses very high permanent tensile set under deformation.<sup>1,2</sup> For example, the tensile sets are 40%, 80% and 230% for PHO under strains of 100%, 150% and 300%, respectively.<sup>1,2</sup> This behavior limits its applicability as a practical thermoplastic elastomer. The permanent tensile set have been attributed to either a change in sample crystallinity or to strain-induced side chain crystallization.<sup>1,2</sup> However, without a convincing way to characterize the chain conformational change, it is difficult to confirm these conjectures.

In this study, we utilized Fourier transform Raman spectroscopy as the principal tool to analyze chain conformation. It is known that Raman active vibrations are extremely sensitive to the changes in chain conformation because of the large polarizability changes expected for the C-C bonds along either the main or side chains. Because quantitative structural information are needed, we have also carried out normal vibrational analyses in conjunction with our experimental result. Generally speaking, a detailed normal vibrational analysis can describe the nature of the normal vibrations, their frequencies, and density of states. Furthermore, most computer programs in literature are really capable of calculating only one specific chain conformation. In this study, we have adopted the computer programs developed by Snyder and his co-workers which would yield both frequency and band intensity for an assembly of disordered chains. The dihedral angles along the chain for each conformation are generated according to the statistical weights calculated using the relative energy of individual rotational isomeric state. The composite spectrum obtained makes it possible to investigate the conformational distribution change of PHO side chains during the crystallization and when being deformed. Our results are reported here.

## 6.2 Experimental Section

The bio-synthetic procedure of PHO and its characterization have been described previously.<sup>1-7</sup> For deformation experiments, PHO which crystallized at 5°C for 36 days was cut to 2 cm by 2 mm stripes with thickness of 1mm. The sample was stretched with a stretcher and kept for 10 min at several elongation ratios. After releasing the stress, the permanent tensile set was recorded.

Raman spectra were obtained on a Bruker 88 Fourier transform Raman bench with laser excitation provided by a Nd:Yag laser (1064 nm) in the near-infrared region. Incident



laser power was maintained at 300mW. Typically, 2000 scans were coadded to achieve an acceptable single-to-noise ratio. All the spectra were obtained with a backscattering geometry. Spectral resolution was maintained at  $4\text{ cm}^{-1}$ . Curve deconvolution was carried out with the software *LAB CALC* (Galactic Ind. Corp.). For the long term phase transformation study, PHO was loaded into the sample die and was heated at  $100^{\circ}\text{C}$  under vacuum for two hours. After cooling to room temperature, the Raman spectrum was taken and was named as "Day 1". Generally each experiment takes 2 hours. There is no evidence that sample changed after being irradiated by the laser beam. After recording each spectrum, individual sample was sealed in a bottle with anhydrous calcium sulfate to keep it dry. Then the sample was kept under  $5^{\circ}\text{C}$  till the next experiment. The induced anisotropy of deformed PHO samples did not affect the isotropic Raman spectra obtained.

Optical circular dichroism (CD) was performed on AVIV 62DS (AVIV Associates, Inc.) equipped with xenon arc lamp and  $\text{MgF}_2$  linear polarizer. Photoelastic modulator (PEM) was operated at 50 kHz. Spectra were taken for the 175 - 400 nm region. PHO samples were casted on the external surface of a 1mm thick quartz cell from a 2% chloroform solution. The solution was filtered with a  $0.2\text{ }\mu\text{m}$  disposable syringe filter. The casted sample film was heated at  $100^{\circ}\text{C}$  for two hours before the spectrum was recorded. The sample storage procedure was the same as used in the Raman study. For each scan the spectral resolution was maintained at 0.5 nm. The averaging time was 5 seconds for each point.

### 6.3 Computational Methods

Normal coordinate calculation for the isotropic Raman spectrum of an assembly of disordered chains was performed with a program written by Snyder and his coworkers. The procedure has been published earlier<sup>8,9</sup> and is briefly summarized as follows. The



intensity of isotropic Raman spectrum,  $I_{iso}(\nu)$ , is determined by scattering activity,  $S(\nu)$ , and a Boltzman factor,  $B(\nu)$ , shown below

$$I_{iso}(\nu) = S(\nu)/B(\nu) \quad (6.1)$$

$$B(\nu) = \nu[1-\exp(-h\nu/kT)] \quad (6.2)$$

where  $\nu$ ,  $h$ ,  $k$  and  $T$  are the vibrational frequency, Planck constant, Boltzman constant, and absolute temperature, respectively. The scattering activity for isotropic Raman spectrum of an assembly of disordered chains was approximated by

$$S(\nu) = \sum_{M=1}^{M_T} S^M(\nu) \quad (6.3)$$

where  $S^M(\nu)$  is the scattering activity of random conformer  $M$  generated by Monte Carlo method, and  $M_T$  is the number of conformers in the ensemble.  $S^M(\nu)$  is calculated by bond polarizability model<sup>9</sup> according to the following expression

$$S_k \propto \left[ \sum_i L_{ik}^R + D \sum_j L_{jk}^\omega \right]^2 \quad (6.4)$$

where  $S_k$  is scattering activity of normal mode  $k$ ,  $L_{ik}^R$  is the normal-coordinate element for the  $i$ th CC stretching (R) internal coordinate, and  $L_{jk}^\omega$  is that for the  $j$ th CCC bending ( $\omega$ ) coordinate.  $D$  in eq.(6.4) is the intensity parameter which is defined as the ratio of mean polarizability derivatives for CCC bending to CC stretching. The intensity parameters for all the backbone CC bonds and CCC angle bendings are assumed to be identical and have been taken to be conformationally invariant. The intensity contribution from C-H stretching and C-C torsion are ignored because we are principally interested in the skeletal modes in the 700-1000  $\text{cm}^{-1}$  region.<sup>8,9</sup> Snyder's method has been demonstrated previously to successfully reproduce the vibrational spectra of several n-alkanes.<sup>8,9</sup> As an

example, the calculated isotropic Raman spectrum of n-hexane and the experimental data are shown in Figure 6.2. Both frequencies and relative intensity of these skeletal vibrations have been reproduced well. All the parameters used in this example have been published previously.<sup>8,9</sup>

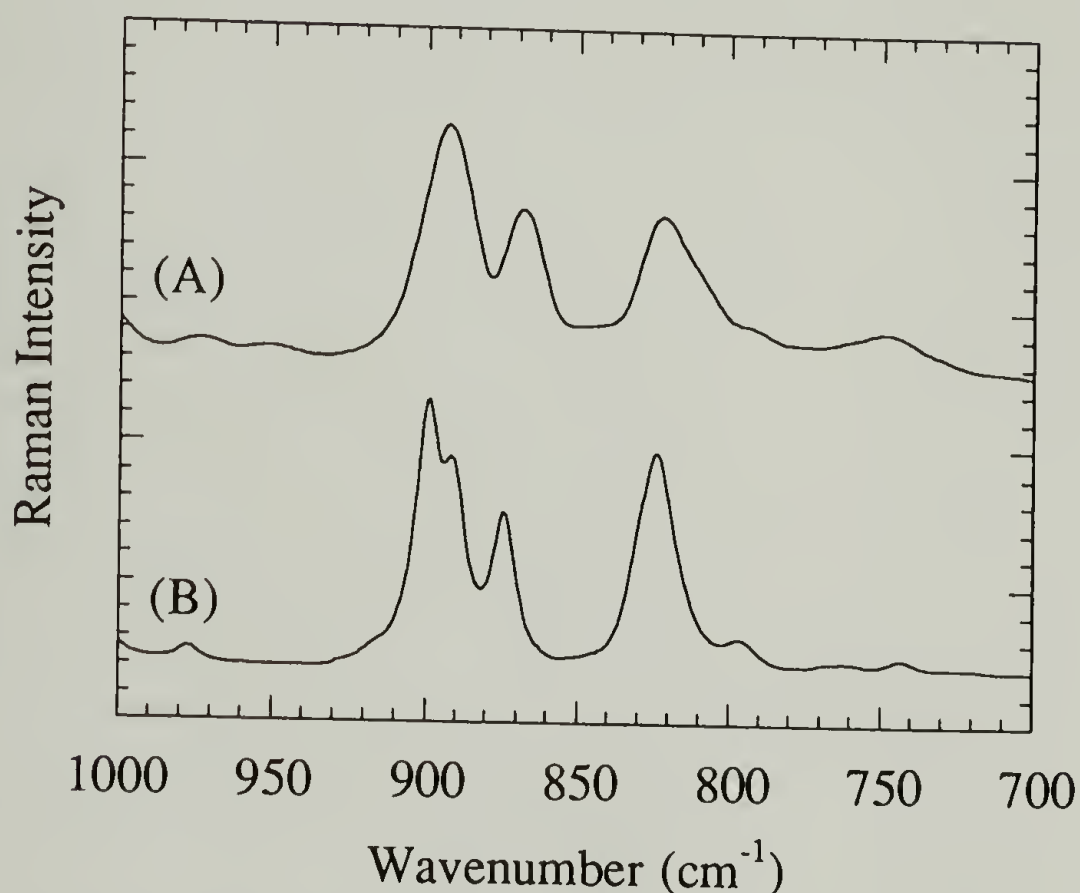


Figure 6.2 Isotropic Raman spectra of n-hexane: (A) Measured FT-Raman spectrum, and (B) calculated spectrum with energy difference of 800 cal/mol between trans and gauche states. 500 conformers were generated for this calculation.

Our objective is to calculate Raman active skeletal vibrations assignable to PHO side chains in order to characterize their conformations. We used the model structure shown in Figure 6.3 as an approximation for PHO side chains. The perturbative effects associated with coupling to the main chain is implicitly incorporated in the effective masses used for the atoms which are attached to the main chain (atoms 2 and 3 in Figure 6.3). The force constants for the model structure are assumed to be unaffected. Therefore, force constants

for aliphatic ether compounds have been used in our analysis.<sup>10</sup> The choice of the effective mass for atoms 2 and 3 are somewhat arbitrarily. In our analysis, the effective mass of atom 2(20 amu) was taken to be  $[(\text{atom } 2 + \text{atom } 6 + \text{atom } 7) + (\text{atom } 5)/2]$ . The effective mass for atom 3(22 amu) was taken as  $[\text{atom } 3 + (\text{atom } 4)/2]$ . Different values chosen for the effective mass of atoms 2 and 3 will shift the calculated frequency and intensity in the skeletal modes somewhat but not significantly.

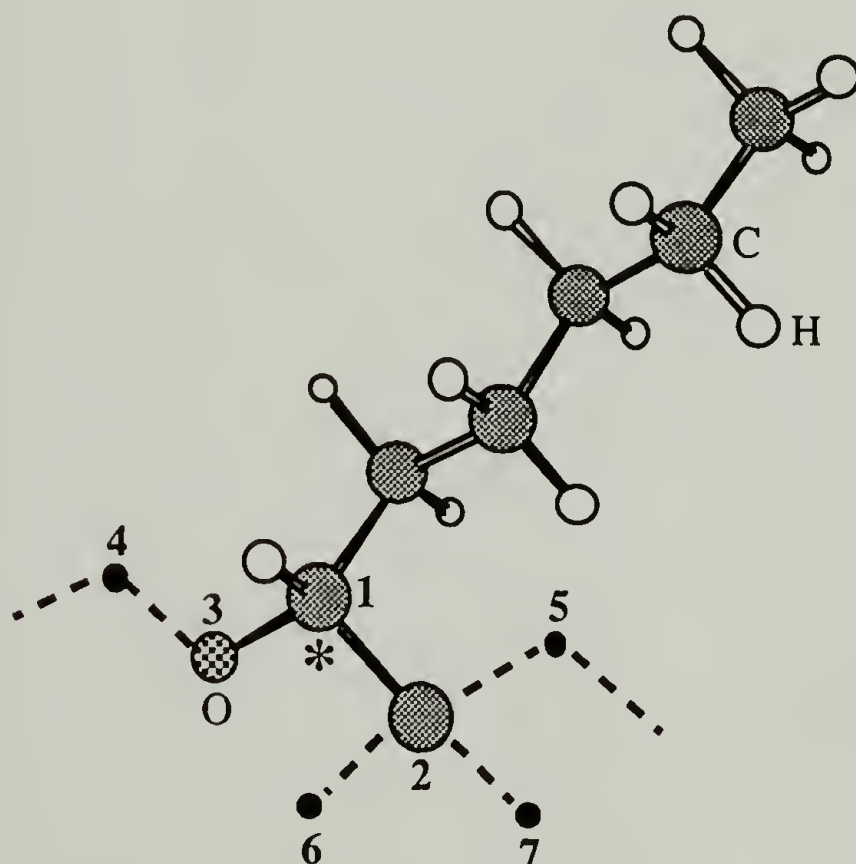


Figure 6.3 Stereochemical representation of the model structure of PHO side chain used in the normal coordinate analysis. Dashed lines and solid spots are used to illustrate the main chain position and are not included in the model structure. Carbons with \* are the chiral centers.

We are interested in the composite spectrum for an ensemble of chains with different chain conformations. We have utilized Flory's rotational-isomeric-state (RIS) model, with one trans and two gauche states.<sup>11</sup> 2000 conformers were generated for

vibrational analysis. The relative population for each conformation is determined by the following condition

$$W^M = n_s^M \exp(-E^M/RT) \quad (6.5)$$

where  $W^M$  is the weight for a particular conformer,  $n_s^M$  is its statistical weight and  $E^M$  is its energy with the all-trans conformation as the zero point. Its value is calculated by

$$E^M = n_G E_G + n_{GG^*} E_{GG^*} \quad (6.6)$$

In equation 6,  $n_G$  is the total number of gauche bonds and  $n_{GG^*}$  is the number of  $GG^*$  pair.  $E_G$  and  $E_{GG^*}$  are the corresponding energies.<sup>11</sup> Pentane effect for the steric hindrance of  $GG^*$  conformation has been taken into consideration.<sup>11</sup> The dihedral angles for the trans and gauche states were taken to be  $180^\circ$  and  $67^\circ$ , respectively. A variation of  $10^\circ$  was used to allow some fluctuations about the local energy minima to incorporate the internal-rotation broadening effect.<sup>8</sup> For each conformer, the dihedral angles were assigned by Monte Carlo method based on the probability of RIS model.<sup>8,9</sup> The population distribution for T, G, and  $G^*$  can be adjusted by changing the energy differences.

Force constants were automatically picked up in a force constant library by checking the atomic type of each atom and its local geometry for each conformer. To calculate relative band intensity, specific parameters related to polarizability changes were adopted from previous studies of n-alkanes.<sup>8,9</sup> We have assumed that the ester unit on the backbone will not change the polarizability derivatives of the aliphatic side chains significantly. The intensity parameters and their corresponding vibrational modes have been published previously.<sup>9</sup> The spectra were constructed by the histograms of scattering power at the frequency region of interest with interval of  $2 \text{ cm}^{-1}$ . A Lorentizan line shape



with bandwidth (FWHM, full width at half maximum) of  $8\text{ cm}^{-1}$  was used for each peak in the histogram. Then spectra including temperature effect were calculated using eq.(6.2).

Finally, molecular simulation was utilized to calculate the contour energy map of a PHO chain repeat using *POLYGRAF* (Molecular Simulations, Inc). Dreiding II force field<sup>12</sup> was used and the electrostatic charges were calculated by the Gasteiger method.<sup>13</sup> Each dihedral angle was varied from  $0^\circ$  to  $360^\circ$  with a  $6^\circ$  increment. Conjugate-gradient method was employed for minimizing energy. Typically, the incremental decrease of the overall energy term per step is less than  $0.1\text{ (kcal/mol)/\AA}$  within 300 steps.

## 6.4 Results and Discussion

**1. Characterization of Chain Conformation.** The principal objective of this study is to evaluation the structural changes of these biodegradable polyesters induced by thermal annealing and during mechanical deformation. The carbonyl stretching region was found to be an appropriate region to monitor the PHO main chain conformational change. Figure 6.4 is the FT-Raman spectra of PHO during the thermal annealing process in the carbonyl stretching region. There are two distinct bands located at  $1742$  and  $1731\text{ cm}^{-1}$ . These 2 components cannot be assigned to crystal field splitting since strong specific intermolecular interactions do not exist. Infrared spectroscopy shows that only negligible amount of residual hydroxy groups in PHO were found. Therefore this splitting is not caused by hydrogen-bonding. In previous Raman study on other ester compounds, similar doublet has been observed and was assigned to different carbonyl groups dispersed in the amorphous and in crystalline phases.<sup>14,15</sup> The lower frequency band is assigned to the crystalline state while the higher one is for amorphous phase.<sup>14,15</sup> The PHO main chain has  $2_1$  helical conformation in the crystalline state.<sup>4</sup> Therefore we have assigned the  $1742$  and  $1731\text{ cm}^{-1}$  components to be associated with carbonyl groups for disordered and

helical chains, respectively. The relative intensity of these two bands can be used to monitor the change in crystallinity even though their absolute amounts are difficult to evaluate.

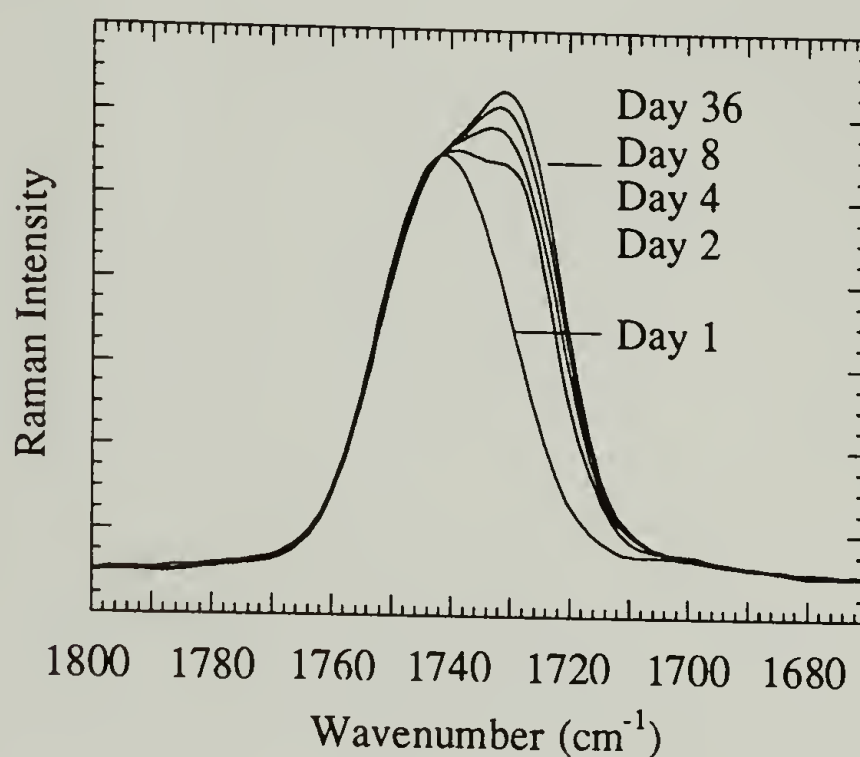


Figure 6.4 Variation of the carbonyl stretching region for PHO crystallization process measured by FT-Raman spectroscopy. Time increases from bottom to top. All of the spectra have been normalized with respect to the  $1742\text{ cm}^{-1}$  intensity.

Figure 6.4 clearly shows that even though most of the crystallization occurs within one week, the process continues for a long period of time at a slower rate. Furthermore, another conformation sensitive region in  $1200\text{--}700\text{ cm}^{-1}$  are depicted in Figure 6.5. From changes in  $870$  and  $1100\text{ cm}^{-1}$  bands in Figure 6.5, it also can be shown that the chain conformation keeps changing even after 36 days. The observed slow crystallization process is consistent with the previous DSC study.<sup>1,2,14,15</sup> These data are inconsistent with previous WAXS and solid NMR studies which indicated that the crystallization process could be completed within a period, as short as 6 hours.<sup>4</sup> The discrepancy may be

attributed to sensitivity limitation of these methods. To assure that the changes in the carbonyl stretching region can really be correlated to changes in main chain conformation, we have also conducted a circular dichroism study.

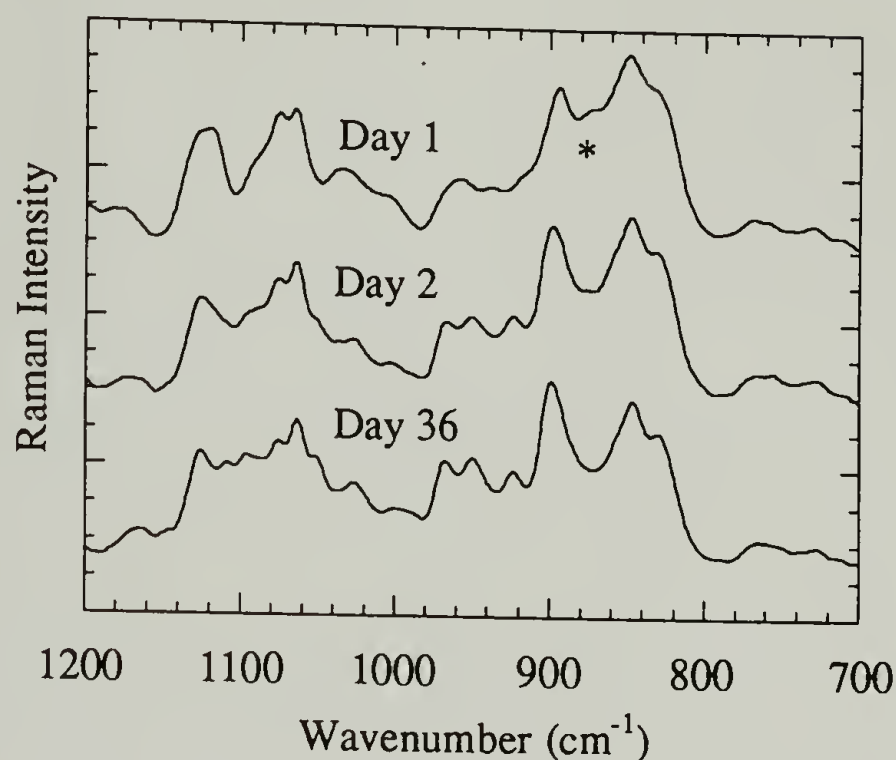


Figure 6.5 Variation of FT-Raman spectra in the region of 700-1200  $\text{cm}^{-1}$  for PHO phase transformation process. The position with \* is one of the side chain skeletal mode band which is sensitive to its conformation.

Circular dichroism (CD) absorption can occur from an asymmetric secondary structure and is known an extremely sensitive tool to monitor the chain conformation change.<sup>16</sup> The optical activity study of PHB and similar compounds were well documented and those results could be used to assign the bands observed for PHO.<sup>17-20</sup> For amorphous PHO, there is a weak CD band locating at 220 nm which is due to the Cotton effect of ester  $n \rightarrow \pi^*$  transition. This feature is shown in Figure 6.6 for the Day 1 curve. The strong ester  $\pi \rightarrow \pi^*$  transition occurs at a wavelength which is lower than the instrument detection limit so it cannot be observed for amorphous PHO. On the other hand, when PHO crystallizes, some of its ester main chains change their conformations to



the left-handed  $2_1$  helix. This asymmetric helical structure will split the ester  $\pi \rightarrow \pi^*$  transition into two peaks with opposite signs.<sup>16,21</sup> The CD spectrum for semi-crystalline PHO clearly shows this splitting (only half of the splitting was detected due to the detection limit). The intensity of this band can be correlated to the degree of phase transformation. Figure 6.6 shows that the crystallization process last for a very long time even though most of the crystallization does occur in the first week. This result is consistent with our Raman finding and the previous DSC observation. Thus the relative intensity of carbonyl stretchings are directly related to the different main chain conformation and can be used to monitor the crystallization process.

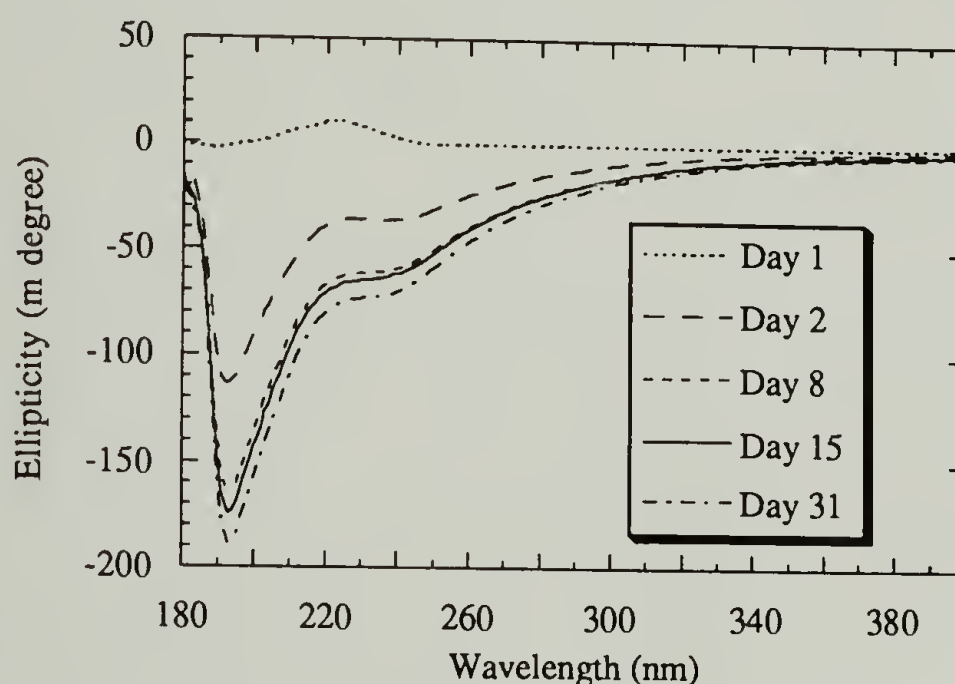


Figure 6.6 Variation of optical circular dichroism for PHO phase transformation process. Time increases from top to bottom.

The preferred  $2_1$  helix associated with main chain conformation of PHO is well established. In contrast, the conformation distribution of side chains is far from clear. Previous solid state NMR study revealed that the conformation of PHO side chains can be different depending on the degree of crystallinity of the sample.<sup>4</sup> Wide angle X-ray diffraction results have suggested that side chains may form ordered sheets with extended



structure in crystalline regions.<sup>3,4</sup> Nevertheless, a convincing structural assignment regarding PHO side chains was never achieved. Raman spectroscopy is particularly suitable for studying chain conformations, especially using the skeletal vibrations( C-C stretching or CCC angle bending vibrations ) in the 800-1000  $\text{cm}^{-1}$  region. Characteristic bands for ester groups on the main chain are expected to be located at 850 and 960  $\text{cm}^{-1}$  . Based on the methyl propionate study, these bands are assignable to ester CC stretching and C-O stretching, respectively.<sup>14</sup> As can be seen from the Raman spectra shown in Figure 6.2, the 870-900  $\text{cm}^{-1}$  region is a suitable region for monitoring side chain conformation without complications from Raman active vibrations associated with the main chain band.

The two bands in the region of 870-900  $\text{cm}^{-1}$  (Figure 6.5) are deconvoluted out from the original spectra using curve fitting technique (A-2 and B-2 in Figure 6.7). To characterize this region, we conducted a normal coordinate calculation for the PHO side chain. We have generated two types of side chains. First, using rotational-isomeric-state model, we generated 2000 random conformers based on the statistical weight for each individual state. In addition, the program allows the possibility to calculate a chain of specific chain conformation, in this case, one with planar zigzag fully extended structure. The population statistics of the generated 2000 random conformers are adjusted to match the experimental result (Figure 6.7A-2). The composite spectrum with overall 80.93% trans structures turns out to be very close to the experimental observation (Figure 6.8A). The detail population statistics is listed in the inset of Figure 6.8A. Furthermore, the calculated Raman spectrum for fully extended side chain is shown in Figure 6.8B. From this calculation it clearly shows that bands at 895 and 880  $\text{cm}^{-1}$  are corresponding to an extended side chain and its less extended structures, respectively. Comparing Figures 6.7 and 6.8 we can conclude that the PHO side chains will possess more extended structure for crystalline PHO than for amorphous PHO. This result is consistent with the previous solid

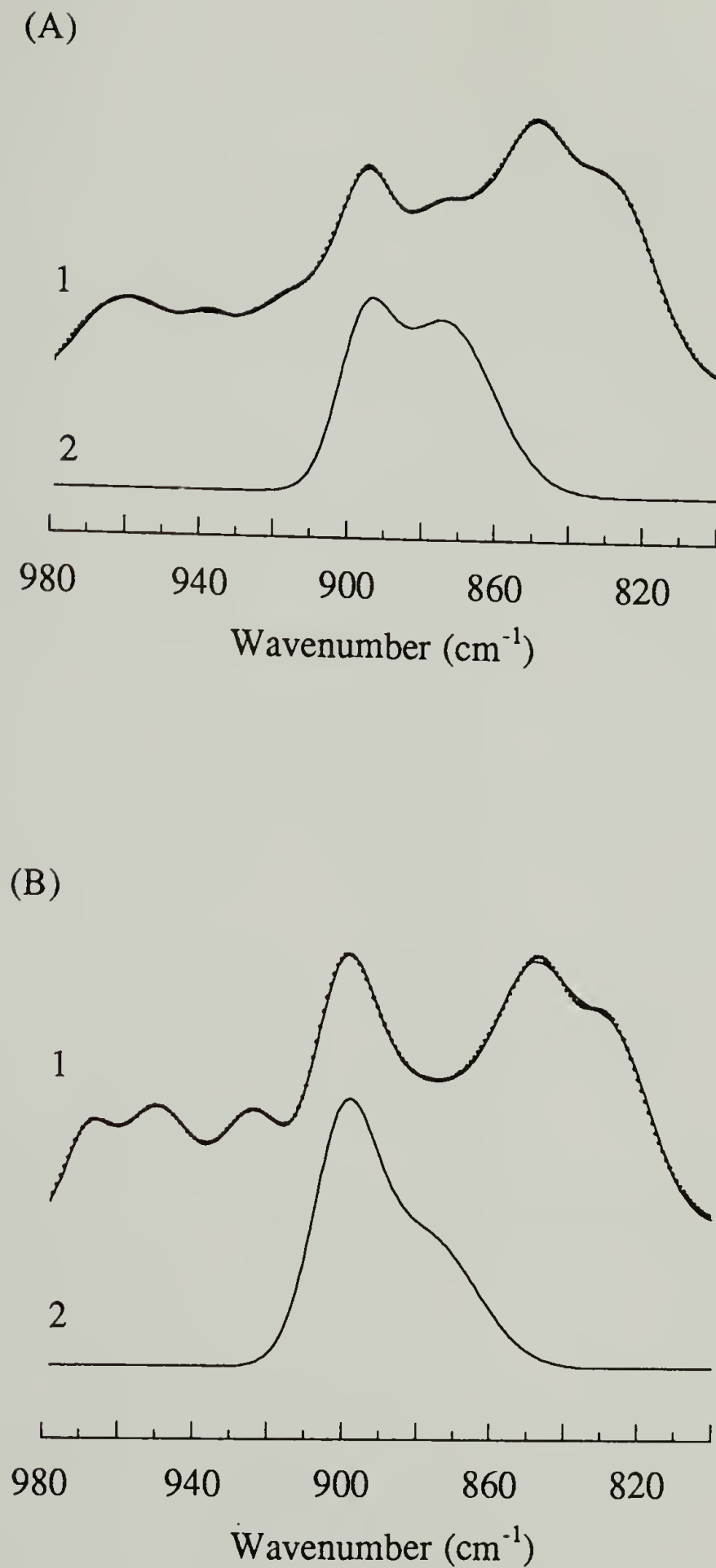


Figure 6.7 Measured isotropic Raman spectra for PHO at different level of phase transformation : (A) Amorphous state; and (B) semi-crystallinity state. (1) : Dots are experimental data while the solid line is the curve-fitting result; (2) : The deconvoluted bands associated with the side chain skeletal mode.

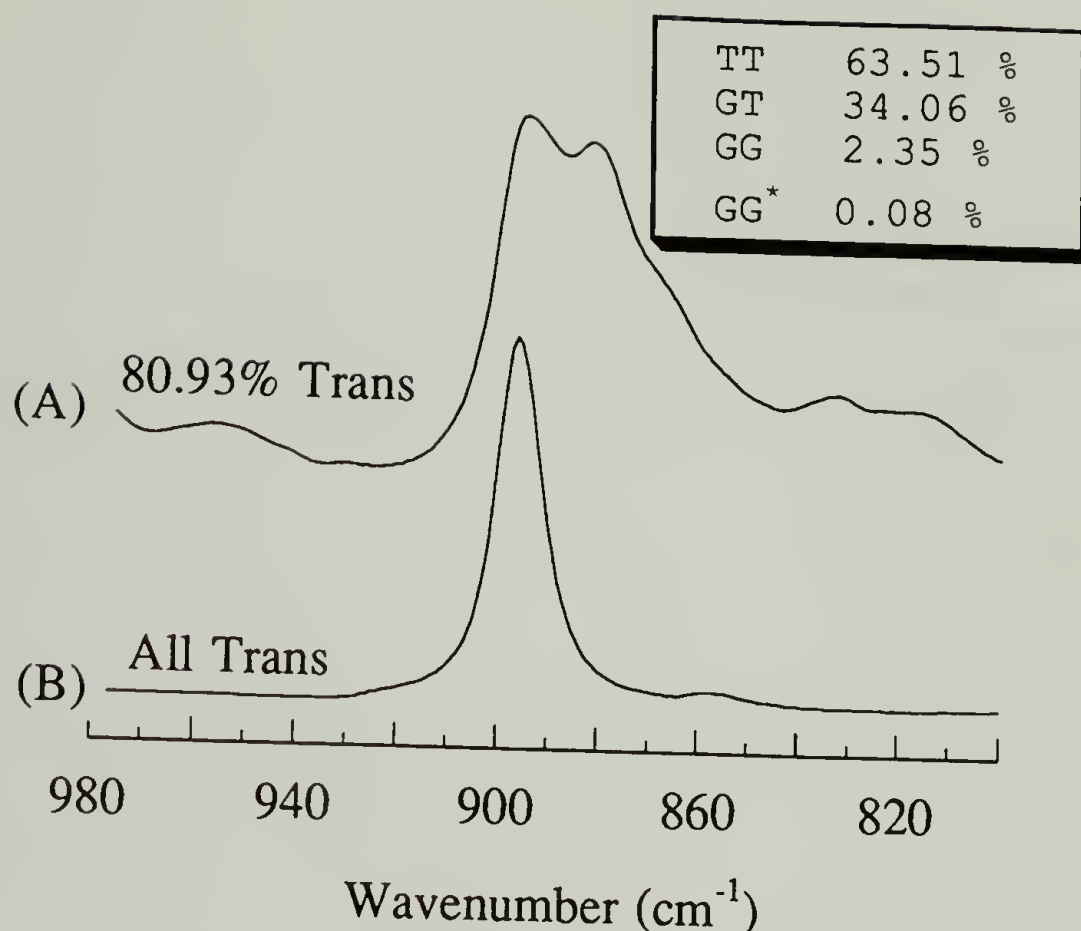


Figure 6.8 Calculated isotropic Raman spectra for the PHO side chain model structure as shown in Figure 6.2 : (A) For non-fully extended structure with the dihedral angle statistics shown in the inset; and (B) for fully extended side chain.

state NMR observation that PHO side chains have different conformations in the amorphous state and in the crystalline state.<sup>4</sup> It also confirms the conjecture by WAXS study that PHO side chains are likely to form sheet-like structure with extended conformation in the crystalline state.<sup>4</sup> Thus by monitoring the change in 870-900  $\text{cm}^{-1}$  region for deformed samples, we can understand whether there is any strain-induced crystallization in the PHO side chains.

**2. Molecular mechanism of Deformation.** Three mechanisms for the permanent tensile set of PHO have been proposed previously:<sup>1,2</sup> (1) permanent orientation or displacement (flow) of the physical crosslinks in the amorphous matrix; (2) irreversible



strain induced crystallization; (3) deformation induced break-up or rearrangement of the physical crosslinks. The second and third hypotheses can be analyzed using carbonyl stretchings and side chain skeletal vibrations. For deformed PHO's with various levels of permanent tensile sets, changes in carbonyl region are shown in Figure 6.9. The degree of crystallinity dropped slightly for samples stretched up to 150% strain (tensile set 85%) (Figure 6.9A). At even higher elongations there indeed is a slight increase in crystallinity (Figure 6.9B). We have no evidence, however, to show any significant strain-induced change in main chain conformation or, indirectly, changes in the degree of crystallinity for deformed PHO's. By examining the side chain skeletal vibrations in the 870-900  $\text{cm}^{-1}$  region (Figure 6.10), there is also no evidence to show any significant strain-induced ordering for PHO side chains. Furthermore, our WAXS study indicated that for deformed PHO sample with a 170% tensile set the change in crystal size is negligible. It should be pointed out, however, previous DSC studies for deformed PHO's have shown an increase in the heat of fusion and a decrease in melting point as a function of strain.<sup>1,2</sup> At the 300% strain (220% tensile set), the heat of fusion increased 60% as compared to the undeformed sample. This result was interpreted as an indication of significant strain-induced crystallization. We have no explanation for those observations.

When deformed, polarized optical microscopy reveals a considerable amount of anisotropy.<sup>4</sup> WAXS study also showed that the chain axis of the crystals will tend to orient parallelly to the stretching direction.<sup>4</sup> With these findings, we suspect that the permanent tensile set results from the irreversible change in chain orientation coupled with changes in chain conformation, but not necessarily crystallinity. We suggest that mechanical elongation induces more extended chains. After releasing from the stress, thermal energy is not sufficiently high to overcome the energy barrier between gauche/trans states thus the amorphous chains are trapped by the more extended conformation. This conjecture can be supported by our molecular simulation study.



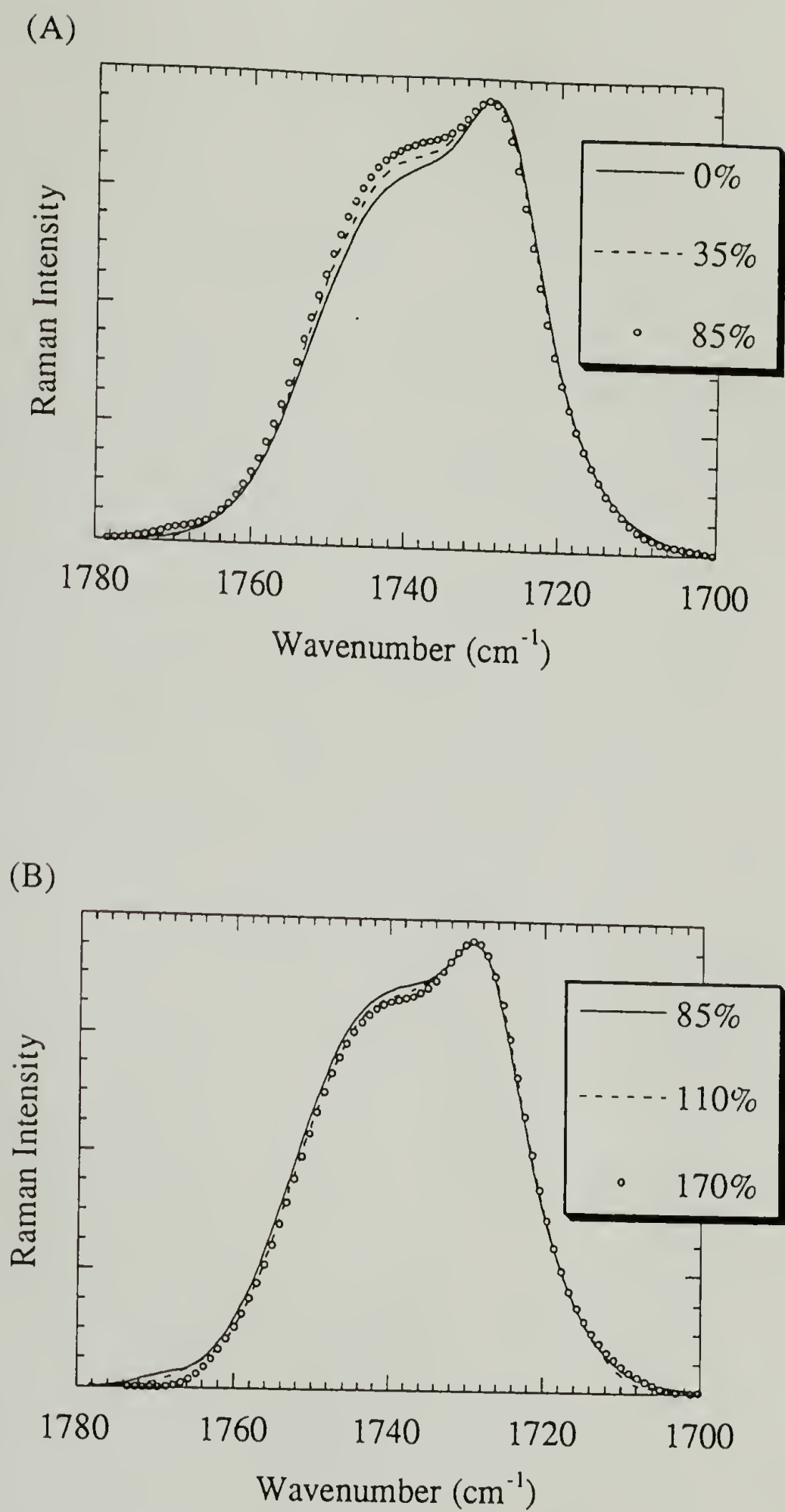


Figure 6.9 Variation of carbonyl stretching region of stretched PHO's measured by FT-Raman spectroscopy. Inset indicates the values of permanent tensile set for PHO samples after various levels of mechanical elongation.

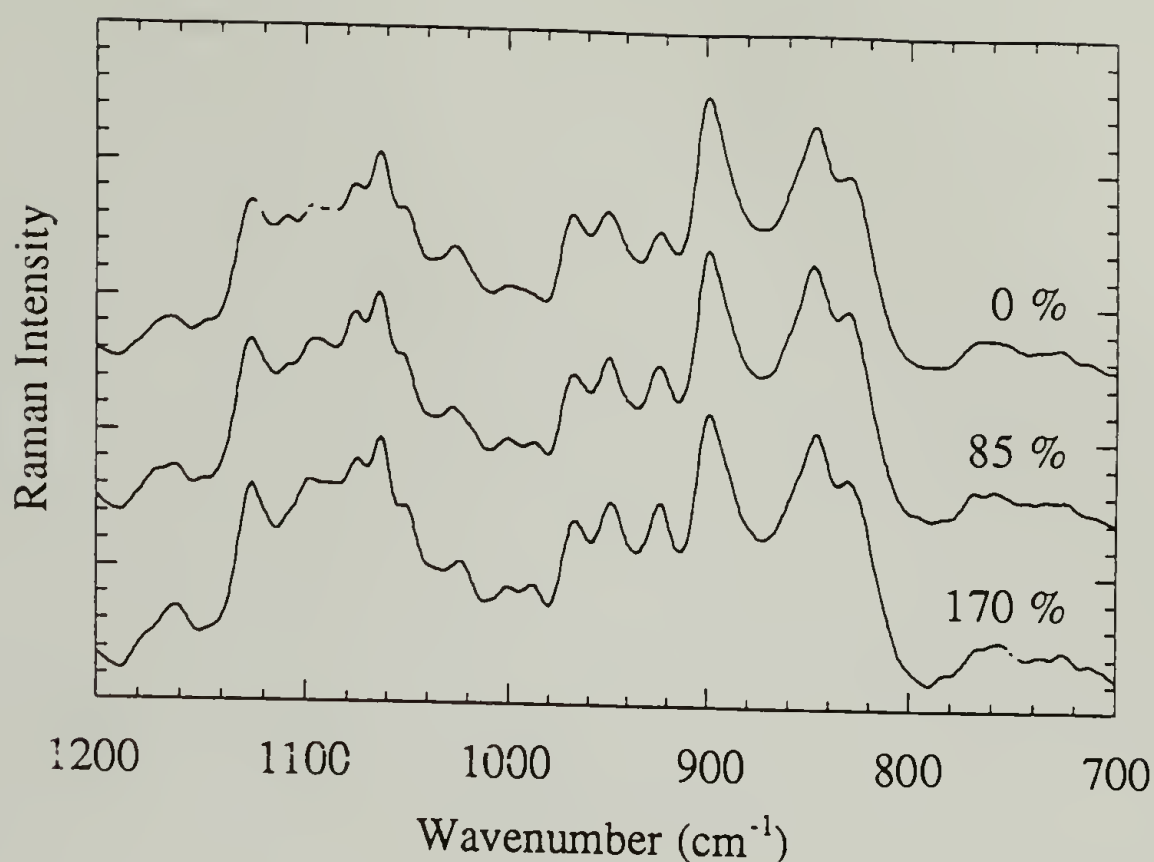


Figure 6.10 Variation of FT-Raman spectra in the region of 700-1200  $\text{cm}^{-1}$  for deformed PHO samples. Listed values are the permanent tensile sets.

In this calculation, we used the PHO structure shown in Figure 6.11. There are four dihedral angles for each repeat unit. However, because each repeat unit has similar structures for both sides with respect to the carbonyl group (Figure 6.11), we can, similar to the approximation used previously, sequentially change  $\phi_1$  and  $\phi_2$  but let rest of the chain relax.<sup>22-24</sup> The calculated contour map is shown in Figure 6.12. The locations of energy minima are exhibited as gray areas. The global minimum is along the line of  $\phi_2=180^\circ$  while other local minima occur at the gauche  $\phi_2$  conformations. The energy barrier between trans and gauche states is very high ( $\approx 10\text{kcal/mol}$ ) due to possible steric interactions with side chains. This result is consistent with our hypothesis. Our proposed model for the permanent tensile set of PHO elastomer is summarized by the schematic representation shown in Figure 6.13. The high rotational energy barrier between different conformations

for the amorphous chains resulting from the long side chains is responsible for this tensile set.

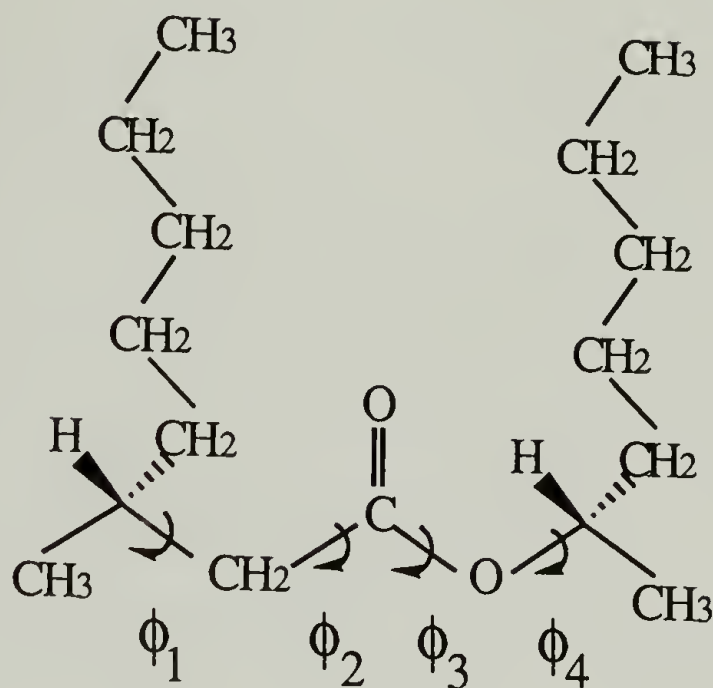


Figure 6.11 Model structure of PHO used for calculating the contour map of conformational energy.  $\phi_1$ - $\phi_4$  are the dihedral angles in the backbone. The dihedral angle is taken to be  $180^\circ$  for trans conformation.

## 6.5 Conclusions

By the FT-Raman measurement associated with normal coordinate analysis we show that the long side-chain of PHO will take more extended structure in the crystal compared with its amorphous state. The carbonyl stretching region can be used to monitor the change in crystallinity during the phase transformation and mechanical deformation processes. It is found that the crystallization process is extremely slow. It is also found that mechanical deformation has no significant effect on the crystallinity. The break-up of crystalline domains and the strain-induced crystallization are believed not to be the important reasons for the high permanent tensile set associated with PHO. The irreversible orientation and displacement of amorphous chains due to the steric interaction between long side-chains is believed to be the dominating factor for this feature.

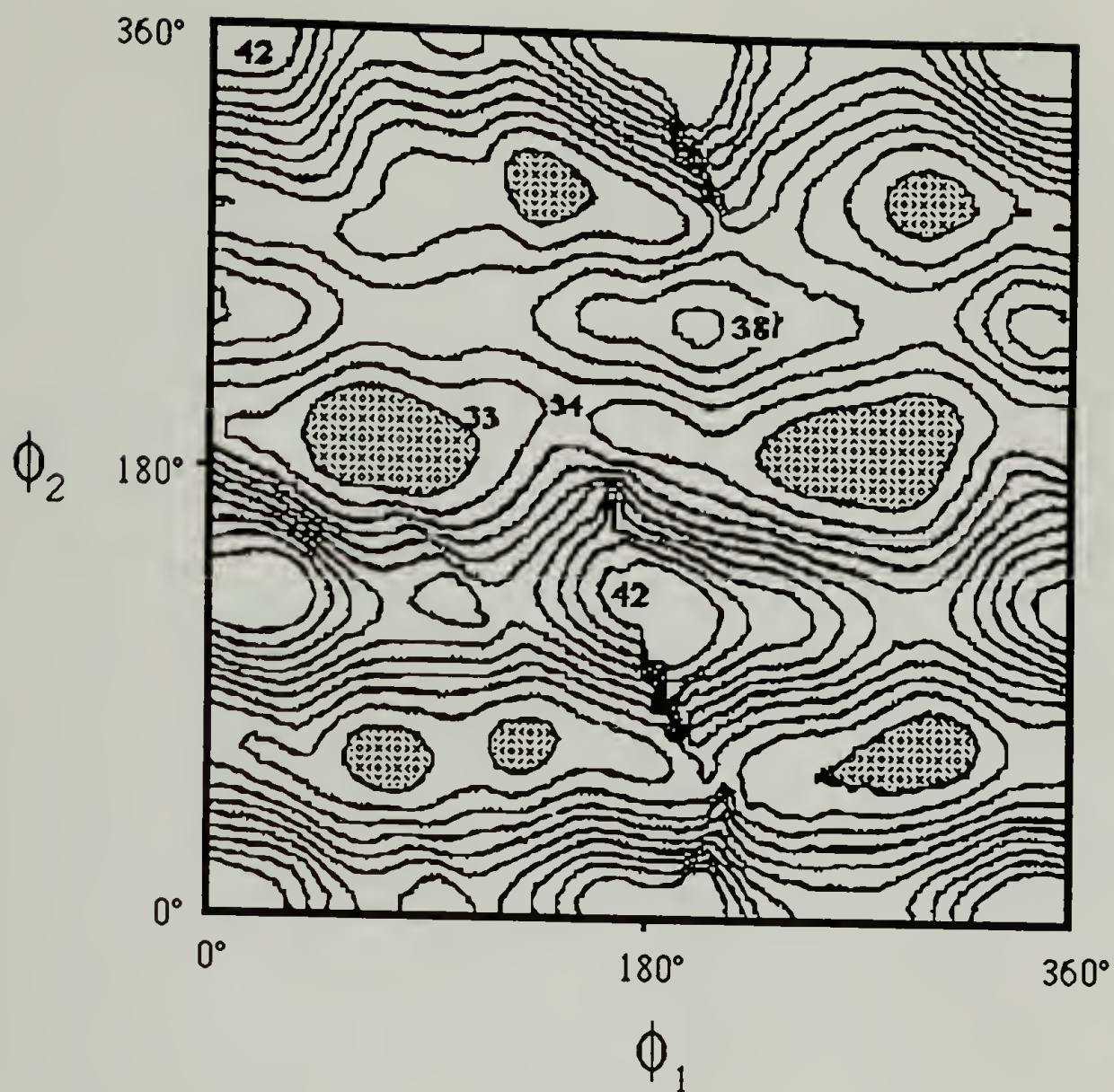


Figure 6.12 The contour map of conformational energy for the model structure shown in Figure 6.10. Listed values are the potential energies in kcal/mol. The increment for each interval is 1kcal/mol.



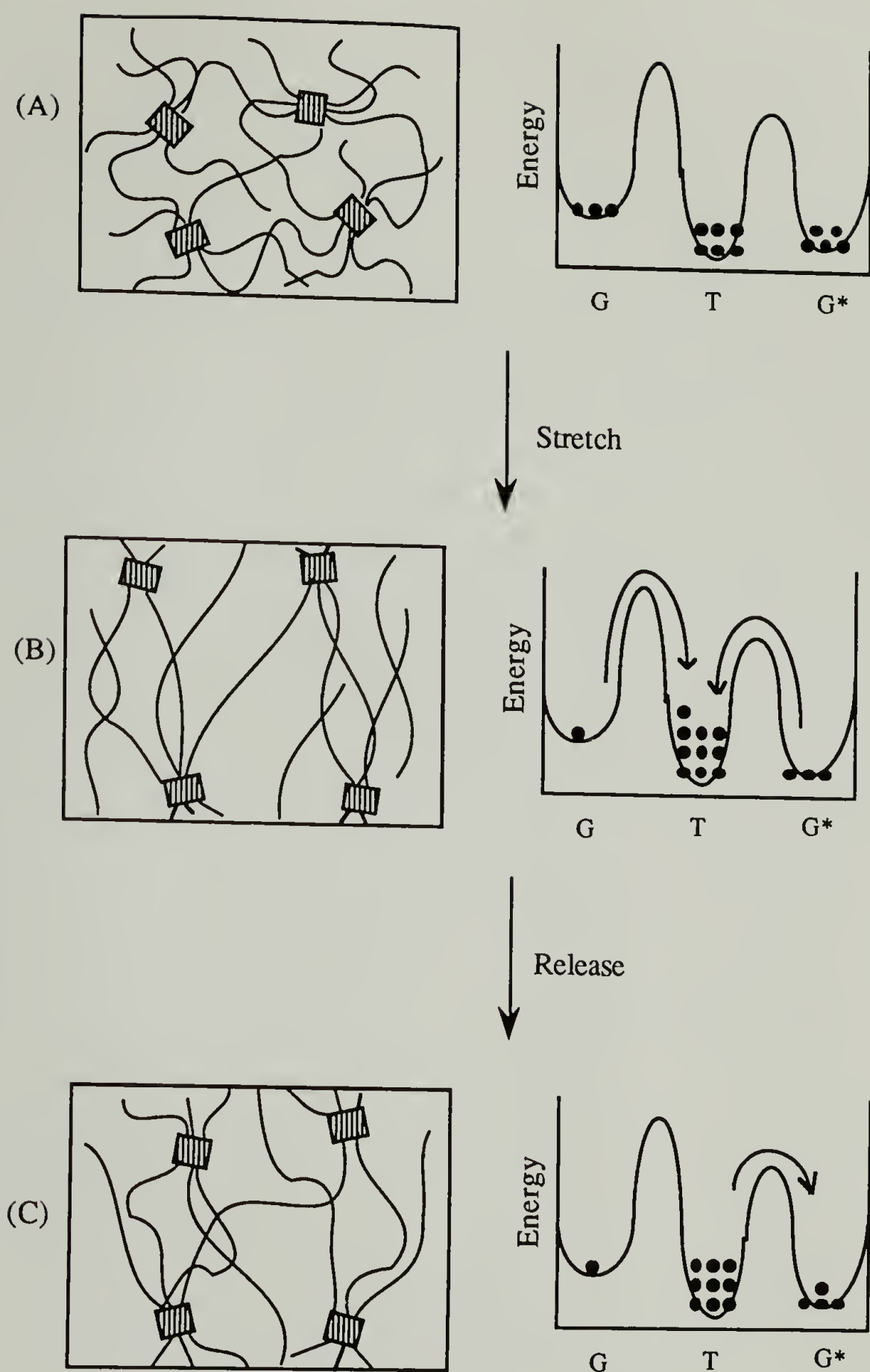


Figure 6.13 Schematic representation of proposed mechanism for the PHO permanent tensile set : (A) Undeformed state, (B) sample under elongation, and (C) sample after releasing from the elongation. Molecular model for chain conformation is shown in the left column with its corresponding conformation distribution in the right column. The number of dots is a representation for the population. T stands for trans conformation. G and G\* stand for gauche conformations. Change in the population in (B) is caused by mechanical deformation. Change in the population in (C) is caused by the thermal energy.

## References

- (1) Gagnon, K. D.; Lenz, R. W.; Farris, R. J.; Fuller, R. C. *Rubber Chem. Tech.* **1992**, *65*, 761.
- (2) Gagnon, K. D.; Lenz, R. W.; Farris, R. J.; Fuller, R. C. *MAcromolecules* **1992**, *25*, 3723.
- (3) Gross, R. A.; DeMello, C.; Lenz, R. W.; Brandl, H.; Fuller, R. C. *Macromolecules* **1989**, *22*, 1106.
- (4) Marchessault, R. H.; Monasterios, C. J.; Morin, F. G.; Sundararajan, P. R. *Int. J. Biol. Macromol.* **1990**, *12*, 158.
- (5) Richtering, H. W.; Gagnon, K. D.; Lenz, R. W.; Fuller, R. C.; Winter, H. H. *Macromolecules* **1992**, *25*, 2429.
- (6) Brandl, H.; Gross, R. A.; Lenz, R. W.; Fuller, R. C. *Appl. Environ. Microbiol.* **1988**, *54*, 1977.
- (7) Gagnon, K. D.; Bain, D. B.; Lenz, R. W.; Fuller, R. C. In ; E. A. Dawes, Ed.; *Novel Biodegradable Microbial Polymers*; Kluwer Academic Publishers: Dordrecht, The Netherlands, 1990; pp 449 and 450.
- (8) Snyder, R. G. *J. Chem. Soc., Faraday Trans.* **1992**, *88*, 1823.
- (9) Snyder, R. G.; Kim, Y. *J. Phys. Chem.* **1991**, *95*, 602.
- (10) Snyder, R. G.; Zerbi, G. *Spectrochim. Acta* **1967**, *23A*, 391.
- (11) Flory, P. J. *Statistical Mechanics of Chain Molecules*; Hanser Publishers: New York, 1989.
- (12) Mayo, S. L.; Olafson, B. D.; Goddard, W. A., III *J. Phys. Chem.* **1990**, *94*, 8897.
- (13) Gasteiger, J. *Tetrahedron* **1980**, *36*, 3219.
- (14) Moravie, R. M.; Corset, J. *J. Mol. Struct.* **1975**, *24*, 91.
- (15) Mido, Y.; Shono, T. *J. Mol. Struct.* **1991**, *246*, 13.
- (16) Charney, E. *The Molecular Basis of Optical Activity*; John Wiley & Sons: New York, 1979.
- (17) Marchessault, R. H.; Okamura, K.; Su, C. J. *Macromolecules* **1970**, *3*, 735.
- (18) Delsarte, J.; Weill, G. *Macromolecules* **1974**, *7*, 450.
- (19) Iwakura, Y.; Iwata, K.; Matsuo, S.; Tohara, A. *Makromolekulare Chem.* **1969**, *122*, 275.
- (20) Akita, S.; Einaga, Y.; Miyaki, Y.; Fujita, H. *Macromolecules* **1976**, *9*, 774.

- (21) Tinoco, I., Jr. *J. Chem. Phys.* **1960**, 33, 1332.
- (22) Fan, C. F.; Hsu, S. L. *Macromolecules* **1991**, 24, 6244.
- (23) Fan, C. F.; Olafson, B. D.; Blanco, M.; Hsu, S. L. *Macromolecules* **1992**, 25, 3667.
- (24) Fan, C. F.; Hsu, S. L. *Macromolecules* **1992**, 25, 266.

## CHAPTER 7

### GENERAL RESULTS AND RECOMMENDATIONS FOR FUTURE WORK

#### 7.1 General Results

In this dissertation, molecular simulation and spectroscopic methods were used to explore the phase separation behavior of thermoplastic elastomers. The results are summarized as follows.

In Chapter 2, a combination of a molecular simulation method and *Monte Carlo* method has been successfully utilized to calculate phase diagrams of model polyurethanes. In our model, the entropic contribution of the Flory-Huggins expression has been modified to incorporate the contribution arising from orientation of hard segments. The constraint associated with chain rigidity of hard segments has been explicitly considered. In addition, the interaction term has been modified to include the relative packing of hard segments. Phase diagrams of various MDI-PPG model polyurethanes have thus been predicted utilizing these modifications. The effects of soft and hard segment lengths have been considered and the actual degree of phase separation calculated. Our predictions have been compared to experimental values. Additionally, the contribution of hydrogen bonding to the miscibility behavior of hard and soft segments needs be re-evaluated.

In Chapter 3, diacetylene-containing segmented polyurethane elastomers with various hard/soft segment lengths have been synthesized. Thermal and spectroscopic studies were conducted to characterize the phase-separated structures of these compounds. Infrared spectroscopic results revealed that the degree of phase separation is higher for



polyurethanes with longer hard-segment or *shorter* soft-segment. This finding is consistent with our previous prediction and it also demonstrates the inapplicability of utilizing thermal analysis to determine the phase compositions. The existence of packing ordering in the non-crystalline hard-segment-rich domains has been confirmed by the capability of cross-polymerization of diacetylene segments. Furthermore, spectroscopic studies showed a better packing in the hard-segment-rich domains for polyurethanes with shorter hard-segment or longer soft-segment.

In Chapter 4, a polyurethane elastomer with monodisperse hard segment, B4 polymer, was examined by two-dimensional solid state wide-line separation (WISE) NMR technique. It was found that the phase separation behavior is quite consistent with our rod-coil model. It was also shown that DSC is not applicable for the phase separation study of thermoplastic elastomers.

In Chapter 5, phase separation behavior associated with ultra-thin films of model polyurethanes has been studied by reflectance infrared spectroscopy. Our data clearly demonstrate that the phase separation behavior and the domain size of polyurethanes in the ultra-thin film region differ significantly from its bulk state. The kinetics measured are considerably slower in thin films as compared to the bulk. In addition, the degree of phase separation is also highly dependent on film thickness. The phase separation obeys an *Avrami* type rate process and have been modeled. The relatively slow rate of phase separation, the ultimate degree of phase separation, and the observed high value of chain orientations on the substrate are consequences of having a polyurethane with semi-rigid hard segments. The predicted phase separation kinetics based on rod-coil model was consistent with the experimental result. Thus we concluded that hard segment chain rigidity effect is the dominating factor controlling the phase separation process for B2 polymer.

In Chapter 6, the chain conformation changes of a bio-degradable polyester elastomer, poly( $\beta$ -hydroxyoctanoate) (PHO), during the phase transformation and mechanical deformation processes were examined by vibrational spectroscopy associated with normal coordinate analysis. It has been shown that the side-chains will take more extended conformation in the crystalline state than in amorphous state. Degree of phase transformation can be monitored by the two distinct bands in carbonyl stretching region which are corresponding to ester groups in amorphous phase and in crystalline phase. It is found that the crystallization process is extremely slow compared with other poly( $\beta$ -hydroxyalkanoates) with shorter side-chains. It is also found that even though mechanical deformation will change the degree of crystallinity, the effect is not significant. We proposed that the permanent tensile set of PHO comes from the irreversible alignment of amorphous chains and crystalline domains rather than from the break-up of the crystalline structure or strain-induced crystallization. The steric hindrance of the long side-chains is responsible for this irreversibility.

## 7.2 Recommended Future Work

For diacetylene-containing polyurethane elastomers, non-linear optical spectroscopy can be utilized to explore the hard segment packing behavior. This conjecture is based on the fact that non-linear response is very sensitive to the conjugate length of cross-polymerized diacetylene, which in turn is sensitive to its local ordering. A possible technique for this work is Degenerate Four-Wave Mixing (DFWM).

The effect of phase separation and mechanical deformation on the chain conformation change of soft segment is another important topic. The Raman spectrum for

PPG in the region of 800-900  $\text{cm}^{-1}$  has been assigned. With this result we can explore this interesting question and try to understand the stress distribution in the elastomers.

For the molecular simulation technique, further work on polyurethane can be extended to polyurethane foam. Molecular simulation can be applied to study the phase separation thermodynamics as well as the cell formation properties which are controlled by the surface tension.

Finally, for PHO work, more detail study on the amorphous chain conformation should be conducted to confirm our mechanism. It will be also helpful to measure or calculate the enthalpic contribution and entropic contribution on the elastic force for deformed samples. It is also interesting to see whether incorporating ester plasticizer can reduce the tensile set because the plasticizer may reduce the rotational energy barrier for the T, G conformations of the amorphous PHO chains (refer to Figure 6.13).



## BIBLIOGRAPHY

1. Akita, S.; Einaga, Y.; Miyaki, Y.; Fujita, H. *Macromolecules* **1976**, *9*, 774.
2. Andrady, A. L.; Sefcik, M. D. *J. Polym. Sci., Polym. Phys. Ed.* **1983**, *21*, 2453.
3. Assink, R. A. *J. Polym. Sci., Polym. Phys. Ed.* **1977**, *15*, 59.
4. Assink, R. A.; Wilkes, G. L. *J. Appl. Polym. Sci.* **1981**, *26*, 3689.
5. Bandekar, J. ; Klima, S. *J. Molec. Struct.*, **1991**, *263*, 45.
6. Bandekar, J.; Klima, S. *Spectrochim. Acta*, **1992**, *48A*, 1363.
7. Baughman, R. H.; Yee, K. C. *Macromol. Rev.* **1978**, *13*, 219.
8. Billon, N.; Escleine, J. M.; Haudin, J. M. *Colloid Polym. Sci.* **1989**, *267*, 668.
9. Binder, K. *J. Chem. Phys.* **1983**, *79*, 6387.
10. Blackwell, J.; Gardner, K. H. *Polymer* **1979**, *20*, 13.
11. Blackwell, J.; Lee, C.D. *J. Polym. Sci., Polym. Phys. Ed.*, **1983**, *21*, 2169.
12. Blackwell, J.; Nagarajan, M. R. *Polymer* **1981**, *22*, 202.
13. Brandl, H.; Gross, R. A.; Lenz, R. W.; Fuller, R. C. *Appl. Environ. Microbiol.* **1988**, *54*, 1977.
14. Cahn, J. W.; Hilliard, J. E. *J. Chem. Phys.* **1958**, *28*, 258.
15. Chang, S.-S. *Polymer* **1992**, *33*, 4768.
16. Charney, E. *The Molecular Basis of Optical Activity*; John Wiley & Sons: New York, 1979.
17. Christenson, C. P.; Harthcock, M. A.; Meadows, M. D.; Spell, H. L.; Howard, W. L.; Creswick, M. W.; Guerra, R. E.; Turner, R. B. *J. Polym. Sci., Polym. Phys. Ed.* **1986**, *24*, 1401.
18. Chu, B.; Gao, T. ; Li, Y. ; Wang, J.; Desper, C.R. ; Byrne, C.A., *Macromolecules*, **1992**, *25*, 5724.
19. Coleman, M. M.; Graf, J. F.; Painter, P. C. *Specific Interactions and the Miscibility of Polymer Blends*; Technomic Publishing Co.: Lancaster, PA, 1991.
20. Culbertson, B.M. (Ed) *Multiphase Macromolecular Systems*, Plenum Publishing Corporation, New York, **1989**.
21. Day, D. R.; Lando, J. B. *J. Appl. Polym. Sci.* **1981**, *26*, 1605.
22. Delsarte, J.; Weill, G. *Macromolecules* **1974**, *7*, 450.
23. Dickinson, L. C.; Shi, J.-F.; Chien, J. C. W. *Macromolecules* **1992**, *25*, 1224.



24. Dixon, W. T. *J. Chem. Phys.* **1982**, 77, 1800.
25. Dixon, W. T. *J. Magn. Reson.* **1980**, 44, 220.
26. Dumais, J. J.; Jelinski, L. W.; Leung, L. M.; Gancarz, I.; Galambos, A.; Koberstein, J. T. *Macromolecules* **1985**, 18, 116.
27. Eisenbach, C. D.; Heinemann, T.; Ribbe, A.; Stadler, E. *Die Angewandte Makromolekulare Chemie* **1992**, 202/203, 221.
28. Eisenbach, C. D.; Nefzger, H. In ; B. M. Culbertson, Ed.; *Multiphase Macromolecular Systems*; Plenum Publishing Corp.: New York, 1989; pp 339.
29. Enkelmann, V. *Adv. Polym. Sci.* **1984**, 63, 91.
30. Escleine, J. M.; Monasse, B.; Wey, E.; Haudin, J. M. *Colloid Polym. Sci.* **1984**, 262, 363.
31. Fan, C. F.; Hsu, S. L. *Macromolecules* **1991**, 24, 6244.
32. Fan, C. F.; Hsu, S. L. *Macromolecules* **1992**, 25, 266.
33. Fan, C.F.; Olafson, B.D.; Blanco, M.; Hsu, S.L. *Macromolecules*, **1992**, 25, 3667.
34. Feger, C.; MacKnight, W. J. *Macromolecules* **1985**, 18, 280.
35. Flory, P. J. *J. Chem. Phys.* **1941**, 9, 660.
36. Flory, P. J. *Principles of Polymer Chemistry*; Cornell Univ. Press: Ithaca, N.Y., 1953.
37. Flory, P. J. *Statistical Mechanics of Chain Molecules*; Hanser Publishers: New York, 1989.
38. Flory, P.J. *Adv. Polym. Sci.*, **1984**, 59, 1.
39. Flory, P.J. *Macromolecules*, **1978**, 11, 1138.
40. Flory, P.J. *Proc. Royal Soc., London*, **1956**, A234, 73.
41. Flory, P.J.; Abe, A. *Macromolecules*, **1978**, 11, 1119.
42. Flory, P.J.; Ronca, G. *Mol. Cryst. Liq. Cryst.*, **1979**, 54, 311.
43. Gagnon, K. D.; Bain, D. B.; Lenz, R. W.; Fuller, R. C. In ; E. A. Dawes, Ed.; *Novel Biodegradable Microbial Polymers*; Kluwer Academic Publishers: Dordrecht, The Netherlands, 1990; pp 449 and 450.
44. Gagnon, K. D.; Lenz, R. W.; Farris, R. J.; Fuller, R. C. *MACromolecules* **1992**, 25, 3723.

45. Gagnon, K. D.; Lenz, R. W.; Farris, R. J.; Fuller, R. C. *Rubber Chem. Tech.* **1992**, *65*, 761.
46. Gasteiger, J. *Tetrahedron* **1980**, *36*, 3219.
47. Gross, R. A.; DeMello, C.; Lenz, R. W.; Brandl, H.; Fuller, R. C. *Macromolecules* **1989**, *22*, 1106.
48. Harrell, L. L. ;. *J. Macromolecules* **1969**, *2*, 607.
49. Helfand, E. *J. Chem. Phys.* **1975**, *63*, 2192.
50. Hepburn, C. *Polyurethane elastomers*; Applied Sciences Publishers: London, 1982.
51. Hildebrand, J. H. *J. Am. Chem. Soc.* **1929**, *51*, 66.
52. Hølyst, R.; Cshick, M. *J Chem. Phys.*, **1992**, *96*, 721; **1992**, *96*, 730.
53. Hu, J.; Park, Y.; Painter, P.C.; Coleman, M.M. *Polym. Prepr. (Am. Chem. Soc. , Div. Polym. Chem.)* **1988**, *29(1)*, 321.
54. Hu, X.; Stanford, J. L.; Day, R. J.; Young, R. J. *Macromolecules* **1992**, *25*, 672.
55. Huggins, M. L. *J. Chem. Phys.* **1941**, *4*, 440.
56. Hwang, K. K. S.; Hemker, D. J.; Cooper, S. L. *Macromolecules* **1984**, *17*, 307.
57. Hwang, K. K. S.; Lin, S. B.; Tsay, S. Y.; Cooper, S. L. *Polymer* **1984**, *25*, 947.
58. Iwakura, Y.; Iwata, K.; Matsuo, S.; Tohara, A. *Makromolekulare Chem.* **1969**, *122*, 275.
59. Jakeways, R.; Ward, I. M.; A., W. M.; Hall, I. H.; Desborough, J.; Pass, M. G. *J. Polym. Sci., Polym. Phys. Ed.* **1975**, *13*, 799.
60. Kintarnar, A.; Jelinski, L.W.; Gancarz, I.; Koberstein, J.T. *Macromolecules*, **1986**, *19*, 1876.
61. Koberstein, J. T.; Galambos, A. F.; Leung, L. M. *Macromolecules* **1992**, *25*, 6195.
62. Koberstein, J. T.; Leung, L. M. *Macromolecules* **1992**, *25*, 6205.
63. Koberstein, J. T.; Morra, B.; Stein, R. S. *J. Appl. Crystallogr.* **1980**, *13*, 34.
64. Koberstein, J. T.; Stein, R. S. *J. Poly. Sci., Polym. Phys. Ed.* **1983**, *21*, 1439.
65. Kollmar, C.; Sixl, H. *J. Chem. Phys.* **1987**, *87*, 5541.
66. Kornfield, J. A.; Spiess, H. W.; Nefzger, H.; Eisenbach, C. D. *Macromolecules* **1991**, *24*, 4787.
67. Lee, H. S.; Wang, Y. K.; Hsu, S. L. *Macromolecules* **1987**, *20*, 2089.

68. Lee, H. S.; Wang, Y. K.; MacKnight, W. J.; Hsu, S. L. *Macromolecules* **1988**, *21*, 270.
69. Lee, H.S. ; Hsu, S.L. ; *Macromolecules*, **1989**, *22*, 1100.
70. Legge, N. R.; Holden, G.; Schroeder, H. E.(Ed)*Thermoplastic Elastomers : A Comprehensive Review* ; Hanser Publishers: New York, 1987.
71. Leung, L. M.; Koberstein, J. T. *Macromolecules* **1986**, *19*, 706.
72. Li, Y.; Kang, W.; Stoffer, J. O.; Chu, B. *Macromolecules* **1994**, *27*, 612.
73. Liang, R.-C.; Lai, W.-Y. F.; Reiser, A. *Macromolecules* **1986**, *19*, 1685.
74. Liu, A.J.; Fredrickson, G.H. *Macromolecules*, **1992**, *25*, 5551; **1993**, *26*, 2817.
75. Lu, X.; Weiss, R.A. *Macromolecules*, **1992**, *25*, 3242.
76. Maier, W.; Saupe, A.Z. *Naturforschg.*, **1959**, *14A*, 882 ; **1960**, *15A*, 287.
77. Marchessault, R. H.; Monasterios, C. J.; Morin, F. G.; Sundararajan, P. R. *Int. J. Biol. Macromol.* **1990**, *12*, 158.
78. Marchessault, R. H.; Okamura, K.; Su, C. J. *Macromolecules* **1970**, *3*, 735.
79. Matheson, R.R.,Jr.; Flory, P.J. *J. Chem. Phys.*, **1980**, *73*, 6327.
80. Mayo, S. L.; Olafson, B. D.; Goddard, W. A., III *J. Phys. Chem.* **1990**, *94*, 8897.
81. Meadows, M. D.; Christenson, C. P.; Howard, W. L.; Harthcock, M. A.; Guerra, R. E.; Turner, R. B. *Macromolecules* **1990**, *23*, 2440.
82. Meuse, C. W.; Tao, H.-J.; Hsu, S. L.; MacKnight, W. J. *Polym. Prepr. (Am. Chem. Soc., Div. Polym. Chem.)* **1993**, *34*(2), 266.
83. Meuse, C. W.; Yang, X.; Yang, D.; Hsu, S. L. *Macromolecules* **1992**, *25*, 925.
84. Mido, Y.; Shono, T. *J. Mol. Struct.* **1991**, *246*, 13.
85. Miller, J. A.; Lin, S. B.; Hwang, K. K. S.; Wu, K. S.; Gibson, P. E.; Cooper, S. L. *Macromolecules* **1985**, *18*, 32.
86. Moravie, R. M.; Corset, J. *J. Mol. Struct.* **1975**, *24*, 91.
87. Nierzwicki, W. *J. Appl. Polym. Sci.* **1984**, *29*, 1203.
88. Nitzsche, S. A.; Hsu, S. L.; Hammond, P. T.; Rubner, M. F. *Macromolecules* **1992**, *25*, 2391.
89. Nitzsche, S. A.; Wang, Y. K.; Hsu, S. L. *Macromolecules* **1992**, *25*, 2397.
90. Okamoto, D. T.; Cooper, S. L.; Root, T. W. *Macromolecules* **1992**, *25*, 1068.



91. Painter, P. C.; Park, Y.; Coleman, M. M. *Macromolecules* **1988**, *21*, 66.
92. Paul, D.R.; Newman, S. (Eds) *Polymer Blends*, Academic Press, New York, **1978**.
93. Petrovic, Z. S.; Ferguson, J. J. *Prog. Polym. Sci.* **1991**, *16*, 695.
94. Petrovic, Z.S.; Javni, I. *J. Polym. Sci., Polym. Phys. Ed.*, **1989**, *27*, 545.
95. Pimentel, G. C.; McClellan, A. L. *The Hydrogen Bond*; Reinhold Publishing Corp.: New York, 1959.
96. Prausnitz, J. M. *Molecular Thermodynamics of Fluid-Phase Equilibria*; Prentice-Hall, Inc.: Englewood Cliffs, N.J., 1969.
97. Priestley, E.B.; Wojtowicz, P.J.; Sheng, P. *Introduction to Liquid Crystals*, Plenum Press, NY and London, **1975**, Chap 3.
98. Richtering, H. W.; Gagnon, K. D.; Lenz, R. W.; Fuller, R. C.; Winter, H. H. *Macromolecules* **1992**, *25*, 2429.
99. Rubner, M. F. *Macromolecules* **1986**, *19*, 2114.
100. Schen, M. A.; Kotowski, K.; Cline, J. *Polymer* **1991**, *32*, 1843.
101. Schmidt-Rohr, K.; Clauss, J.; Spiess, H. W. *Macromolecules* **1992**, *25*, 3273.
102. Schoen, P. E.; Yager, P.; Priest, R. G. In ; D. Bloor and R. R. Chance, Ed.; *Polydiacetylenes : Synthesis, Structure and Electronic Properties*; Martinus Nijhoff Publishers: Dordrecht, The Netherlands, 1985; pp 223.
103. Schott, M.; Wegner, G. In ; M. S. Chemla and J. Zyss, Ed.; *Nonlinear Optical Properties of Organic Molecules and Crystals*; Academic Press: Orlando, 1987; Vol. 2, chapter III-1; pp 3.
104. Snyder, R. G. *J. Chem. Soc., Faraday Trans.* **1992**, *88*, 1823.
105. Snyder, R. G.; Kim, Y. *J. Phys. Chem.* **1991**, *95*, 602.
106. Snyder, R. G.; Zerbi, G. *Spectrochim. Acta* **1967**, *23A*, 391.
107. Stein, R. S.; Powers, J. *J. Polym. Sci.* **1962**, *56*, S9.
108. Stouch, T.R.; Jurs, P.C. *J. Chem. Inf. Comput. Sci.*, **1986**, *26*, 4.
109. Sun, H. *Macromolecules* **1993**, *26*, 5924.
110. Tao, H.-J.; Hsu, S. L.; MacKnight, W. J. *Polym. Prepr., (Am. Chem. Soc., Div. Polym. Chem.)* **1992**, *33(2)*, 575.
111. Tao, H.-J.; MacKnight, W. J.; Hsu, S. L. *Macromolecules* **1994**, in press.
112. Tekely, P.; Palmas, P.; Mutzenhardt, P. *Macromolecules* **1993**, *26*, 7363.



113. Theodoro, D. N. *Macromolecules* **1988**, *21*, 1411.
114. Theodoro, D. N. *Macromolecules* **1988**, *21*, 1422.
115. Tinoco, I., Jr. *J. Chem. Phys.* **1960**, *33*, 1332.
116. Treloar, L. R. G. *The Physics of Rubber Elasticity*; Clarendon Press: Oxford, 1975.
117. Utracki, L. A. *Polymer Alloys and Blends*; Hanser Publishers: Munich, Germany, 1989.
118. Warner, M.; Flory, P.J. *J. Chem. Phys.*, **1980**, *73*, 6327.
119. Wegner, G. *Makromol. Chem.* **1971**, *145*, 85.
120. Wunderlich, B. *Macromolecular Physics*; Academic Press: New York, 1976; pp chapter 6 .
121. Yokouchi, M.; Sakakibara, Y.; Chatani, Y.; Tadokoro, H.; Tanaka, T.; Yoda, K. *Macromolecules* **1976**, *9*, 266.
122. Yoon, D. Y.; Flory, P. J. . *Macromolecules* **1984**, *17*, 868.





